

Supplemental information

Highly potent quinoxalinediones inhibit

α -hemolysin and ameliorate

Staphylococcus aureus lung infections

Aditya Shekhar, Raffaella Di Lucrezia, Karoline Jerje, Vadim S. Korotkov, Kirsten Harmrolfs, Katharina Rox, Herbert A. Weich, Ishan Ghai, Florent Delhommel, Isabelle Becher, Carsten Degenhart, Eyad Fansa, Anke Unger, Peter Habenberger, Bert Klebl, Peer Lukat, Stefan Schmelz, Steffi Henke, Sebastian Borgert, Julia C. Lang, Florenz Sasse, Randi Diestel, Clémentine Richter, Nicole Schneider-Daum, Bettina Hinkelmann, Jana Niemz, Claus-Michael Lehr, Lothar Jänsch, Jochen Huehn, Richard Alm, Mikhail Savitski, Tobias Welte, Thomas Hesterkamp, Michael Sattler, Mathias Winterhalter, Wulf Blankenfeldt, Eva Medina, Ursula Bilitewski, Klaus Dinkel, and Mark Brönstrup

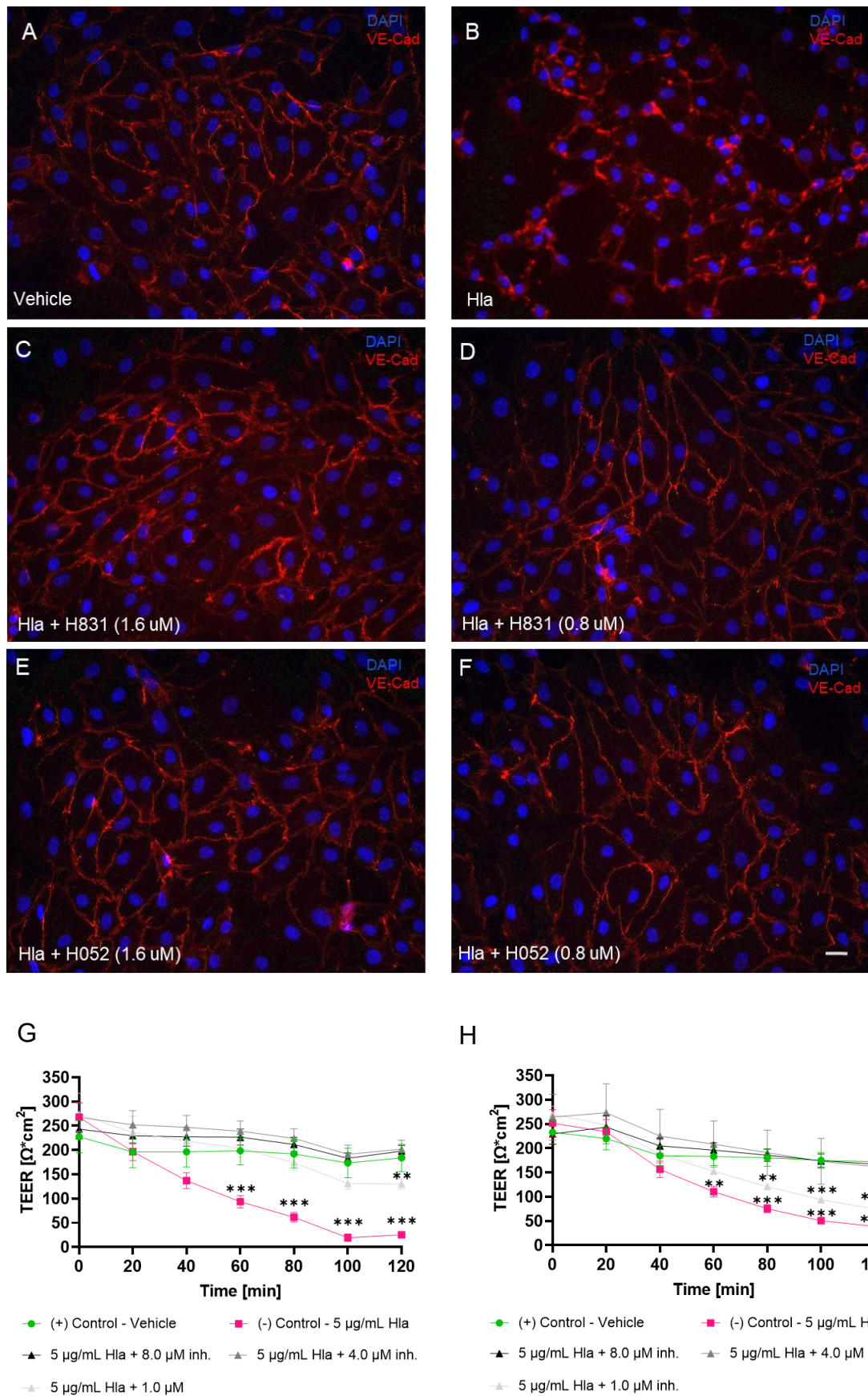


Figure S1. Prevention of Hla-induced degradation of adherens junctions by QDS in human lung cells, related to Figure 3. Primary human pulmonary microvascular endothelial cells were grown on 8-well coverslips (A), incubated with 1 $\mu\text{g/ml}$ Hla (B) in the presence of 1.6 μM H831 (C), 0.8 μM H831 (D), 1.6 μM H052 (E) or 0.8 μM H052 (F). Cells were fixed in MeOH/Acetone (50:50) and immunostained

with VE-cadherin antibodies and Alexa647 IgG as secondary antibodies (red). DNA was visualized by DAPI staining (blue). Scale bar, 20 μm . (G)-(H) Protection of pulmonary barrier against Hla-induced loss of transepithelial resistance (TEER). Calu-3 monolayers were cultivated on Transwells[®] and the TEER was measured using an EVOM2 with a pair of chopstick electrodes STX2 (all World Precision Instruments). After 11 days, a typical TEER around 250 $\text{Ohm} \cdot \text{cm}^2$ was reached. However, when exposed to 5 $\mu\text{g/ml}$ Hla, TEER dropped to <50 $\text{Ohm} \cdot \text{cm}^2$ within 90-120 min, indicating a nearly complete loss of epithelial barrier function. In presence of either QDS H831 (G) or H052 (H), the Hla-induced loss of epithelial barrier function could be prevented in a dose dependent way, with H831 appearing to be more potent than H052, but leading to a complete protection of the epithelial barrier at 4.0 μM for either drug. N = 4 out of one experiment; One-way ANOVA with post-hoc Dunnett's test; *P* 0.12 (ns), 0.002 (**), <0.001 (***)

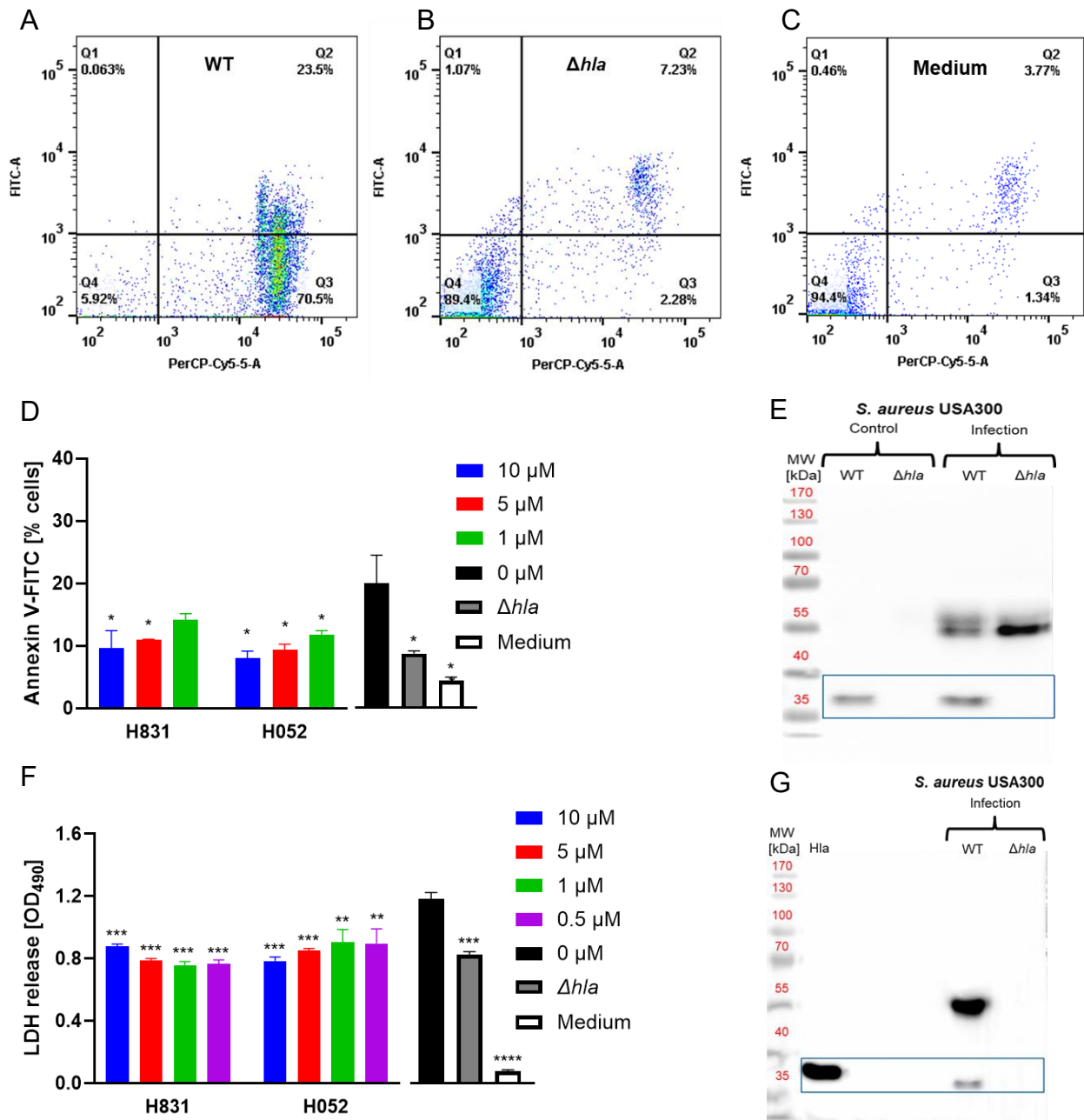


Figure S2. Co-culture of A549 cells and differentiated THP1 cells with *S. aureus* USA300, related to Figure 3. (A) – (C) Representative flow cytometry plots gated for Annexin V (FITC-A, apoptosis) and PI (PerCP-CY5-5-A, necrosis) labelled cells after incubation at 37 °C for 6 h at MOI 10. (A) Incubation of A549 cells with *S. aureus* USA300 wild type: 94% of the cells were necrotic (Q2+Q3), 5.92% were healthy (Q4). (B) Incubation of A549 cells with *S. aureus* USA300 Δhla : 9.51% of the cells were necrotic (Q2+Q3), 89.4% were healthy (Q4) and comparable to medium-treated cells (C) wherein 5.11% were necrotic (Q2+Q3) and 94.4% were healthy (Q4). (D) Annexin V (apoptosis) labelled cells from three experiments are shown (mean values \pm SD). Statistical significance was determined by unpaired, two tailed *t*-test (**** $P < 0.0001$, *** $P < 0.001$, ** $P < 0.01$, * $P < 0.05$). (E) Proteins in the culture medium were separated by 10% SDS-PAGE and transferred to a PVDF membrane. Hla was detected (blue box) by incubation with mouse anti-Hla mAb 8B7, followed by anti-mouse IgG-HRP. (F) LDH release in culture medium after co-culture of PMA-differentiated THP1 cells with *S. aureus* USA300 for 6 h at MOI of 10 in the presence of H831 or H052. Bars represent mean values \pm SD of one representative experiment done in triplicate. Statistical significance was determined by unpaired, two tailed *t*-test compared to inhibitor-free 0 μ M control (**** $P < 0.0001$, *** $P < 0.001$, ** $P < 0.01$, * $P < 0.05$). (G) Proteins in the culture medium were separated by 10% SDS-PAGE and transferred to a PVDF membrane. Hla was detected (blue box) by subjecting the blot to mouse anti-Hla mAb 8B7 followed by anti-mouse IgG-HRP.

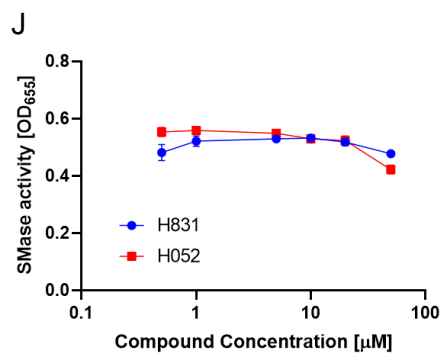
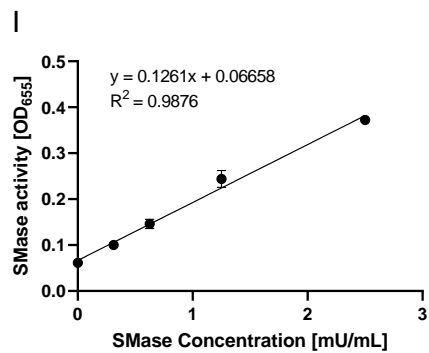
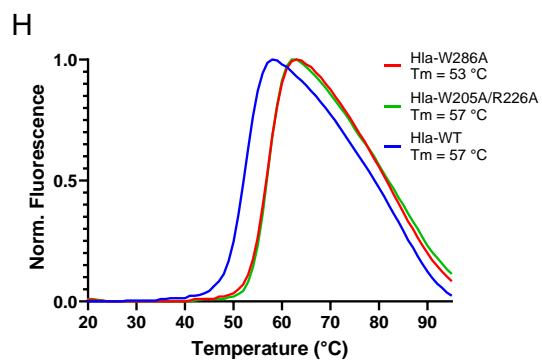
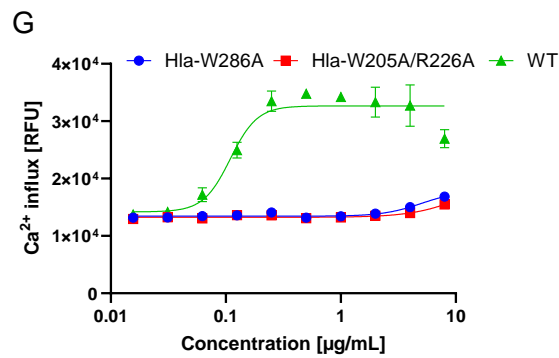
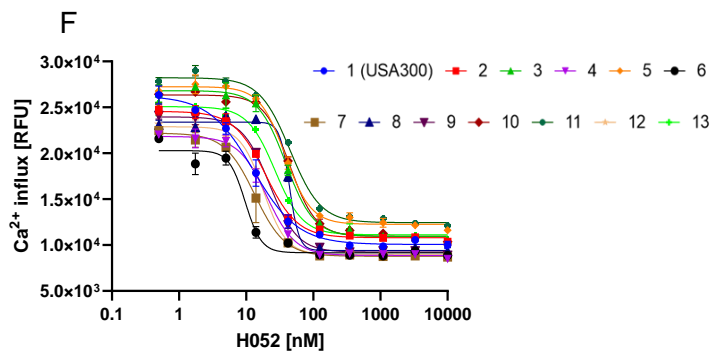
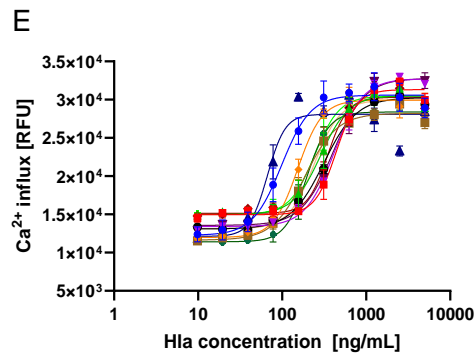
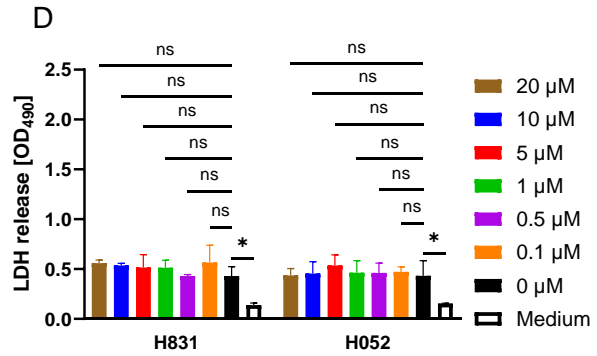
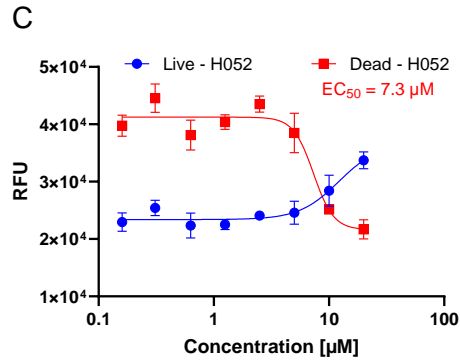
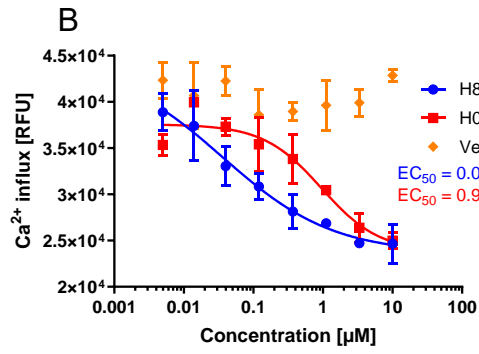
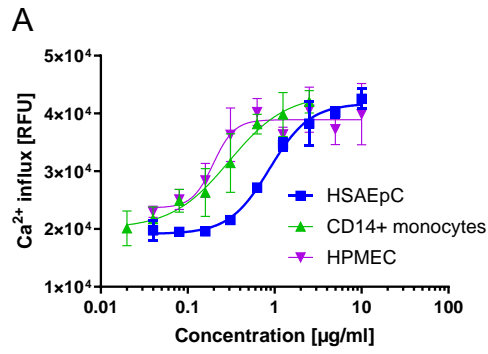


Figure S3. QDS prevent Hla-dependent Ca^{2+} influx, cytotoxicity and do not interfere with sphingomyelinase activity, related to Figure 3-5. (A) Hla-induced Ca^{2+} influx in primary human small airway epithelial cells, human CD14⁺ monocytes and primary human pulmonary microvascular endothelial cells. Data points represent at least three experiments (mean values \pm SD). (B) Ca^{2+} influx in HSAEpC. Cells were treated with 2 $\mu\text{g}/\text{ml}$ Hla in the presence of increasing amounts of H052 or H831. Data points represent two independent experiments (mean values \pm SD). (C) Cytotoxicity assay with HSAEpC. Cells were treated with 2 $\mu\text{g}/\text{ml}$ Hla and grown in the presence of increasing amounts of H052 and for 20 h. After treating with multi-tox fluor buffer for 30 min, live cell fluorescence (505 nm) and dead cell fluorescence (520 nm) was measured. Data points represent three independent experiments (mean values \pm SD). (D) QDS do not prevent LDH release from *S. aureus* USA300 Δhla co-cultured with A549 cells. LDH release in culture medium after co-culture of A549 cells with *S. aureus* USA300 Δhla for 6 h at MOI of 10 in the presence of H831 or H052. Bars represent mean values \pm SD of two independent experiments. Statistical significance was determined by two-way ANOVA compared to inhibitor-free 0 μM control (* $P < 0.05$, ns $P > 0.05$). (E) Concentration-response curves of Hla-subtypes on Ca^{2+} influx in U937 cells. Data points indicate three experiments (mean values \pm SD). EC_{50} values of Hla-subtypes are shown in table S2. (F) Activity of H052 on Ca^{2+} influx in U937 cells induced by 13 Hla-subtypes at 1 $\mu\text{g}/\text{ml}$. Data points indicate two experiments (mean values \pm SD). (G) Activity of site-specific amino acid variants of Hla on Ca^{2+} influx in U937. Related to Figure 5. Site-specific amino acid variants were constructed to validate the identified binding site (W286A). Data points indicate three experiments (mean values \pm SD). (H) The stability of Hla variants was validated by determining their melting temperatures in a thermal shift assay. (I)-(J) Effect of QDS on sphingomyelinase activity. Related to Figure 4. (I) Standard curve of sphingomyelinase activity. (J) H831 or H052 were incubated with sphingomyelin for 30 min, followed by addition of 2 mU/ml of sphingomyelinase. Each data point represents mean values, \pm SD of three replicates. Bars represent mean values \pm SD of one representative experiment done in triplicate.

The chemical structure of H831 is shown at the top. It is a pyrimidine-2,4-dione derivative with a 4-(trifluoromethyl)phenyl group attached to the 6-position. The structure is labeled H831.

Below the structure are three ^1H NMR spectra stacked vertically, sharing a common x-axis representing the chemical shift in ppm, ranging from 7.9 to 6.2.

- The top spectrum (red) is labeled "Ref: STD (831 w/o Hla)". It shows a noisy baseline with no significant peaks.
- The middle spectrum (blue) is labeled "sample: STD (831 + Hla)". It shows several sharp peaks in the aromatic region, specifically around 7.6, 6.9, 6.8, and 6.7 ppm.
- The bottom spectrum (green) is labeled " ^1H (p3919) 831". It shows a similar pattern of peaks to the blue spectrum, with major peaks around 7.6, 6.9, 6.8, and 6.7 ppm.

D

STD intensities [%]

saturation time [s]

H831

Saturation time [s]	H1 (grey)	H2 (blue)	H3 (green)	H4 (pink)	H5 (orange)
0.5	39	32	32	25	45
1.0	60	53	45	42	68
1.5	78	67	59	49	78
2.0	88	75	65	55	83
2.5	93	82	68	57	88
3.0	98	85	71	60	89
3.5	93	82	68	57	89
4.0	100	88	69	59	89

A bar chart showing the Chemical Shift Perturbation (CSP) in ppm for residues 30 to 310. The y-axis is labeled 'CSP (ppm)' and ranges from 0 to 0.04. The x-axis is labeled 'Residues' and ranges from 30 to 310. A red horizontal line indicates a threshold at 0.013 ppm, labeled '> 0.013'. The bars are blue, and the chart shows several peaks, with the highest peak around residue 225 reaching approximately 0.04 ppm.

Amount of modified peptides (%)

Eq 15 Eq 16

Y54 Y66 W106 W205 W213 W286

Figure 2 is a scatter plot showing the amount of modified peptides (%) for various peptides. The y-axis represents the percentage of modified peptides, ranging from 0 to 50. The x-axis lists 15 different peptides, each with a unique identifier (e.g., Y54, K63, V64, Y66, Y94, W106, Y174, W205, W213, Y217, W286). The data points are colored circles representing different peptides. Y54 shows the highest modification levels, peaking at ~30% for the first instance and ~40% for the second. W106 and Y174 show moderate modification levels around 10-15%. Most other peptides show very low modification levels below 5%.

Figure S4. QDS inhibitors interact directly with Hla, related to Figure 5. (A) STD –NMR experiments with H831 and (B) H052 demonstrate that ligand signals (aromatic section is shown) are affected by saturation transfer from Hla. (C) Comparison of STD –NMR results of different active (in vitro) ligands (H831, H052, **S3**) and inactive (in vitro) ligand **17**. (D) Dependence of STD strength on saturation time. Individual curves of the STD strength correspond to individual protons, whose positions are indicated by color. Curves are normalized to the most affected signal set, which is related to the protons with the closest contact to the protein.^{S1} (E)-(F) ¹⁹F–NMR experiments with H052 (E) and H831 (F) demonstrate that increasing concentration of Hla induces line-broadening effects and chemical shift changes (on the left in E and F). Comparison with non-functional, but structurally similar OCF₃- or F-carrying sulfonamides do not cause line broadening (on the right in E and F). (G) Chemical shift perturbations (CSPs) between H-N TROSY of ¹⁵N-labeled Hla before and after addition of 0.6 equivalent of H831, reported along Hla sequence. CSPs higher than 0.013 are indicated in red. (H)-(I) Degree of amino acid modifications after incubation with photoprobes. (H) Modification after 1 h incubation with one equivalent of the photoprobes 15 and 16 and irradiation for 15 and 45 min. Data for all irradiation times are plotted. (I) Degree of peptide modifications after 1 h incubation with 10 and 50 equivalents of the photoprobes 15 and 16 and irradiation for 15 min.

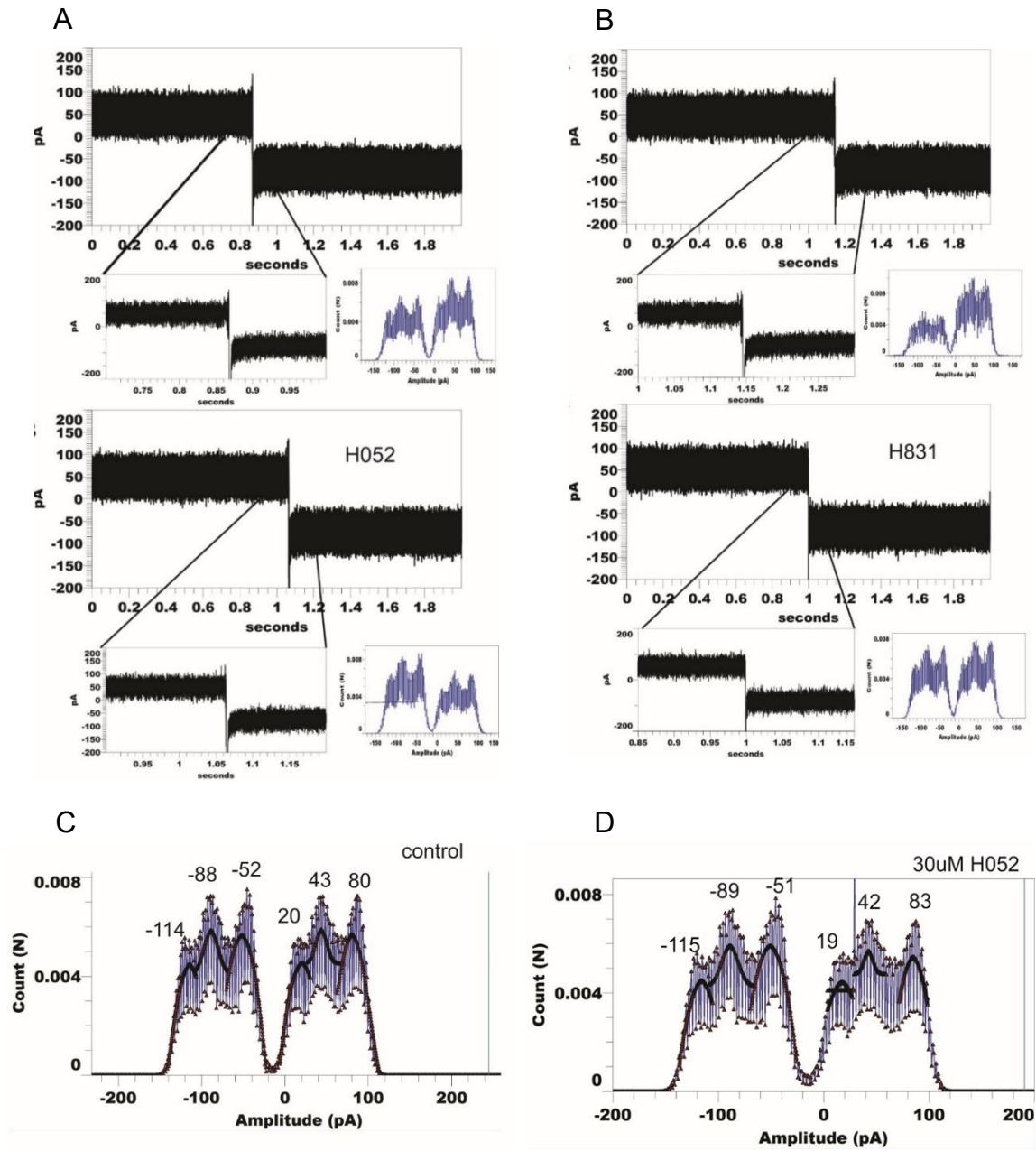


Figure S5. Effect of QDS on the activity of pre-formed pores, related to Figure 4. (A)-(B) Selected ion-trace recordings from bilayers containing a single reconstituted Hla in 200 mM NaCl. Total recording time 2 seconds, ± 100 mV voltage step, the insert shows a 0.3 second zoom-in and the full range amplitude histogram. (A) Baseline recording (top). The same channel but ten minutes after addition of 30 μ M H052 in DMSO to both cis and trans compartments (bottom). (B) Baseline recording (top). In presence of 30 μ M H831 in DMSO added to cis and trans (bottom). (C)-(D) Histogram from ion trace recordings from bilayers containing single reconstituted Hla. (C) Control and (D) 30 μ M H052 in DMSO was added to cis and trans, ± 100 mV (lower). Histogram from longer traces with a histogram fit using Gaussian, 1st order all 12 fit in both histograms were successful. No significant difference between both control and H052-treated traces was observed.

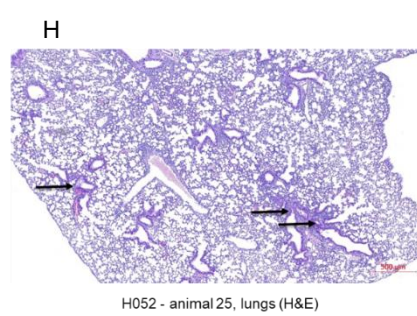
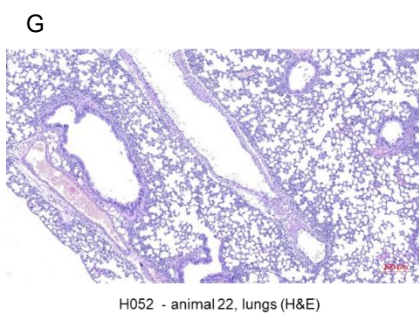
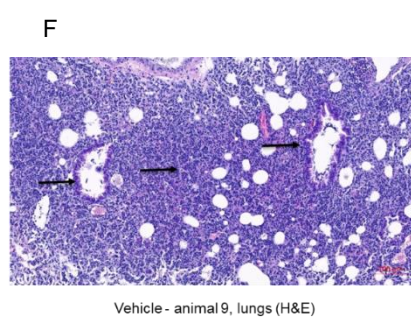
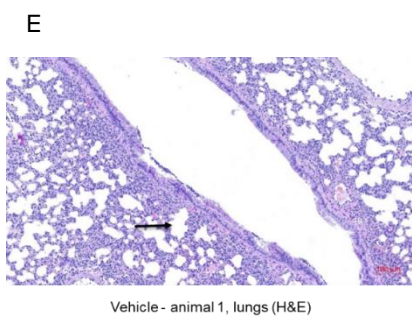
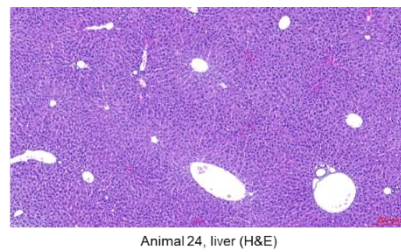
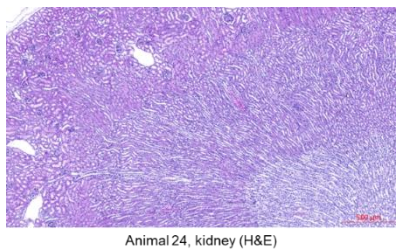
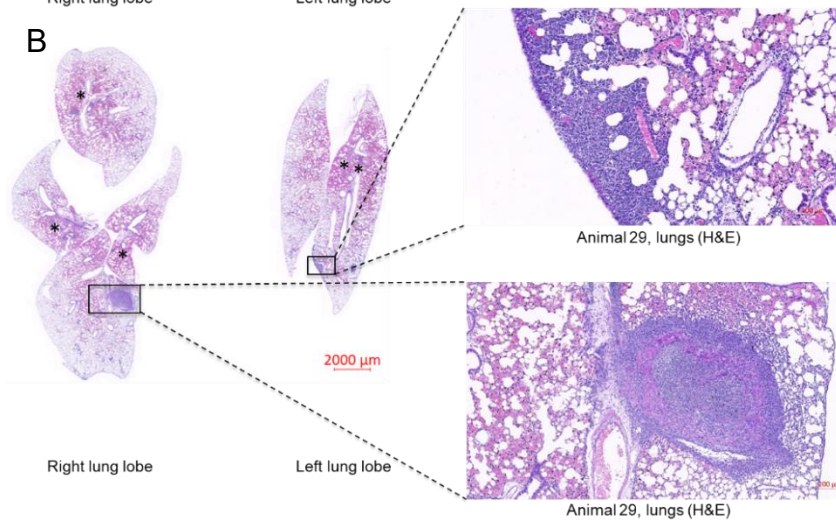
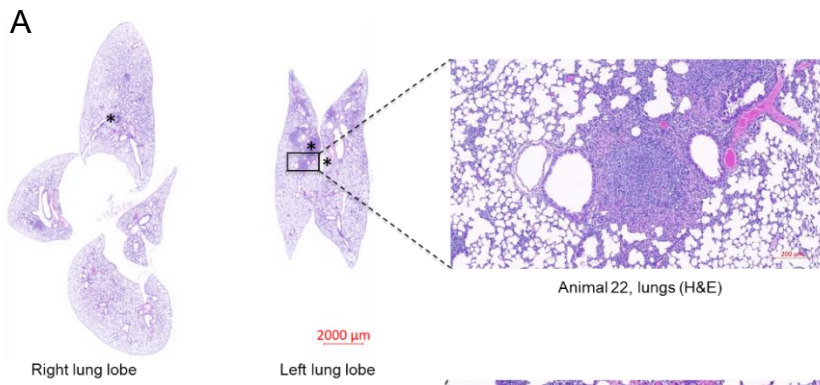


Figure S6. Histopathology analysis from the in vivo studies, related to figure 6. (A)-(B) Lung histopathology examination from two of the four mice that survived in the H052 treatment group (60 mg/kg, IP, BID). Related to Figure 6C. Animals were sacrificed on day 4 (96 h post infection). (A) H&E staining showed multi-focal peri-bronchial inflammation in both lung lobes with beginning of resolution (asterisks). One abscess in left lung lobe (0.3 x 0.2 mm). (B) H&E staining revealed multifocal peri-bronchial inflammation (asterisks) with diffuse hemorrhage in the lung interstitium (hemosiderosis). One abscess in inferior right lung lobe (1.3 x 0.8 mm). (C)-(D) Kidney and liver histopathology analysis. Related to Figure 6C. Material was obtained from animal 24 that survived in the H052 treatment group (60 mg/kg, IP, BID). The animals was sacrificed on day 4 (96 h post infection). No histopathological changes were observed by H&E staining of kidneys (C) and liver (D) tissues. (E)-(H) Lung histopathology analysis 24 h after intranasal infection with 5×10^7 CFU/mouse. (E) Animal from the vehicle-treated group. Destruction of the bronchial epithelial cell and a mixture of neutrophils, bacteria and apoptotic/necrotic debris was observed in animal 1 of the vehicle group. (F) Animal from the vehicle-treated group. Interstitial inflammation with alveolar damage and multifocal edema (arrows) was observed in animal 9 of the vehicle group. (G) Animal from the H052-treated group (60 mg/kg, IP, BID). Mild to moderate multifocal peri-bronchial inflammation was observed in animal 22 of the H052 treatment group. (H) Animal from the H052-treated group (60 mg/kg, IP, BID). Moderate multifocal inflammation (arrows) with focal hemorrhage and edema was observed in animal 25 of the H052 treatment group.

Table S2. Characteristics of Hla subtypes investigated in this study, related to Figure 3.

#	Frequency [%] ^{a)}	Cluster type ^{b)}	Sequence type ^{c)}	CarbX Type	No. of mutations	Hla EC ₅₀ [ng/ml] ^{d)}
1 (USA300)	14.9	Cluster 1		Type B	- (Ref. seq.)	98.6
2	40.5	Cluster 11		Type A	2	439.1
3	8.2	Cluster 4		Type D	1	288.5
4	6.1	Cluster 51		Type G	6	416.3
5	3.5	Cluster 23		Type R	3	153.5
6	2.9	Cluster 43		Type I	5	312.5
7	2.0	Cluster 39		Type K	4	186.1
8 ^{e)}	1.4	Cluster 54			29	66.9
9	0.9	Cluster 42		Type H	5	405.6
10	0.6	Cluster 3	ST5		1	347.8
11	n/a		ST45		1	197.2
12	n/a			Type T	5	240.4
13 ^{f)}	n/a				1	243.1

a) Frequency based on total number of isolates (984) from 57 cluster in Tabor *et al.*^{S2} b) Taken from Tabor *et al.*^{S2} c) taken from Tavares *et al.*^{S3} d) EC₅₀ of Hla variant for induction of Ca²⁺ influx in U937 cells; e) Sequence from *Staphylococcus agalactiae*; f) Sequence is an intermediate (K314N) from construct generation and was additionally included in the analysis.

1 - Type B

MADSDINIKTGTTDIGSNTTVKTGDLVTYDKENGMHKKVFYSFIDDKNHNNKLLVIRTKGTIAGQYRVY
SEEGANKSGLAWPSAFKVQLQLPDNEVAQISDYYPRNSIDTKEYMSTLTGFGNGNVTGDDTGKIGGLI
GANVSIGHTLKYVQPDFKTIESTDCKVGVKVFNNMVNQNWGPYDRDSWNPVYGNQLFMKTRNG
SMKAADNFLDPNKASSLLSSGFSPDFATVITMDRKASKQQTNIIDVIYERVRDDYQLHWTSTNWKGTN
TKDKWIDRSSERYKIDWEKEEMTN

#2

MADSDINIKTGTTDIGSNTTVKTGDLVTYDKENGMHKKVFYSFIDDKNHNNKLLVIRTKGTIAGQYRVY
SEEGANKSGLAWPSAFKVQLQLPDNEVAQISDYYPRNSIDTKEYMSTLTGFGNGNVTGDDTGKIGGLI
GANVSIGHTLKYVQPDFKTIESTDCKVGVKVFNNMVNQNWGPYDRDSWNPVYGNQLFMKTRNG
SMKAAENFLDPNKASSLLSSGFSPDFATVITMDRKASKQQTNIIDVIYERVRDDYQLHWTSTNWKGTN
TKDKWIDRSSERYKIDWEKEEMTN

#3

MADSDINIKTGTTDIGSNTTVKTGDLVTYDKENGMHKKVFYSFIDDKNHNNKLLVIRTKGTIAGQYRVY
SEEGANKSGLAWPSAFKVQLQLPDNEVAQISDYYPRNSIDTKEYMSTLTGFGNGNVTGDDTGKIGGLI
GANVSIGHTLKYVQPDFKTIESTDCKVGVKVFNNMVNQNWGPYDRDSWNPVYGNQLFMKTRNG
SMKAADNFLDPNKASSLLSSGFSPDFATVITMDRKASKQQTNIIDVIYERVRDDYQLHWTSTNWKGTN
TKDKWIDRSSERYKIDWEKEEMTN

#4

MADSDINIKTGTTDIGSNTIVKTGDLVTYDKENGMHKKVFYSFIDDKNHNNKLLVIRTKGTIAGQYRVY
EEGANKSGLAWPSAFKVQLQLPDNEVAQISDYYPRNSIDTKEYMSTLTGFGNGNVTGDDSGKIGGLI
ANVSIGHTLKYVQPDFKTIESTDCKVGVKVFNNMVNQNWGPYDRDSWNPVYGNQLFMKTRNGS
MKAADNFLDPNKASSLLSSGFSPDFATVITMDRKATKQQSNIDVIYERVRDDYQLHWTSTNWKGTNT
KDKWIDRSSERYKIDWEKEEMTN

#5

MADSDINIKTGTTDIGSNTTVKTGDLVTYDKENGMHKKVFYSFIDDKNHNNKLLVIRTKGTIAGQYRVY
SEEGANKSGLAWPSAFKVQLQLPDNEVAQISDYYPRNSIDTKEYMSTLTGFGNGNVTGDDTGKIGGLI
GANVSIGHTLKYVQPDFKTIESTDCKVGVKVFNNMVNQNWGPYDRDSWNPVYGNQLFMKTRNG

SMKAAENFLDPNKASSLLSSGFSPDFATVITMDRKASKQQTNIDVIYERVRDDYQLHWTSTNWKGTN
TKDKWTDROSSERYKIDWENEEMTN

#6

MADSDINIKTGTTDIGSNTTVKTGDLVTYDKENGMHKKVFYSFIDDKNHNKKILVIRTKGTIAGQYRVYS
EEGANKSGLAWPSAFKVQLQLPDNEVAQISDYYPNSIDTKEYMSTLTYGFGNVTGDDSGKIGGLIG
ANVSIGHTLKYYVQPDFKTILESPTDKKVGWKVIFNNMVNQNWGPYDRDSWNPVYGNQLFMKTRNGS
MKAADNFLDPNKASSLLSSGFSPDFATVITMDRKATKQQTNIDVIYERVRDDYQLHWTSTNWKGTNT
KDKWTDRCSEYKIDWEKEEMTN

#7

MADSDINIKTGTTDIGSNTTVKTGDLVTYDKENGMHKKVFYSFIDDKNHNKKILVIRTKGTIAGQYRVYS
EEGANKSGLAWPSAFKVQLQLPDNEVAQISDYYPNSIDTKEYMSTLTYGFGNVTGDDSGKIGGLIG
ANVSIGHTLKYYVQPDFKTILESPTDKKVGWKVIFNNMVNQNWGPYDRDSWNPVYGNQLFMKTRNGS
MKAADNFLDPNKASSLLSSGFSPDFATVITMDRKATKQQTNIDVIYERVRDDYQLHWTSTNWKGTNT
KDKWTDROSSERYKIDWEKEEMTN

#8

MADSDINIKPGTTDIGSNTTIKTGDLVTYDKVNGMHKKIFYSFIDDKNHNKKLLVIRTKGTIAGQYRVYSE
EGSNKSGLAWPSAFKVHLEIPDNEAAQISDYYPNSIDTKEYMSTLNYGFNGSISADDTGKIGGGIGGT
VSIGHTLKYYVQPDFKTILESPTDKKVGWKVIFNNMMNQNWGPYDRDSWNPYGNQLFMKTRNGSMK
ASENFLDPNKASSLLSSGFSPDFATVLVMDRKAQNQQTNIDIVYERVRDDYQLHWTSTNWKGTNTKD
KWTDROSSERYKIDWKKEEMTN

#9

MADSDINIKTGTTDIGSNTTVKTGDLVTYDKENGMHKKVFYSFIDDKNHNKKILVIRTKGTIAGQYRVYS
EEGANKSGLAWPSAFKVQLQLPDNEVAQISDYYPNSIDTKEYMSTLTYGFGNVTGDDSGKIGGLIG
ANVSIGHTLKYYVQPDFKTILESPTDKKVGWKVIFNNMVNQNWGPYDRDSWNPVYGNQLFMKTRNGS
MKAAENFLDPNKASSLLSSGFSPDFATVITMDRKATKQQTNIDVIYERVRDDYQLHWTSTNWKGTNT
KDKWTDROSSERYKIDWEKEEMTN

#10

MADSDINIKTGTTDIGSNTTVKTGDLVTYDKENGMHKKVFYSFIDDKNHNKKLLVIRTKGTIAGQYRVY
SEEGANKSGLAWPSAFKVQLQLPDNEVAQISDYYPNSIDTKEYMSTLTYGFGNVTGDDTGKIGGLI
GANVSIGHTLKYYVQPDFKTILESPTDKKVGWKVIFNNMVNQNWGPYDRDSWNPVYGNQLFMKTRNG
SMKAAENFLDPNKASSLLSSGFSPDFATVITMDRKASKQQTNIDVIYERVRDDYQLHWTSTNWKGTN
TKDKWIDROSSERYKIDWEKEEMTN

#11

MADSDINIKTGTTDIGSNTTVKTGDLVTYDKENGMHKKVFYSFIDDKNHNKKLLVIRTKGTIAGQYRVY
SEEGANKSGLAWPSAFKVQLQLPDNEVAQISDYYPNSIDTKEYMSTLTYGFGNVTGDDTGKIGGLI
GANVSIGHTLKYYVQPDFKTILESPTDKKVGWKVIFNNMVNQNWGPYDRDSWNPVYGNQLFMKTRNG
SMKAADNFLDPNKASSLLSSGFSPDFATVITMDRKATKQQTNIDVIYERVRDDYQLHWTSTNWKGTN
TKDKWIDROSSERYKIDWEKEEMTN

#12

MADSDINIKTGTTDIGSNTIVKTGDLVTYDKENGMHKKVFYSFIDDKNHNKKILVIRTKGTIAGQYRVYS
EEGANKSGLAWPSAFKVQLQLPDNEVAQISDYYPNSIDTKEYMSTLTYGFGNVTGDDSGKIGGLIG
ANVSIGHTLKYYVQPDFKTILESPTDKKVGWKVIFNNMVNQNWGPYDRDSWNPVYGNQLFMKTRNGS
MKAADNFLDPNKASSLLSSGFSPDFATVITMDRKATKQQTNIDVIYERVRDDYQLHWTSTNWKGTNT
KDKWTDROSSERYKIDWEKEEMTN

#13

MADSDINIKTGTTDIGSNTTVKTGDLVTYDKENGMHKKVFYSFIDDKNHNKKLLVIRTKGTIAGQYRVY
SEEGANKSGLAWPSAFKVQLQLPDNEVAQISDYYPNSIDTKEYMSTLTYGFGNVTGDDTGKIGGLI
GANVSIGHTLKYYVQPDFKTILESPTDKKVGWKVIFNNMVNQNWGPYDRDSWNPVYGNQLFMKTRNG
SMKAADNFLDPNKASSLLSSGFSPDFATVITMDRKASKQQTNIDVIYERVRDDYQLHWTSTNWKGTN
TKDKWIDROSSERYKIDWENEEMTN

Table S3. Bioactivity, physicochemical, ADME, permeability and pharmacokinetic (PK) data of QDS, related to Figure 3 and Figure 6.

Bioactivity	H052	H831
Ca ²⁺ Influx assay [U937 cells] EC ₅₀ (μM)	0.01	0.04
LDH assay [A549 cells] IC ₅₀ (μM)	0.002	0.04
Hemolysis [rabbit erythrocytes] IC ₅₀ (μM)	0.79	0.33
Ca ²⁺ -influx [human monocytes] (μM)	0.09	0.03
Ca ²⁺ -influx [human NK cells] (μM)	0.4	0.5
Ca ²⁺ -influx [lung endothelial cells] (μM)	0.83	0.11
Impedance of endothelial cell layer (μM)	0.98	0.20
Selectivity index [hPBMC/Ca ²⁺ Influx] IC ₅₀	>3000	>810
Selectivity index [CTG-U937/Ca ²⁺ Influx] IC ₅₀	>1000	>270
Selectivity index [hERG Binding/Ca ²⁺ Influx] IC ₅₀	>1200	>115
Selectivity index [HepToxH / Ca ²⁺ Influx] IC ₅₀	>3000	>810
Physiochemical, ADME and PK data	H052	H831
Kinetic Solubility pH 7.4 (μM)	202	337
pKa	7.21	Not determined
HLM CL _{int} (μl/min/mg)	2	0.1
MLM CL _{int} (μl/min/mg)	~0	~0
Plasma Stability Human (%Remaining)	97.6	86
Plasma Stability Mouse (%Remaining)	89.5	100
PPB Human (%Bound)	99.7	99.6
PPB Mouse (%Bound)	95.6	94.8
t _{1/2} (h)	1.67	1.25
C _{max} (ng/ml)	1283	1204
AUC 0-inf_obs (h*ng/ml)	2060	1586
Cl _{obs} (ml/min/kg)	8.2	10.5
V _{z_obs} (l/kg)	1.2	1.1
NMDA antagonist radioligand @ 10 μM	54.5%	41.8%
NMDAR (1A/2B) agonist in functional assay	EC ₅₀ > 10 μM	Not determined
NMDAR (1A/2B) antagonist in functional assay	EC ₅₀ > 10 μM (44% @ 10 μM)	Not determined
Permeability in CaCo-2 cells across artificial membranes	H052	H831
Caco-2 pH 6.5/7.4 P _{app} A->B (10 ⁻⁶ cm/s)	0.12	0.39
Caco-2 pH 6.5/7.4 P _{app} B->A (10 ⁻⁶ cm/s)	6.62	11.2
Caco-2 pH 6.5/7.4 Ratio B->A : A->B	57.5	28.9
PAMPA pH 7.4 (% Flux)	2.6	≈ 0

PK parameters after 1 mg/kg iv*	H052	H831
t _{1/2} [h]	1.67	1.25
C ₀ [ng/ml]	1448	1386
AUC _{0-t} [ng/ml *h]	2001	1570
V _z [l/kg]	1.17	1.14
Cl [ml/kg/ min]	8.2	10.5

Compound levels in µM after 60 mg/kg**	H052	H831
Lung tissue SC (CD)	0.45	0.08
Lung tissue IP	0.54	0.08
BALF SC (CD)	0.32	0.09
BALF IP	0.85	0.11
Plasma SC (CD)	17.6	1.43
Plasma IP	35.5	1.37

* The formulations were: 20% DMSO, 50% PEG400, 30% 10x PBS; with cyclodextrin (CD): 10% DMSO, 20% PEG400, 20% HP-β-CD in water, 50% water.

+ Determined 8 h post administration

Table S4: Study group, treatment, dosage regime and clinical score in different in vivo infection models, related to Figure 6.

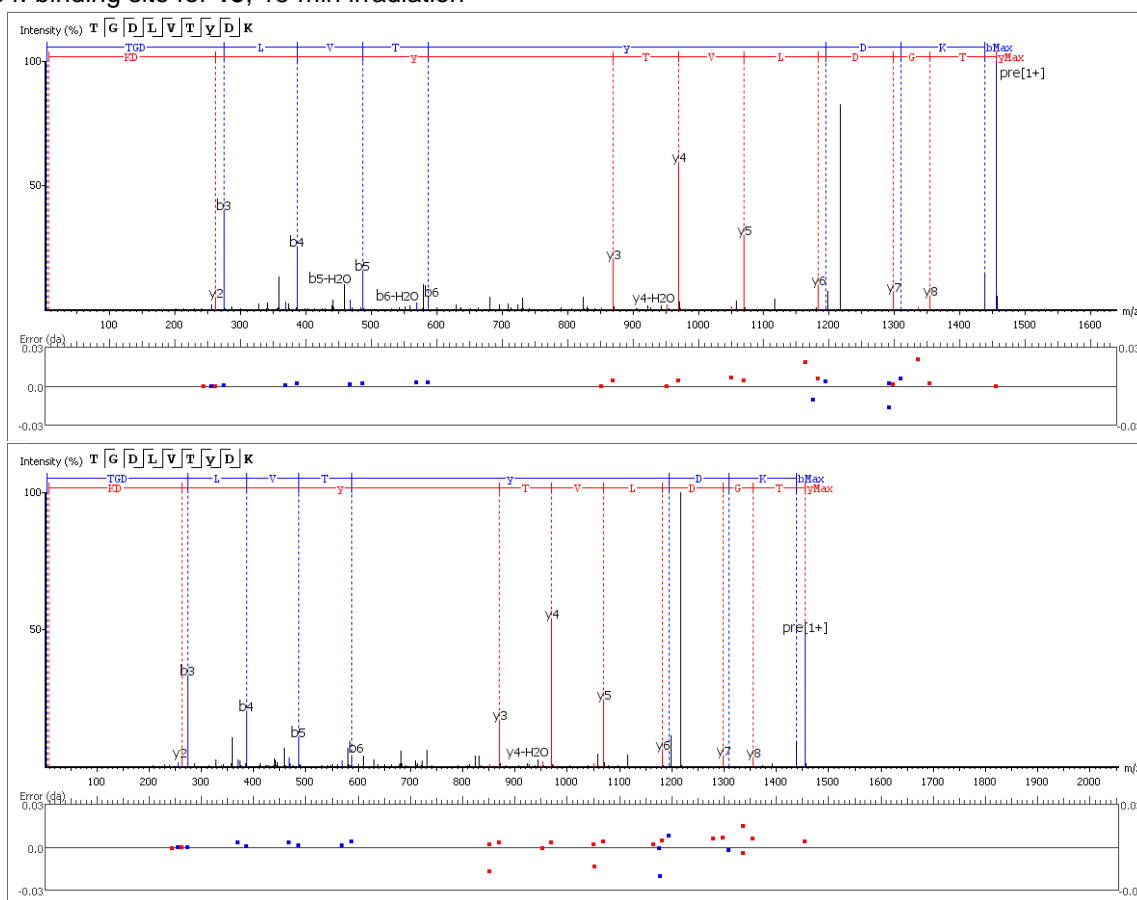
Pneumonia survival model					
Group	Treatment	N/group	Dose regime	Infection d0	Read-outs (d0 - d4)
1	Vehicle	10	N/A	5x10 ⁸ CFU/mouse; IN; 50 µL/mouse	- Survival, body weight, and clinical score d0-d4 - Terminal bleeding for plasma - Terminal sampling of lungs, kidneys and liver for potential histopathological analyses
3	H052		60 mg/kg BW, IP BID 10-12h between doses, d-1 – d4 p.i.		
Lung infection model for bacterial load and IL-6					
Group	Treatment	N/group	Dose regime	Infection d0	Read-outs
1	Vehicle (20% DMSO / 50% PEG400 / 30% 10x PBS)	5	N/A	5x10 ⁸ CFU/mouse in 20 µL PBS; IN	CFU loads 24h p.i., body weight and clinical score
2	H052		60 mg/kg BW IP BID (10-12h between doses) d-1 – d1 p.i.		
Pneumonia survival model for prophylactic and therapeutic monotherapy					
Group	Treatment	N/group	Dose regime	Infection d0	Read-outs
1	Vehicle (20% DMSO / 50% PEG400 / 30% 10x PBS)	10	5 ml/kg IP Start +1h, and then BID d4 p.i.	4x10 ⁸ CFU/mouse in 50 µL; IN on d0	Survival, body weight and clinical scores monitoring up to d5 p.i.
2	Linezolid (0.5% MC)		2.5 mg/kg SC Start +1h, and then 12h, 24h and 36h p.i.		
3	H052		60 mg/kg IP Start +1h and then BID to d4 p.i.		
4	Linezolid + H052		2.5 mg/kg SC Start +1h, and then 12h, 24h and 36h p.i. + 60 mg/kg IP Start +1h and then BID to d4 p.i.		

5	H052 from d-1		60 mg/kg IP d-1 – d4 p.i., BID				
6	Linezolid (model control) (0.5% MC)		100 mg/kg IP +6h and +24h p.i.				
Clinical scores in the pneumonia survival model							
Group	Treatment	Clinical score (h p.i.)					
		12	24	36	48	72	96
1	Vehicle	4 in 10/10	5 in 10/10				
2	H052	4 in 10/10	4 in 10/10	5 in 2/10; 4 in 8/10	5 in 3/8; 4 in 1/8; 1 in 4/8	5 in 1/5; 0 in 4/5	0 in 4/4
Score	Description						
0	No clinical signs						
1	Piloerection						
2	Piloerection, labored respiration						
3	Piloerection, labored respiration, hunched posture						
4	Piloerection, labored respiration, hunched posture; lethargic and/or thin/dehydration						
5	Dead						

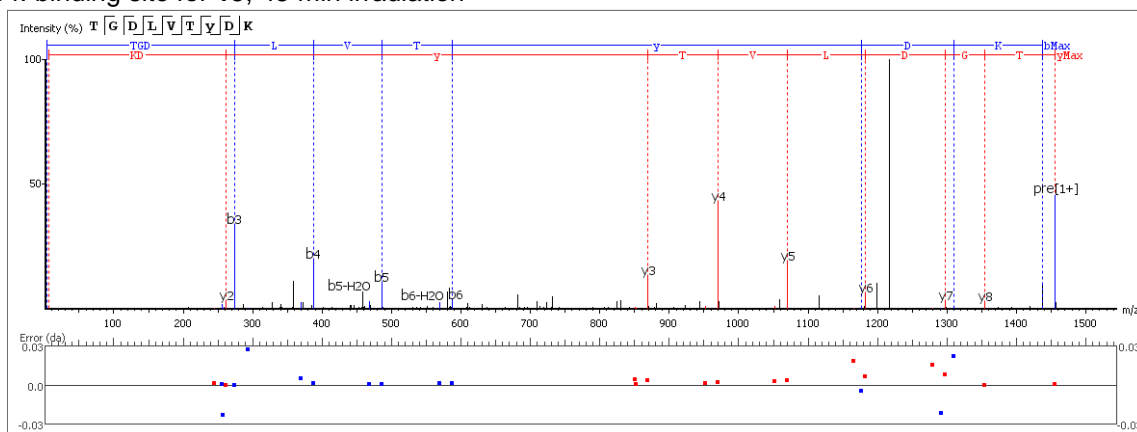
Data S1: MS/MS spectra of peptides and NMR Spectra of synthesized compounds, related to Figure 2 and Figure 5.

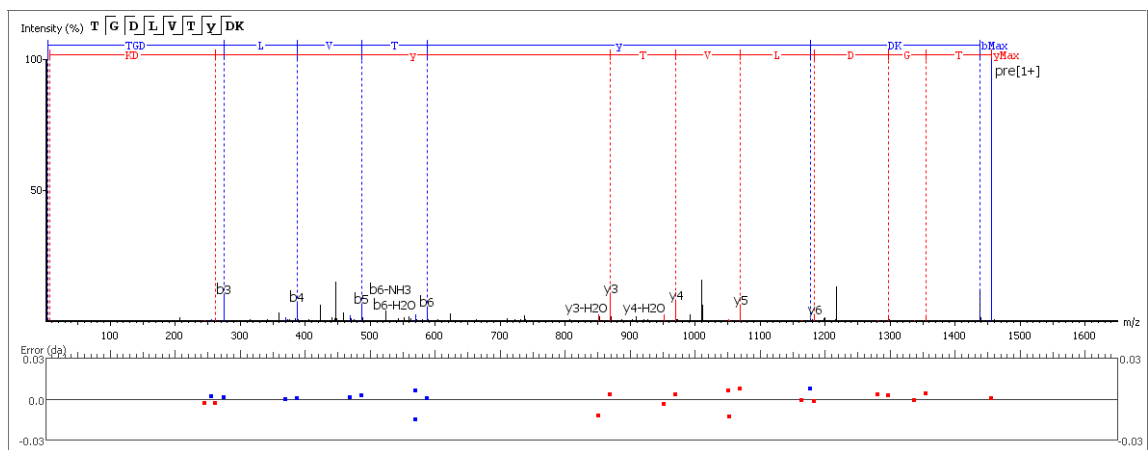
MS/MS spectra

Y54: binding site for **15**, 15 min irradiation

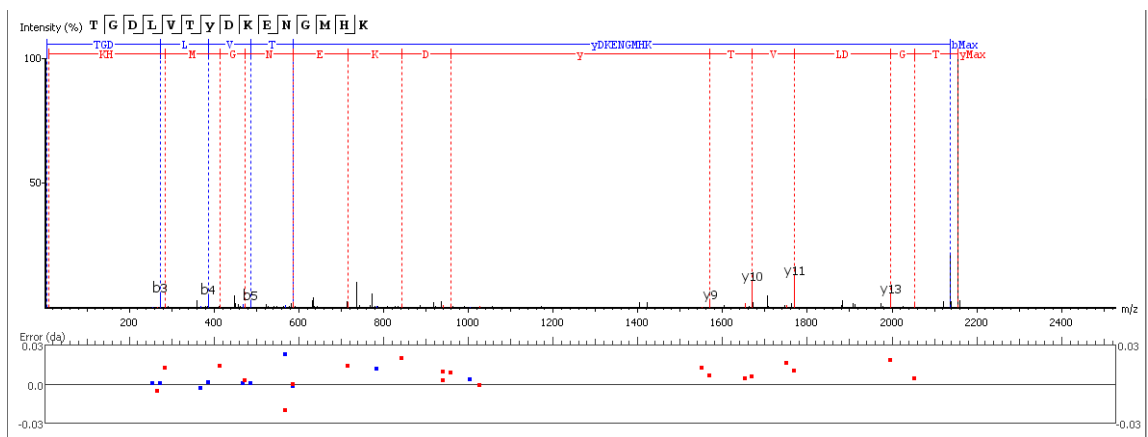
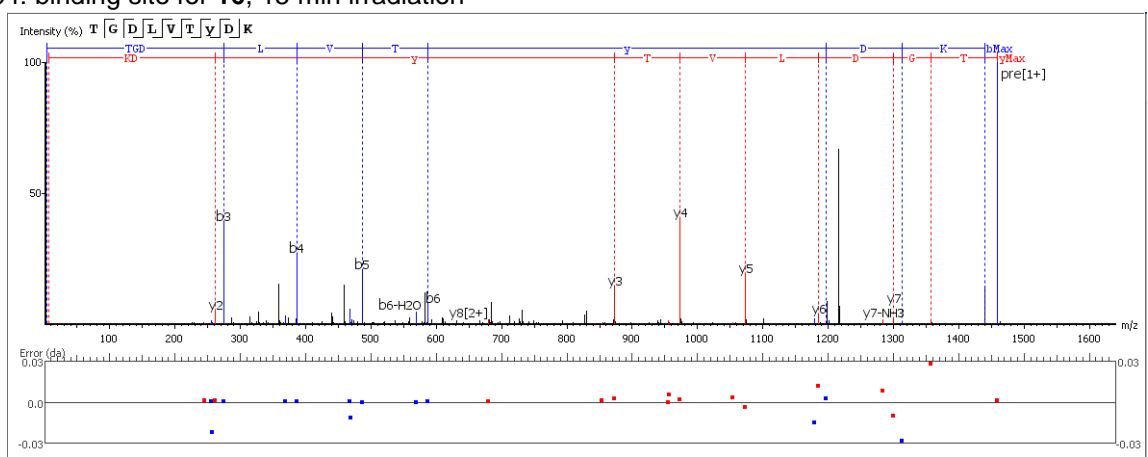


Y54: binding site for **15**, 45 min irradiation

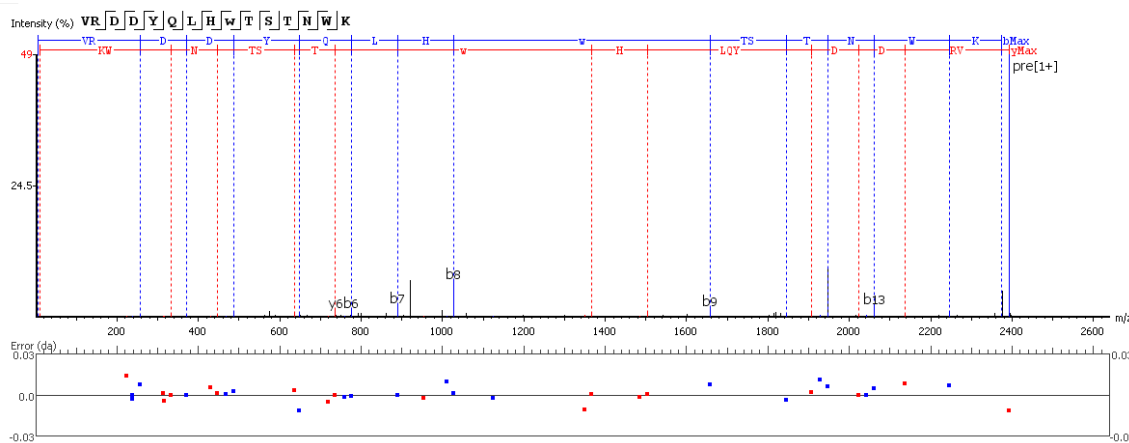
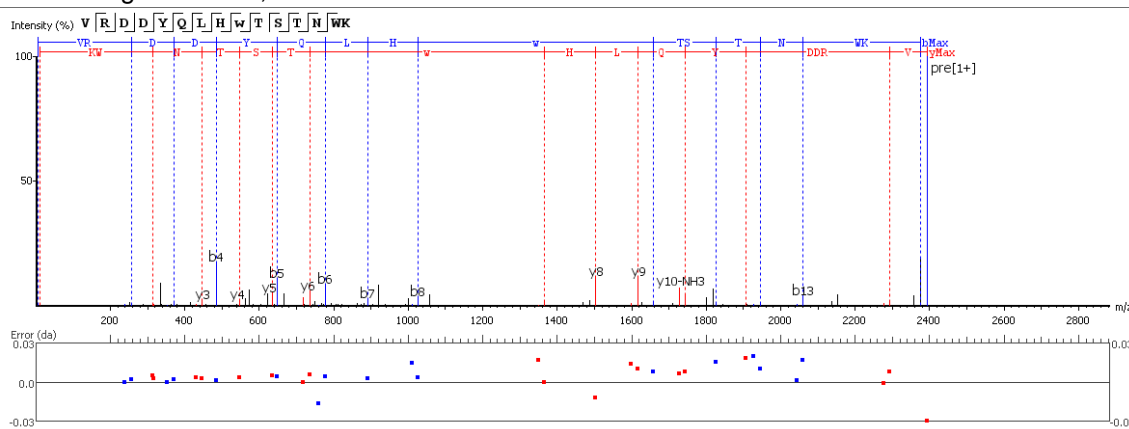




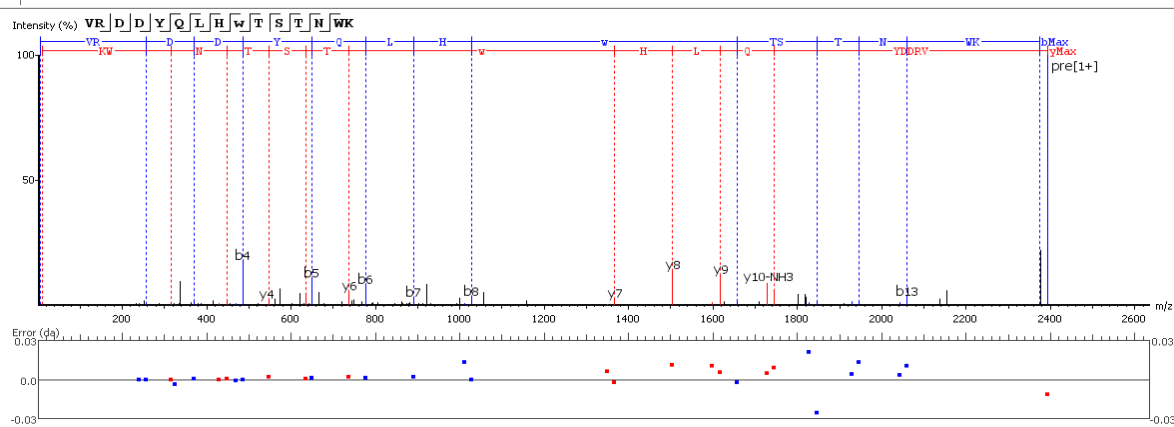
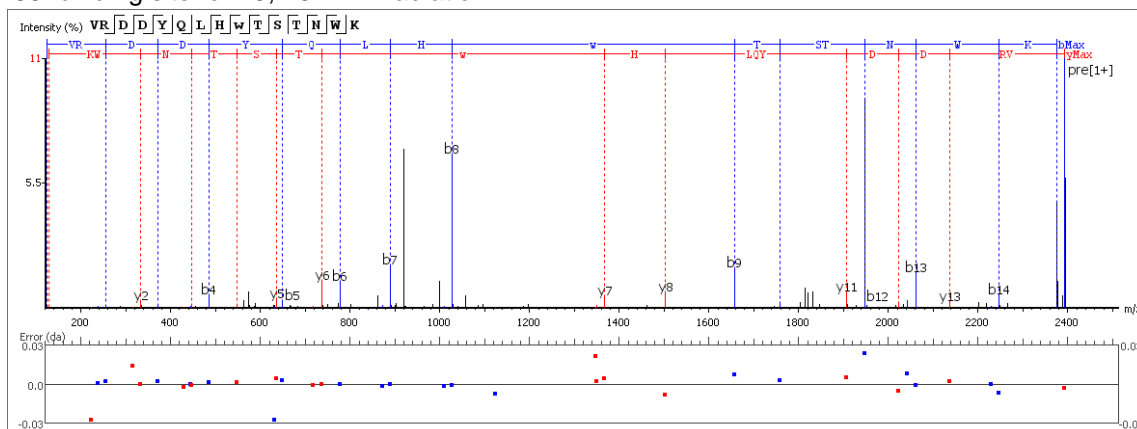
Y54: binding site for **16**, 15 min irradiation



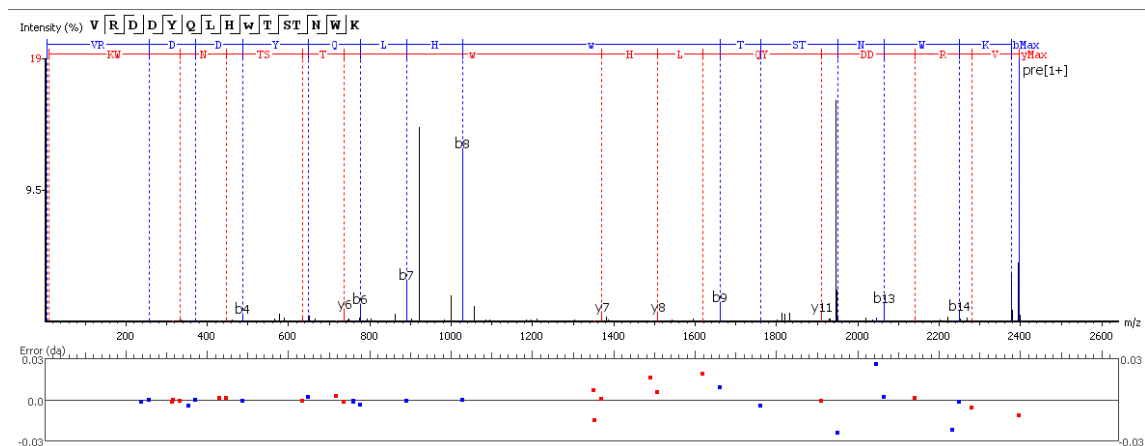
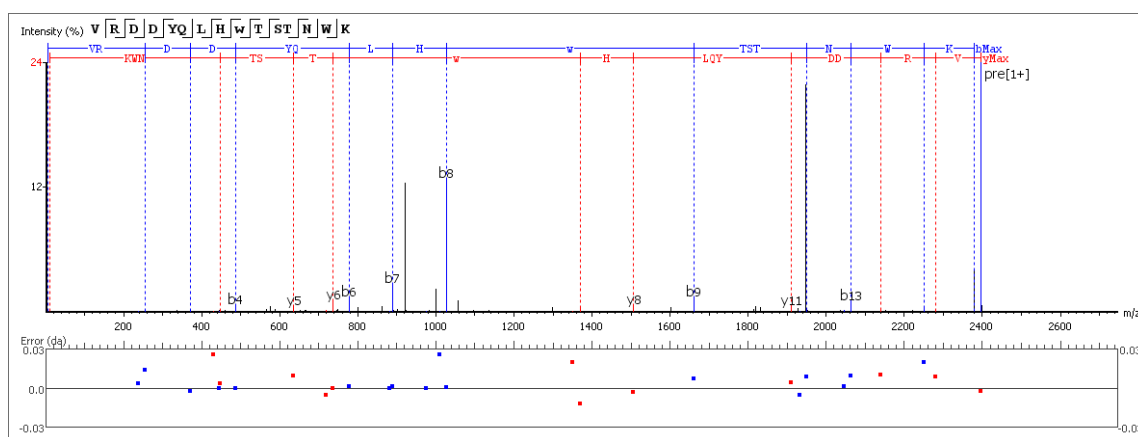
W286: binding site for 15, 15 min irradiation



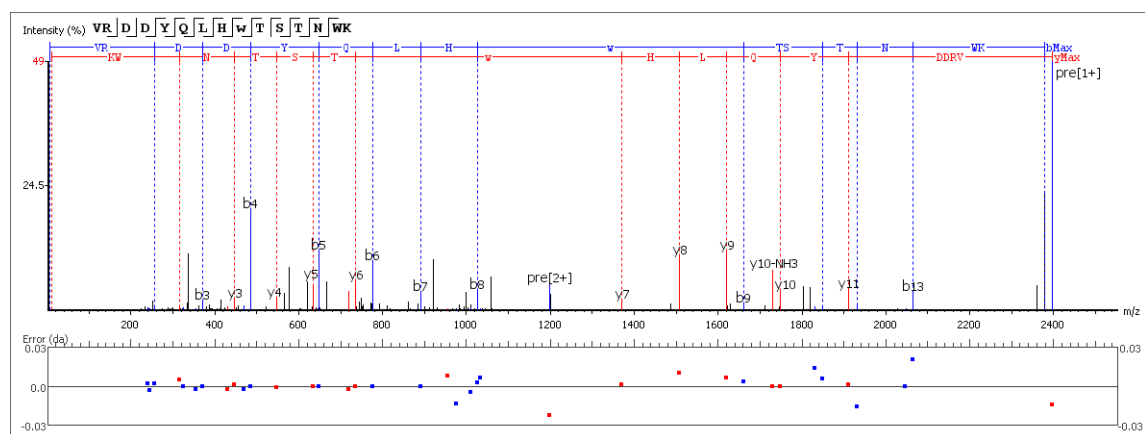
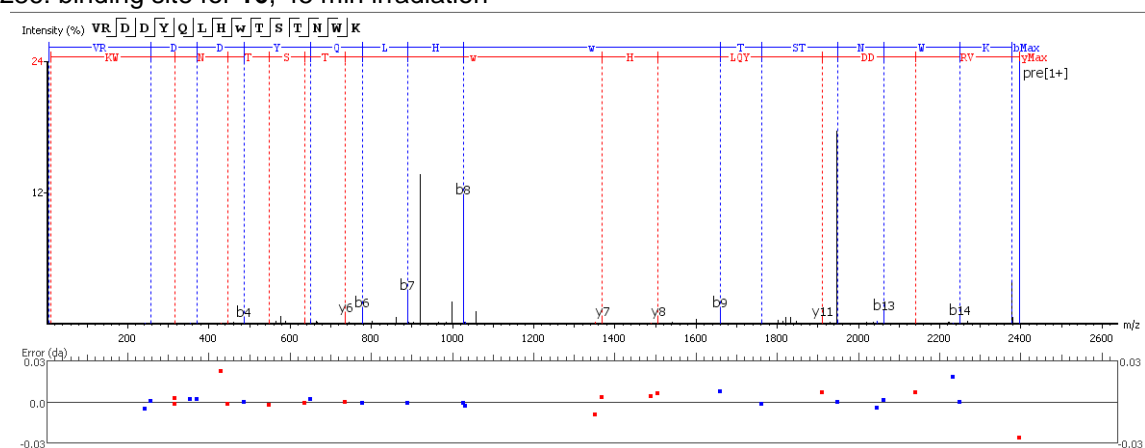
W286: binding site for 15, 45 min irradiation



W286: binding site for **16**, 15 min irradiation

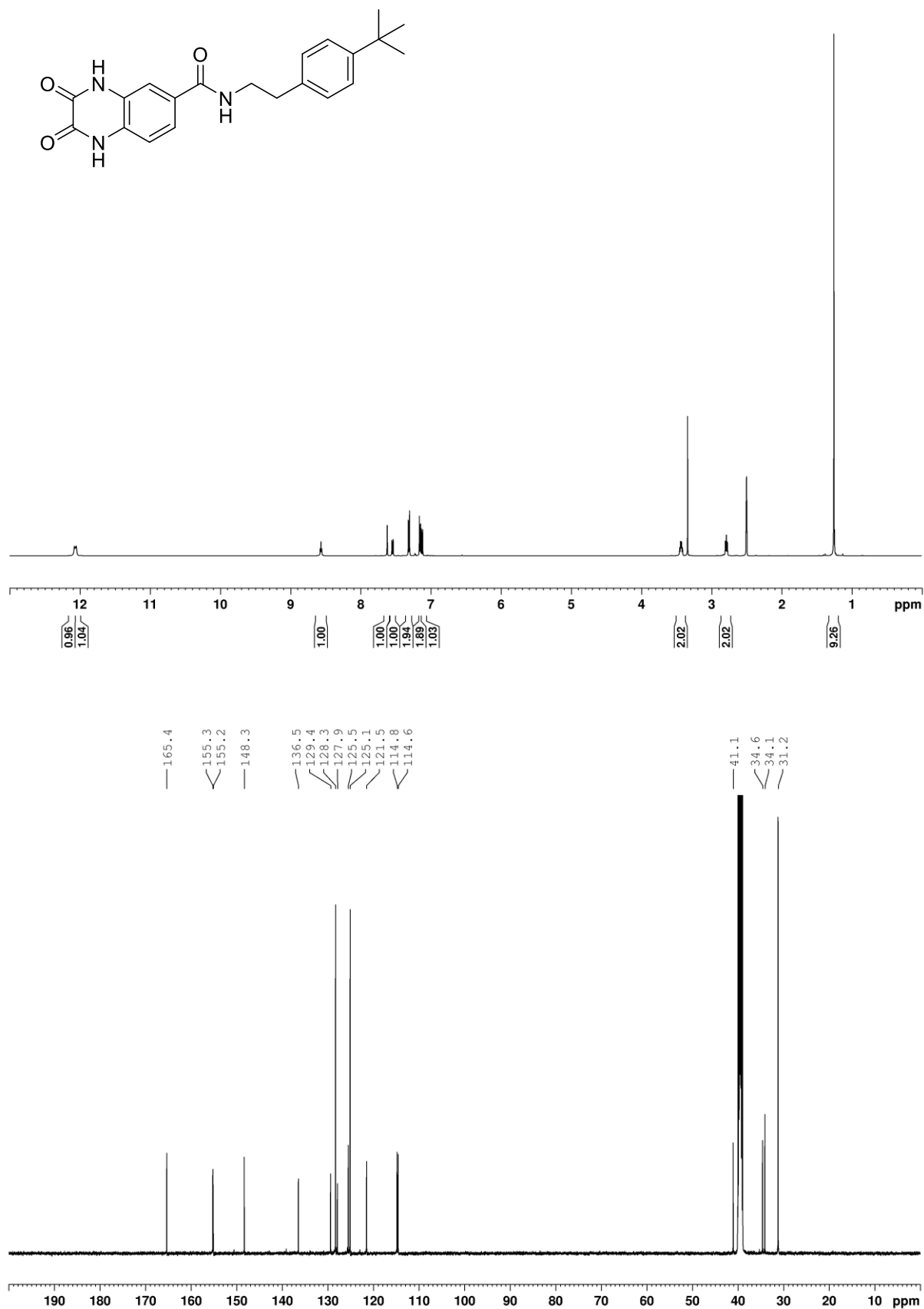


W286: binding site for **16**, 45 min irradiation

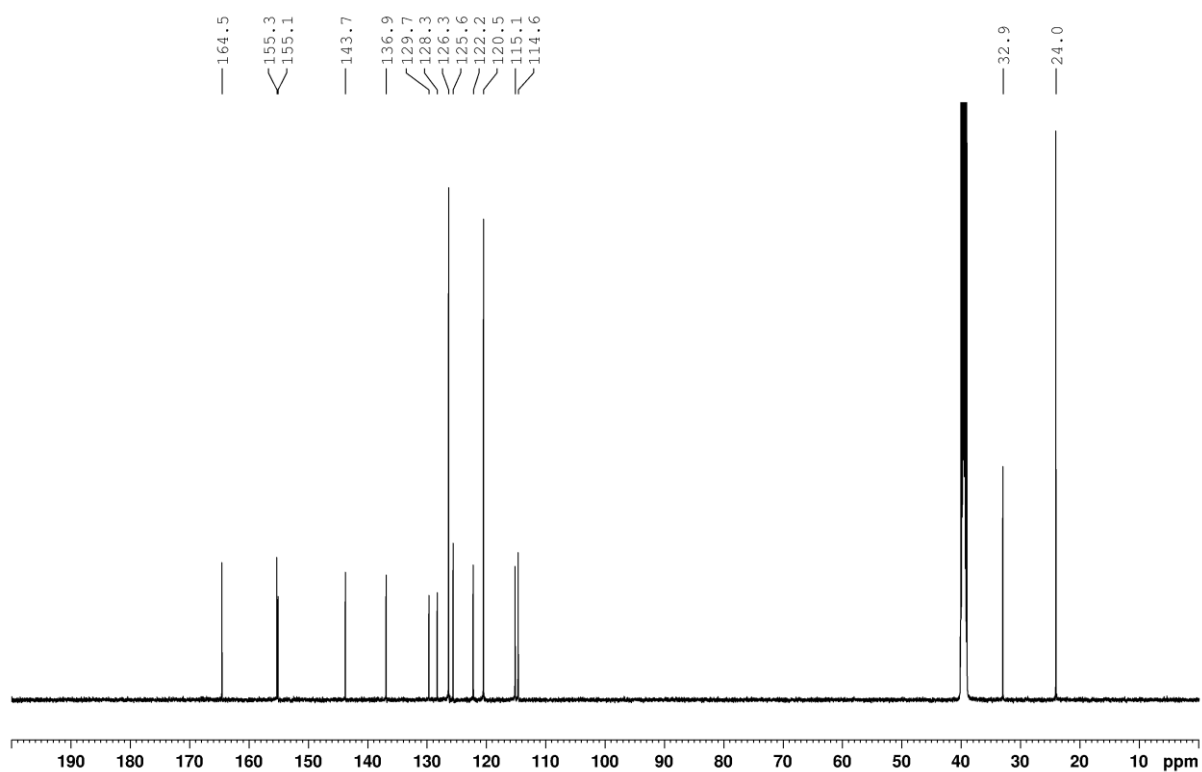
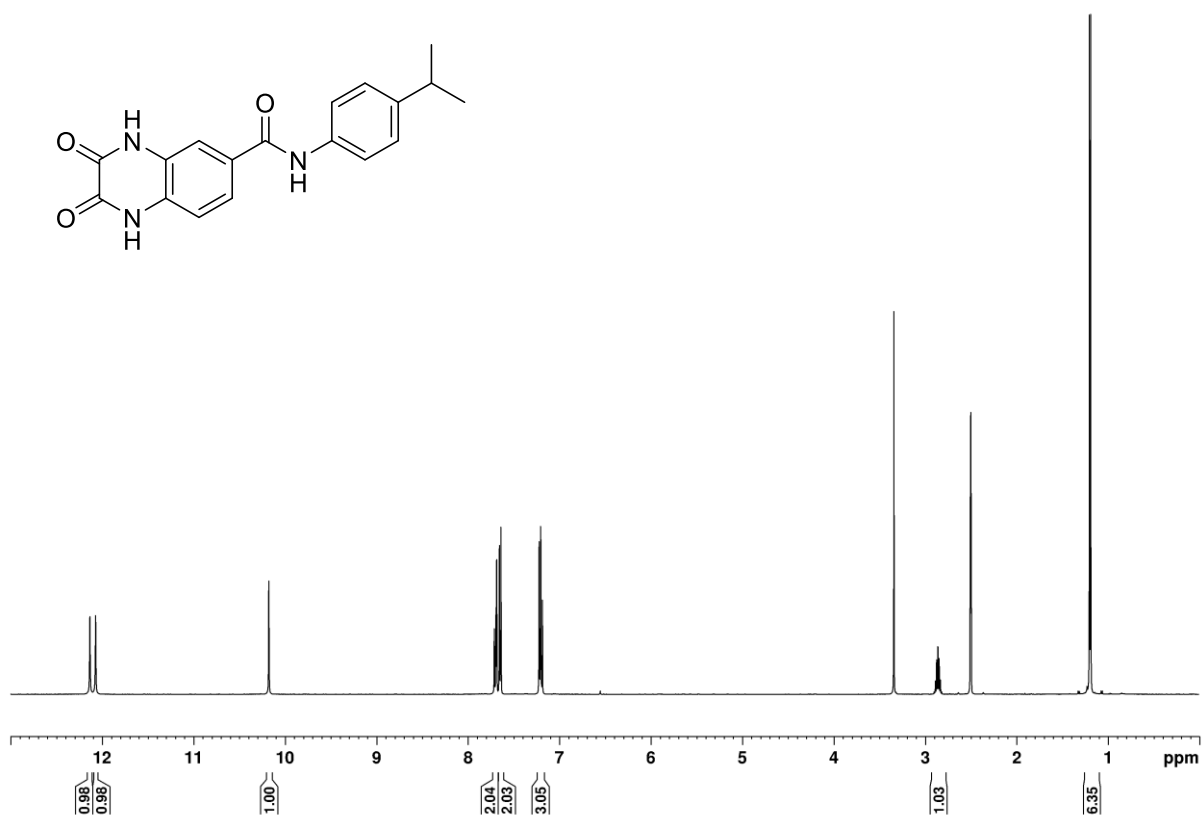


NMR spectra

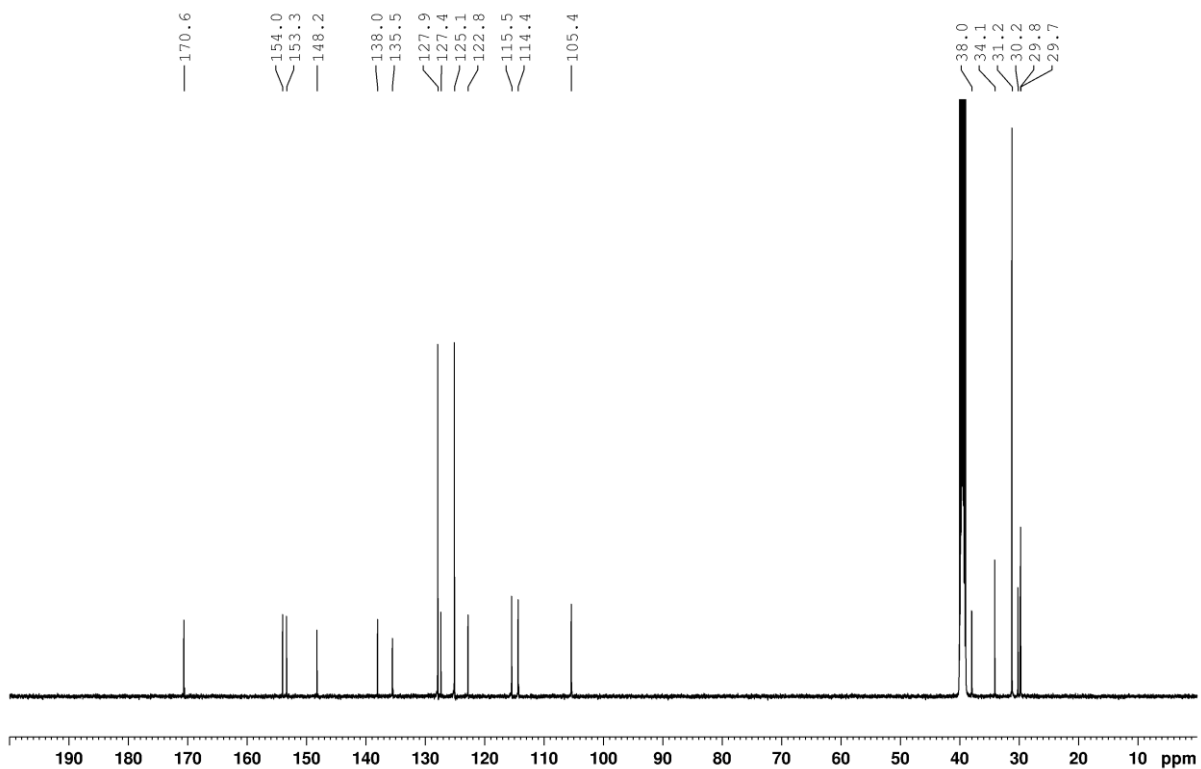
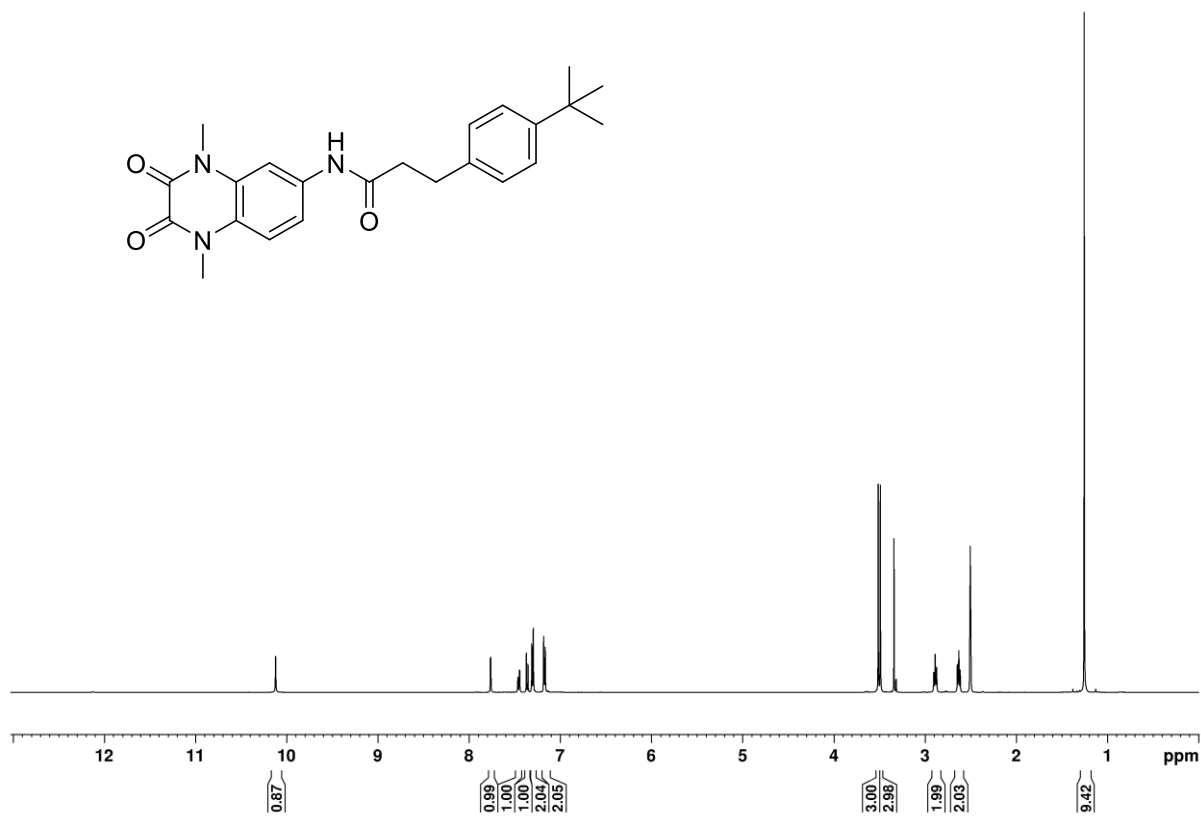
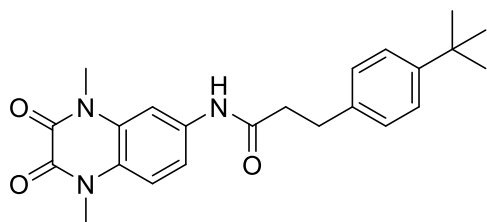
N-(4-(*tert*-Butyl)phenethyl)-2,3-dioxo-1,2,3,4-tetrahydroquinoxaline-6-carboxamide (2)



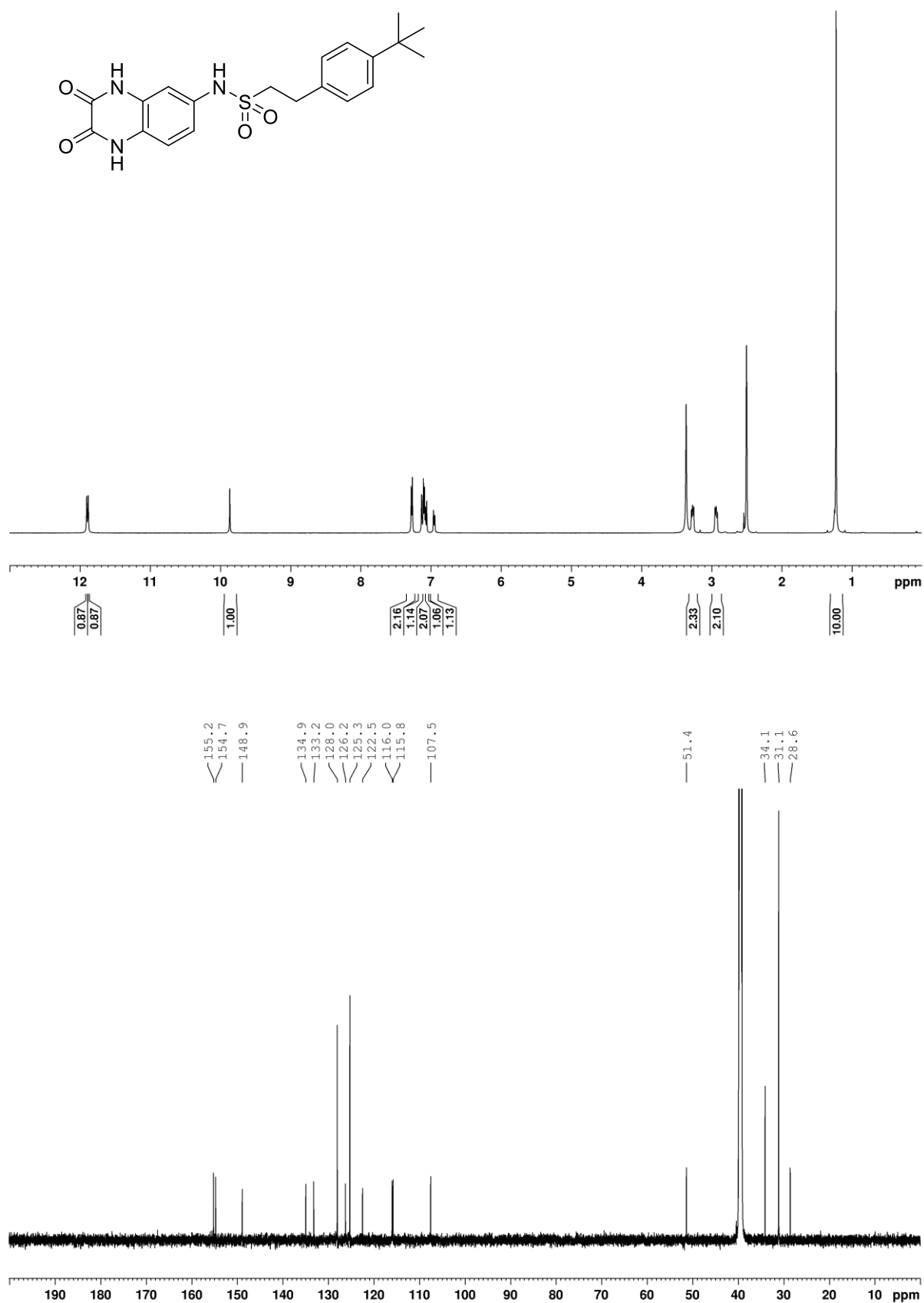
***N*-(4-Isopropylphenyl)-2,3-dioxo-1,2,3,4-tetrahydroquinoxaline-6-carboxamide (8)**



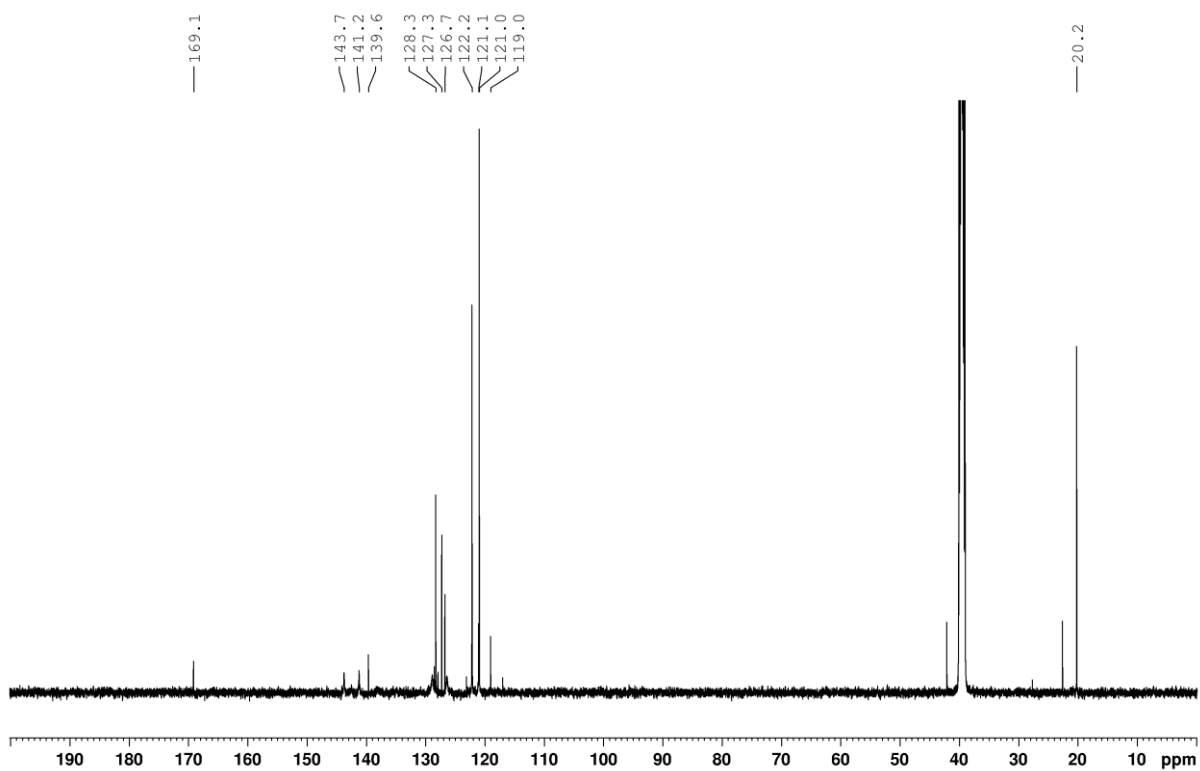
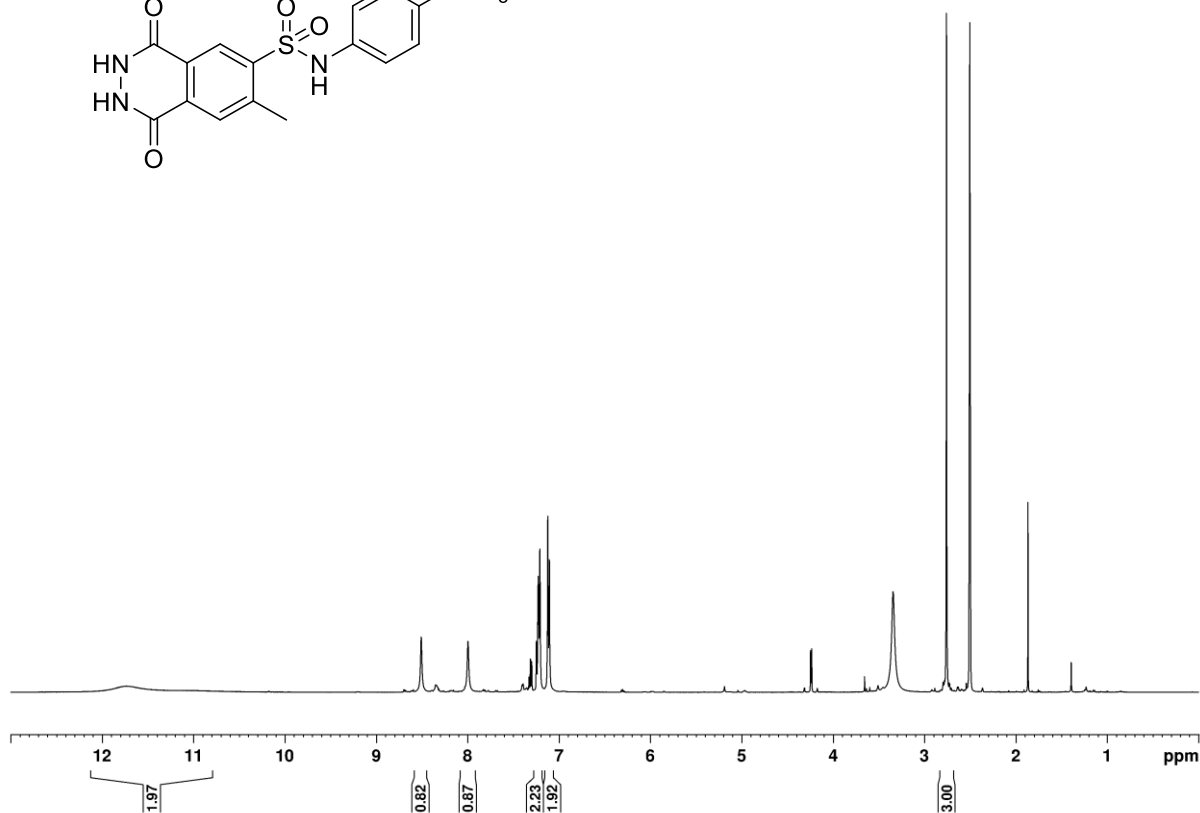
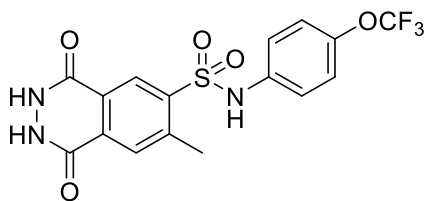
3-(4-(*tert*-Butyl)phenyl)-N-(1,4-dimethyl-2,3-dioxo-1,2,3,4-tetrahydroquinoxalin-6-yl)propanamide (S16)



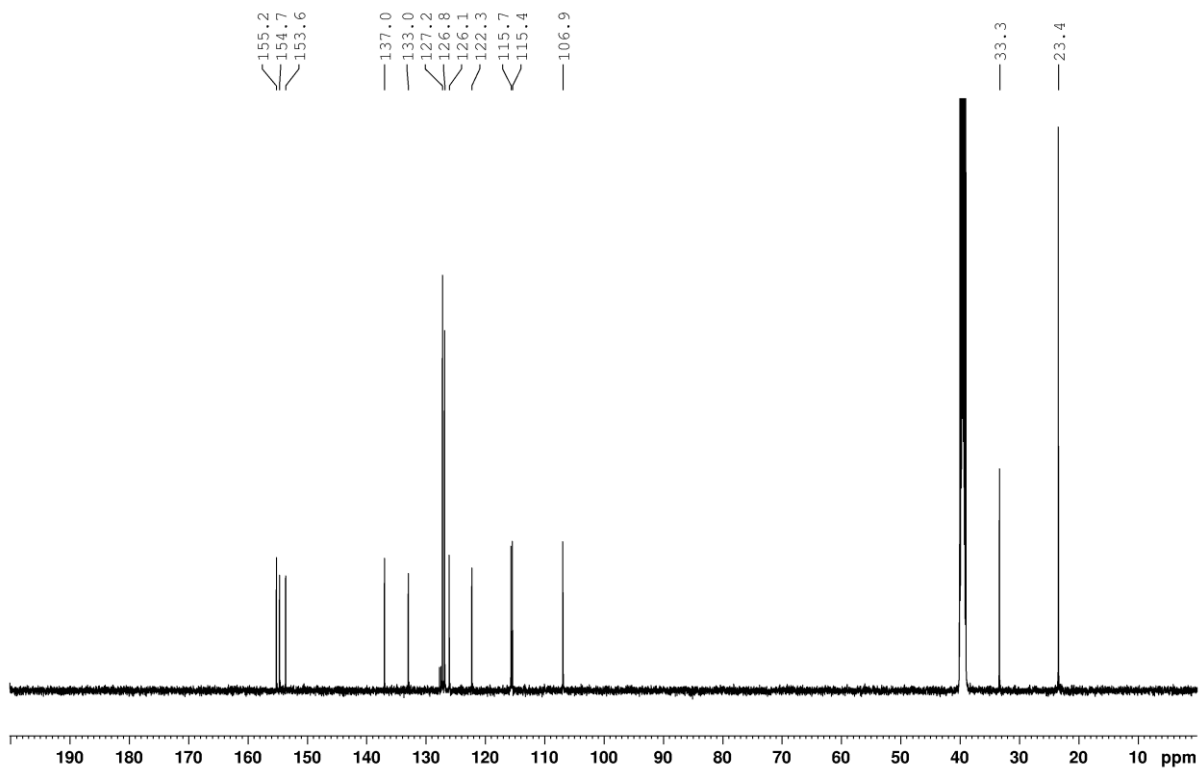
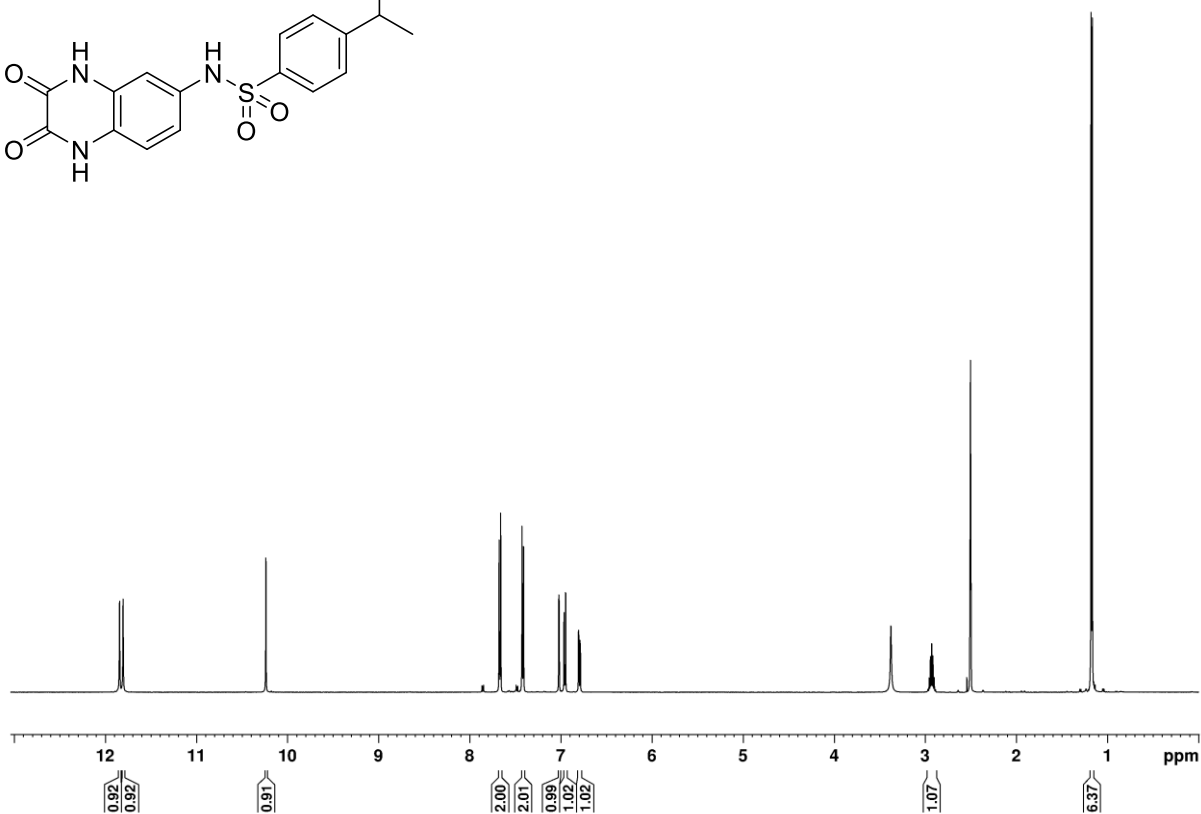
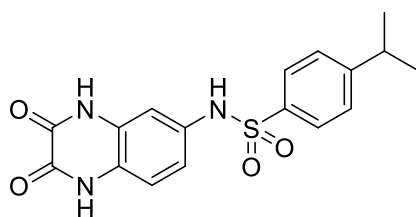
2-(4-(*tert*-Butyl)phenyl)-*N*-(2,3-dioxo-1,2,3,4-tetrahydroquinoxalin-6-yl)ethane-1-sulfonamide (3)



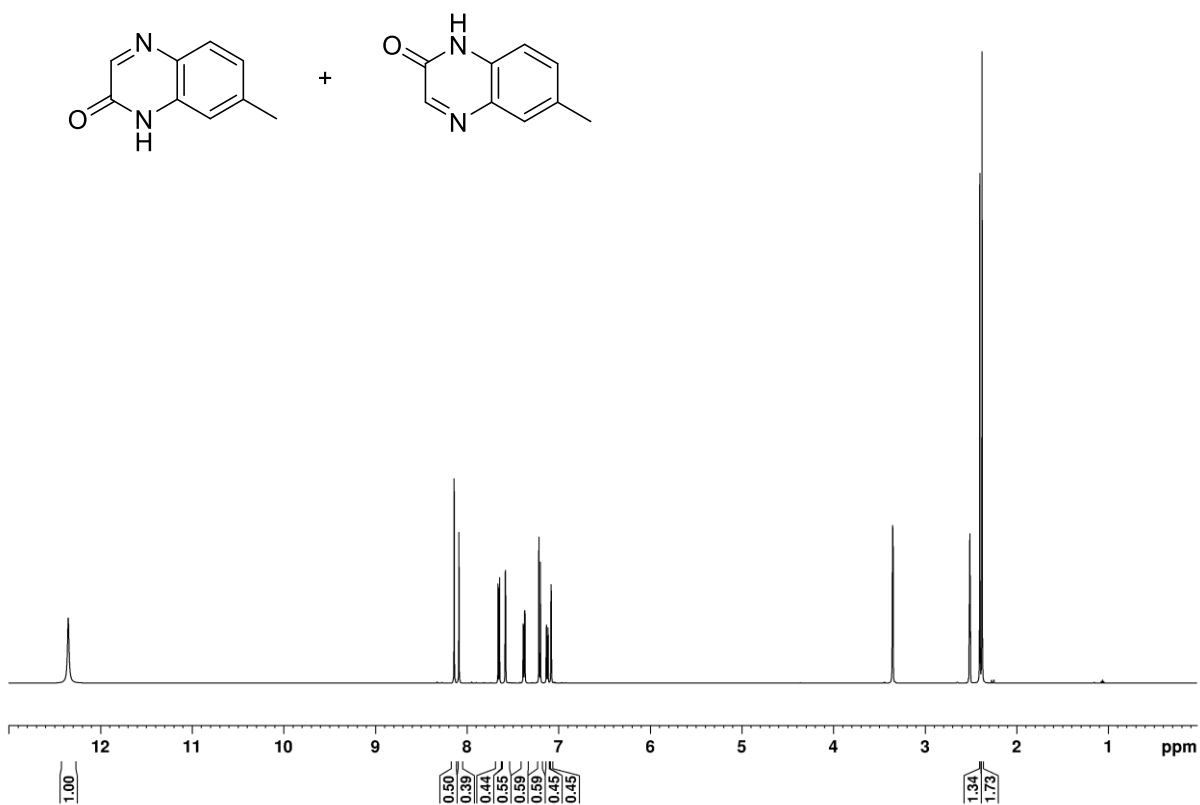
7-Methyl-1,4-dioxo-*N*-(4-(trifluoromethoxy)phenyl)-1,2,3,4-tetrahydrophthalazine-6-sulfonamide (13)



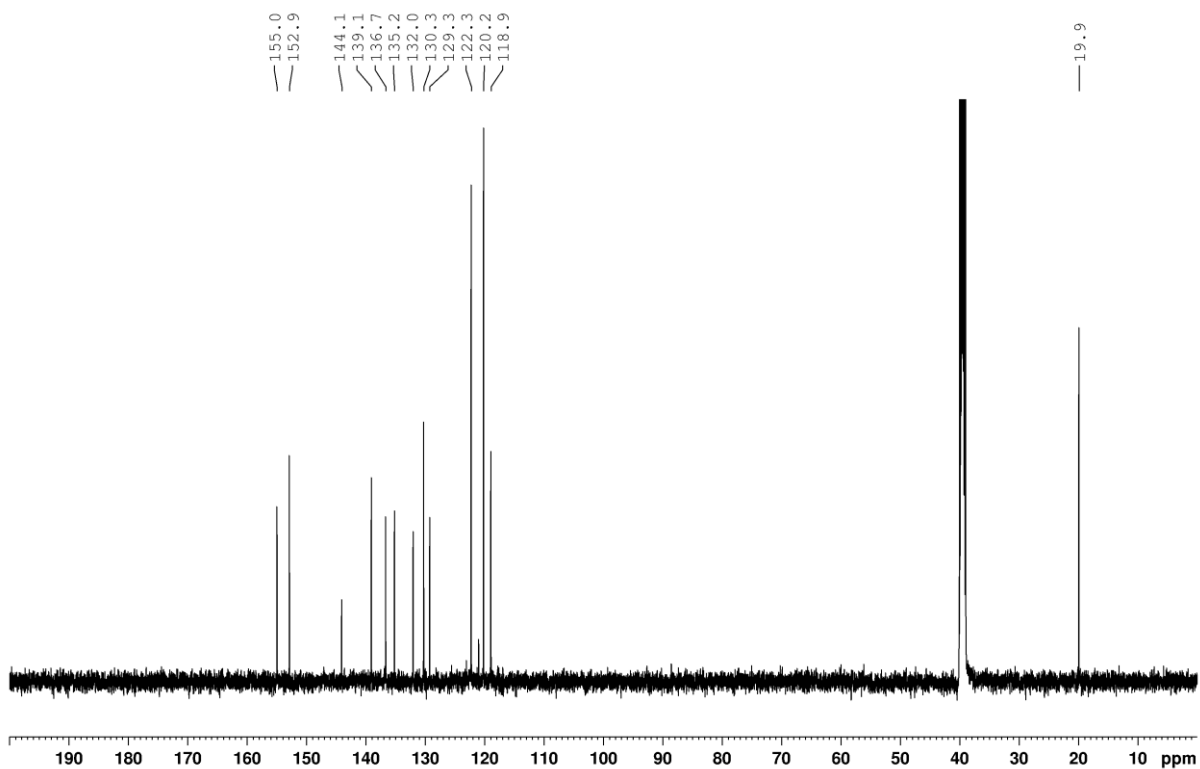
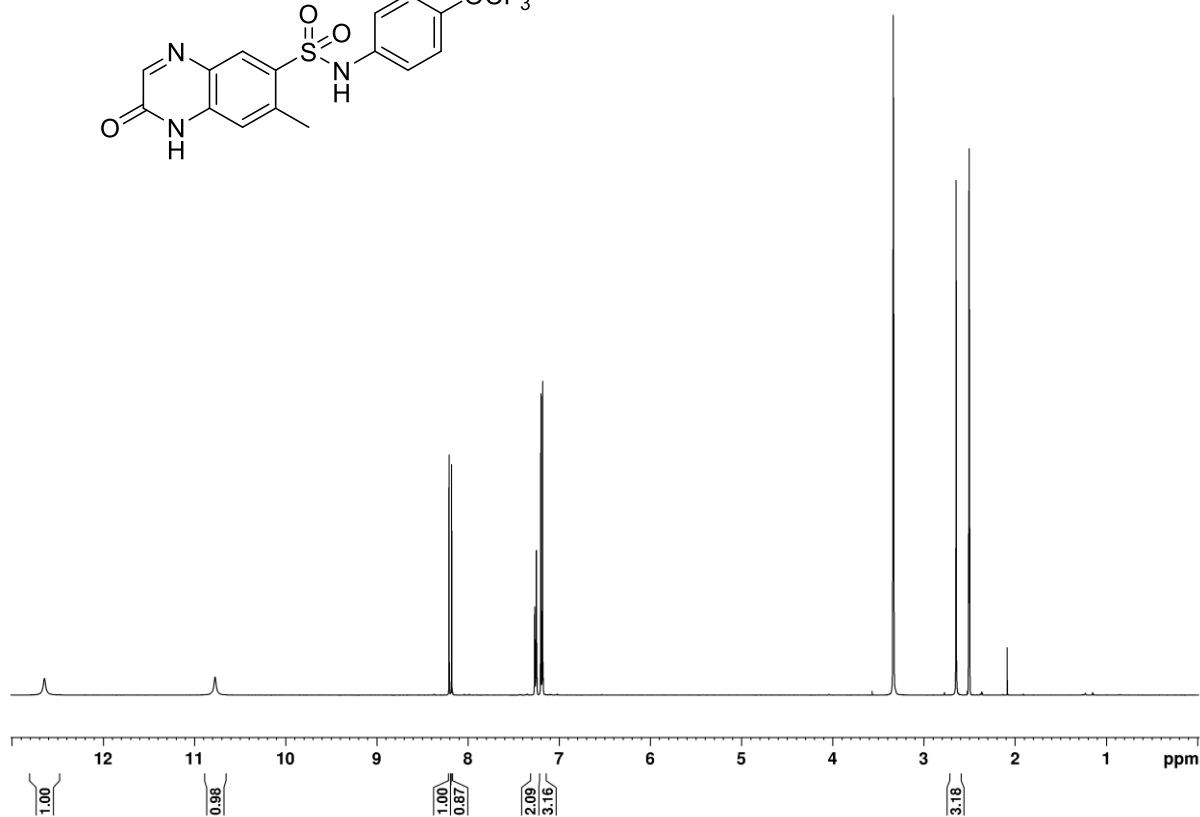
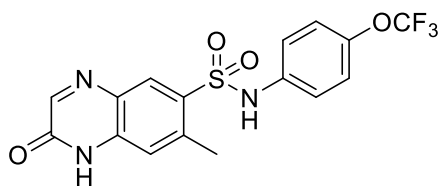
***N*-(2,3-Dioxo-1,2,3,4-tetrahydroquinoxalin-6-yl)-4-isopropylbenzenesulfonamide (9)**



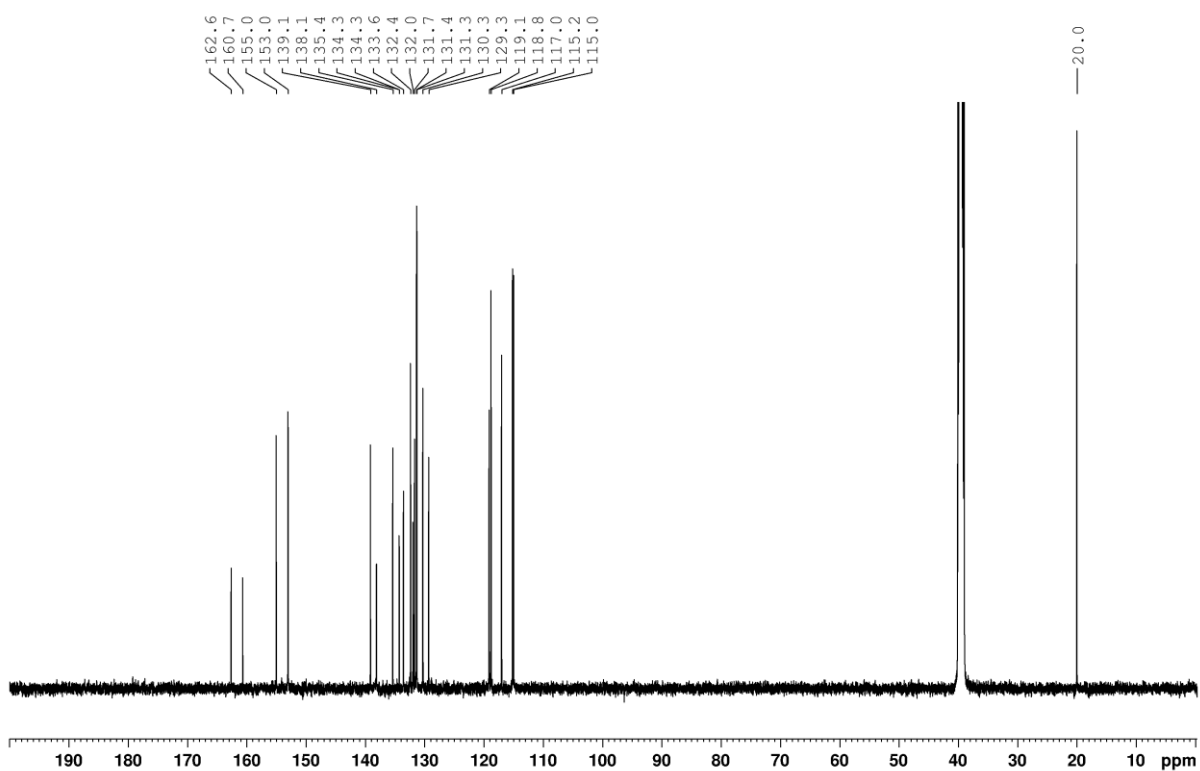
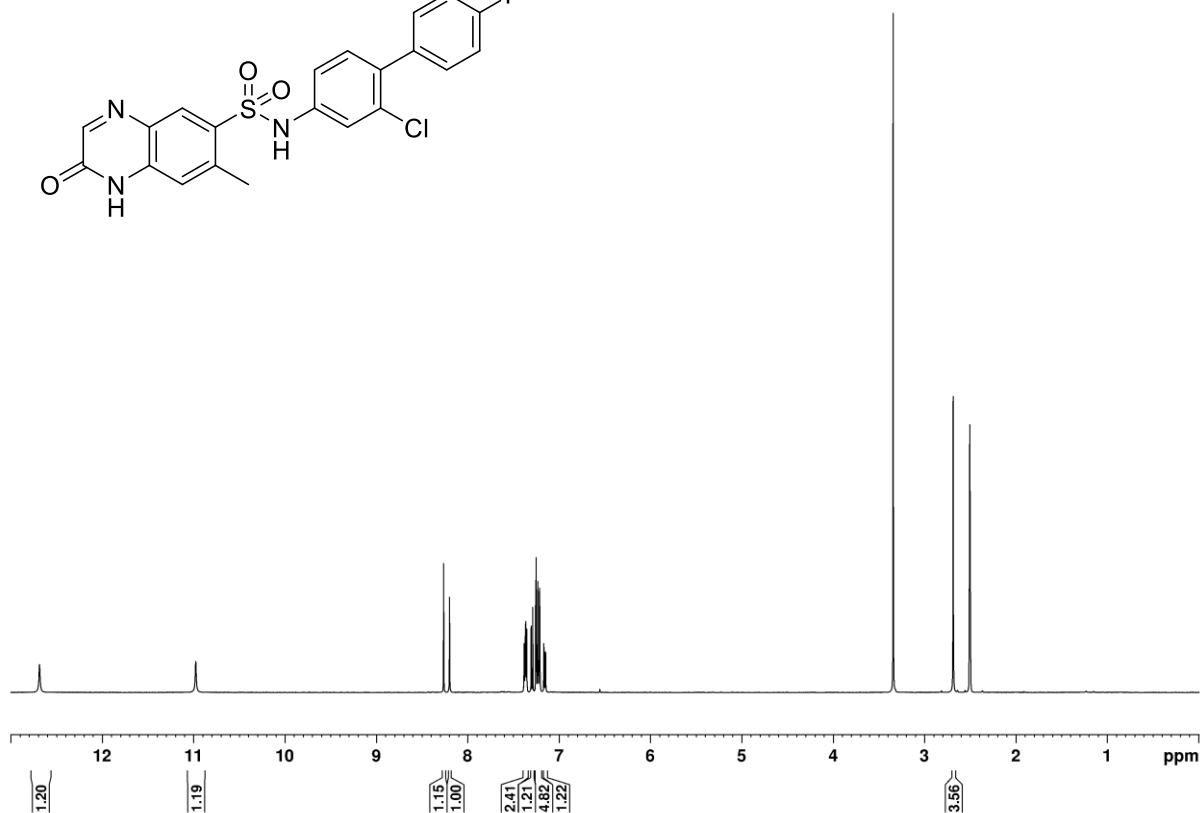
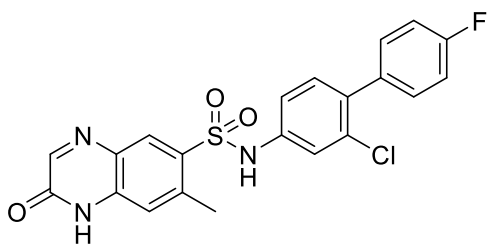
Mixture of 7-methylquinoxalin-2(1*H*)-one (S23) and 6-methylquinoxalin-2(1*H*)-one (S24)



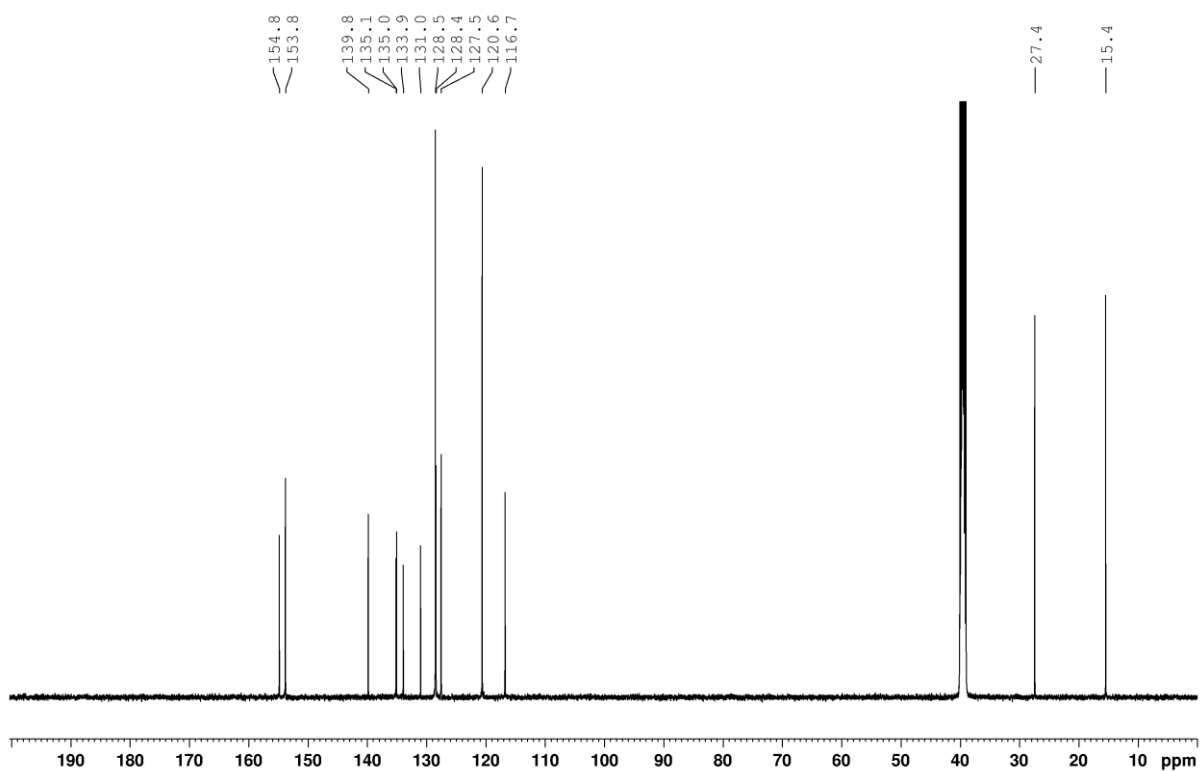
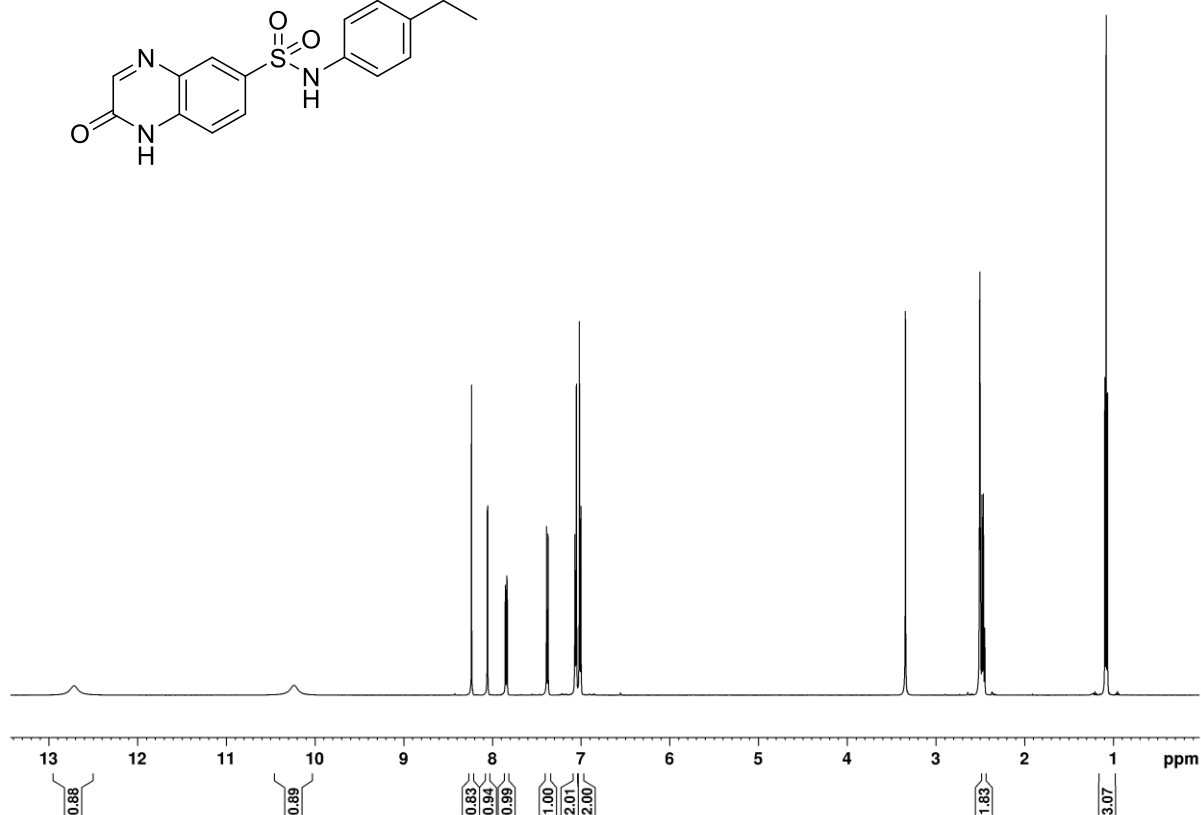
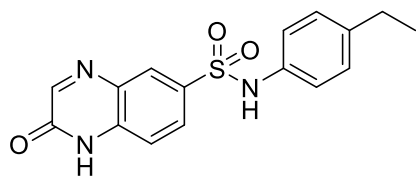
7-Methyl-2-oxo-N-(4-(trifluoromethoxy)phenyl)-1,2-dihydroquinoxaline-6-sulfonamide (S11)



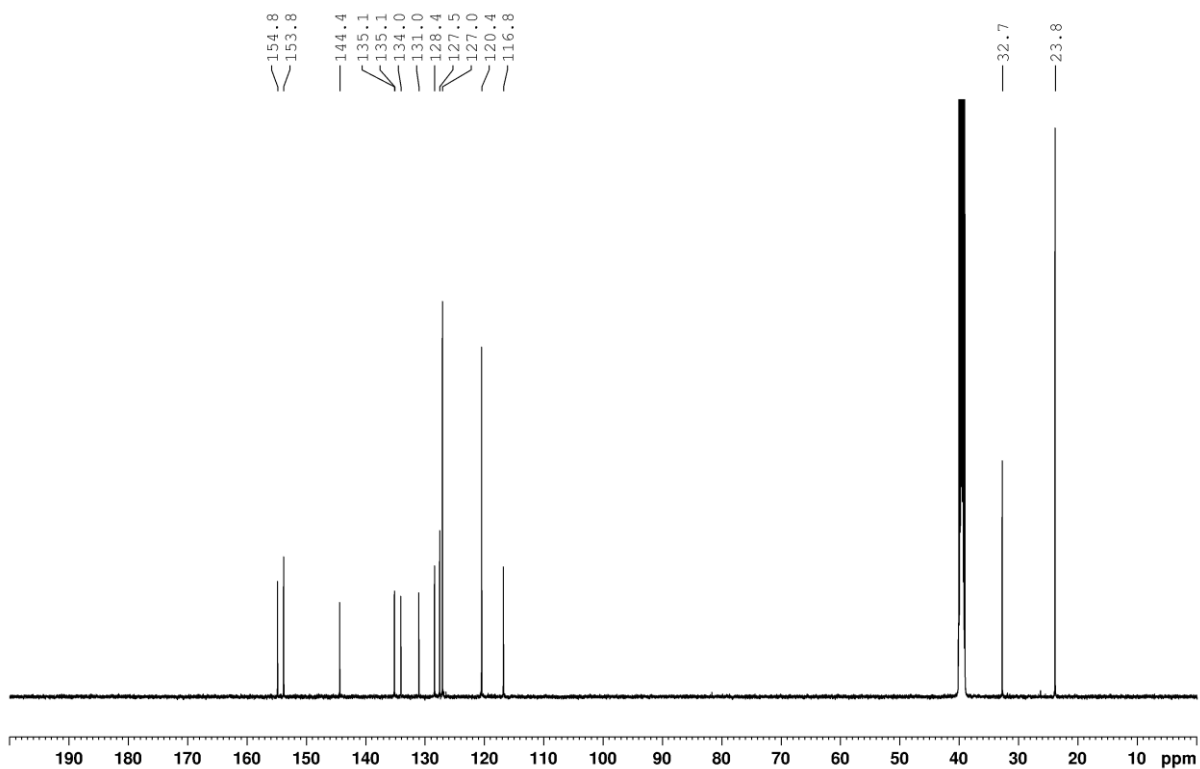
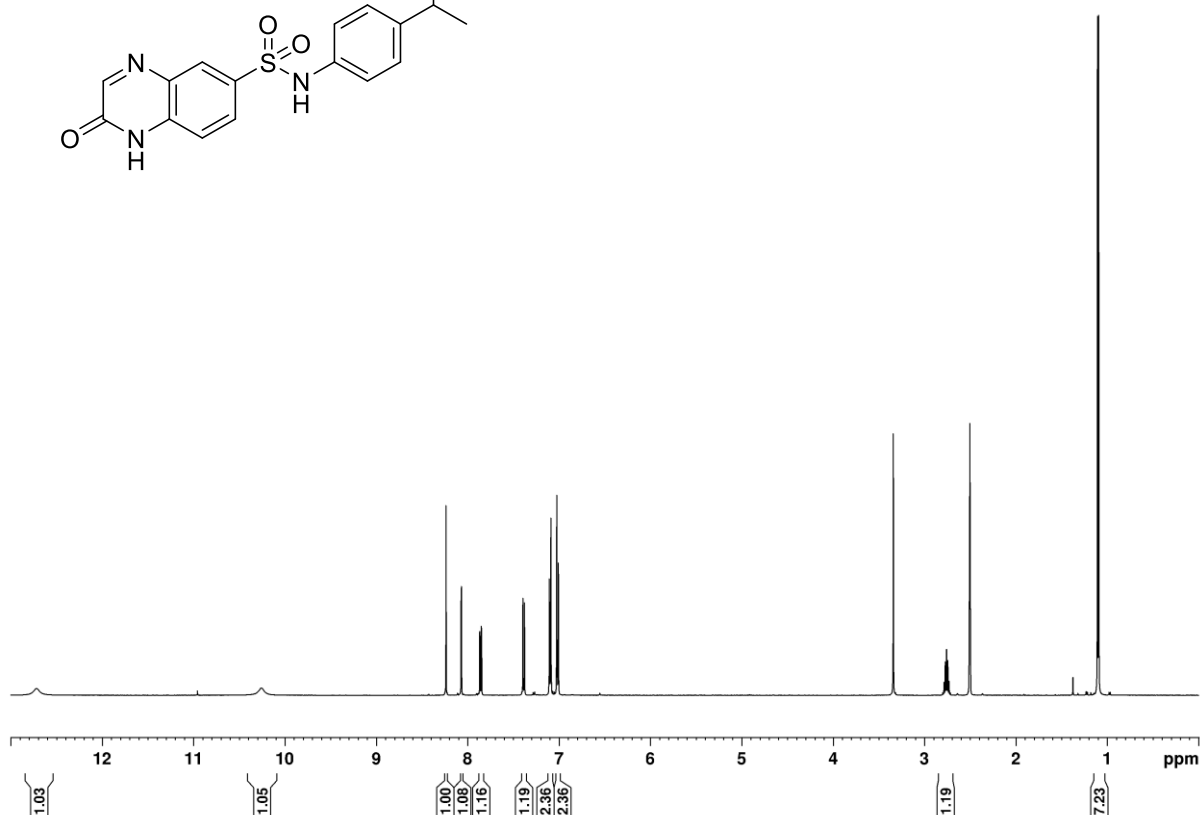
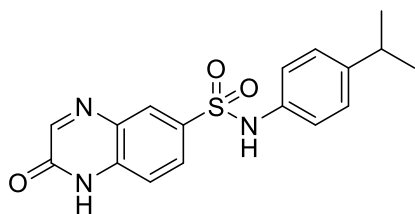
***N*-(2-Chloro-4'-fluoro-[1,1'-biphenyl]-4-yl)-7-methyl-2-oxo-1,2-dihydroquinoxaline-6-sulfonamide (S12)**



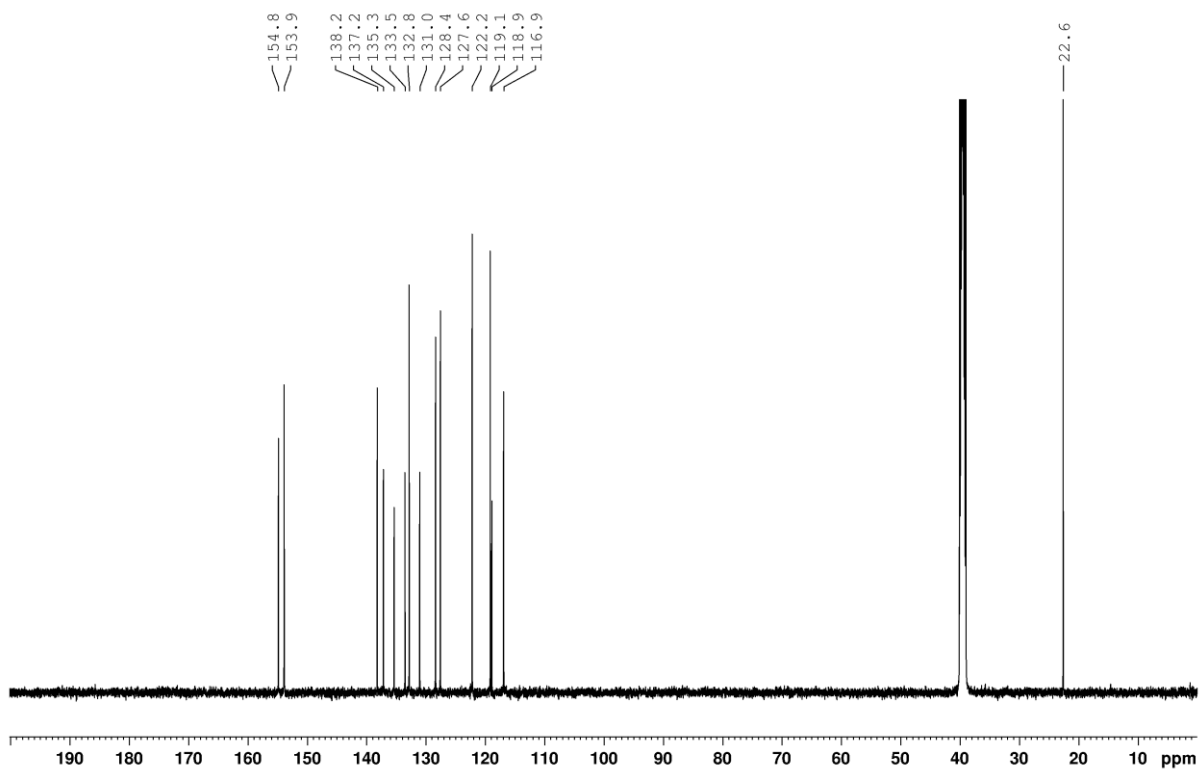
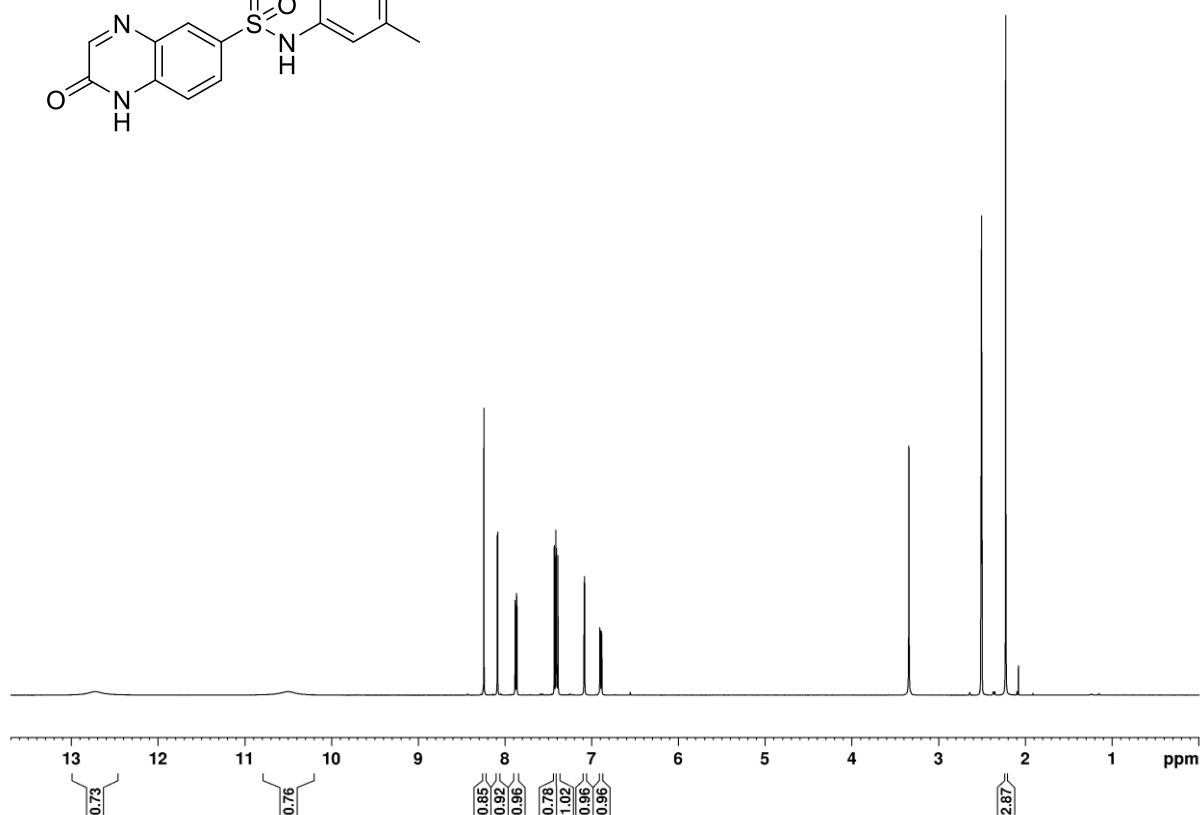
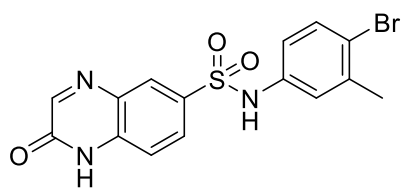
***N*-(4-Ethylphenyl)-2-oxo-1,2-dihydroquinoxaline-6-sulfonamide (S6)**



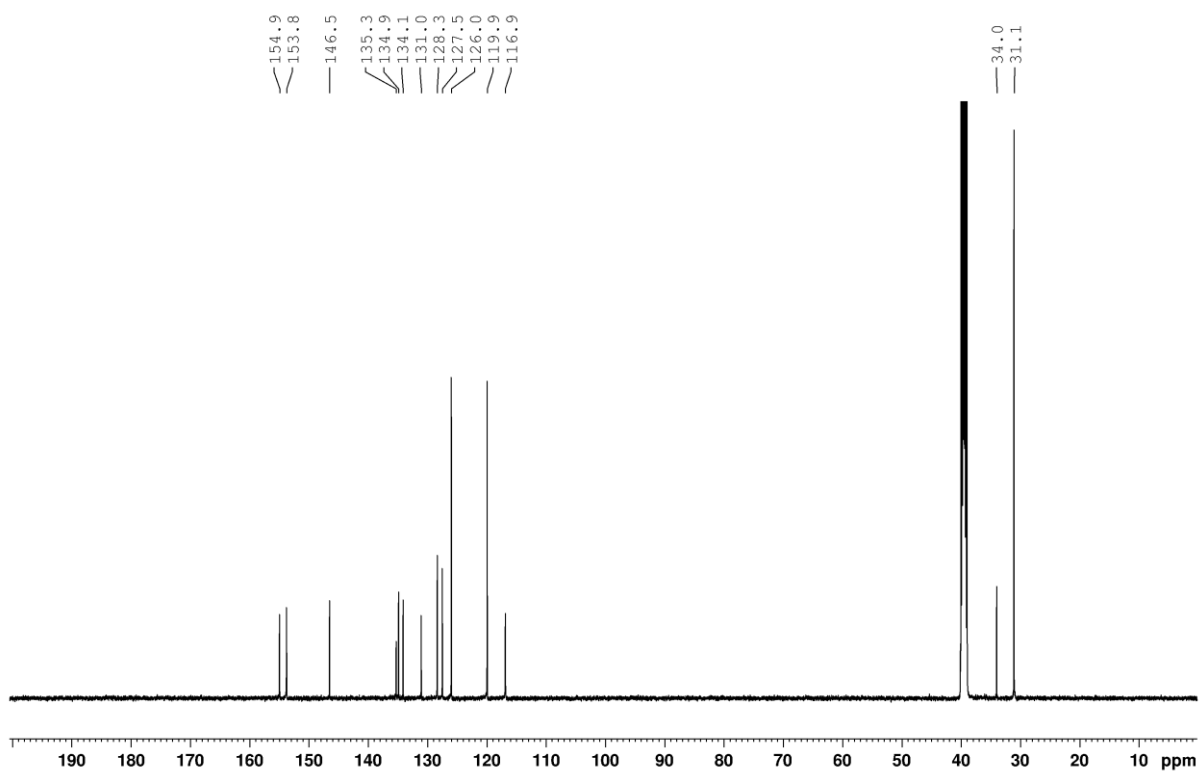
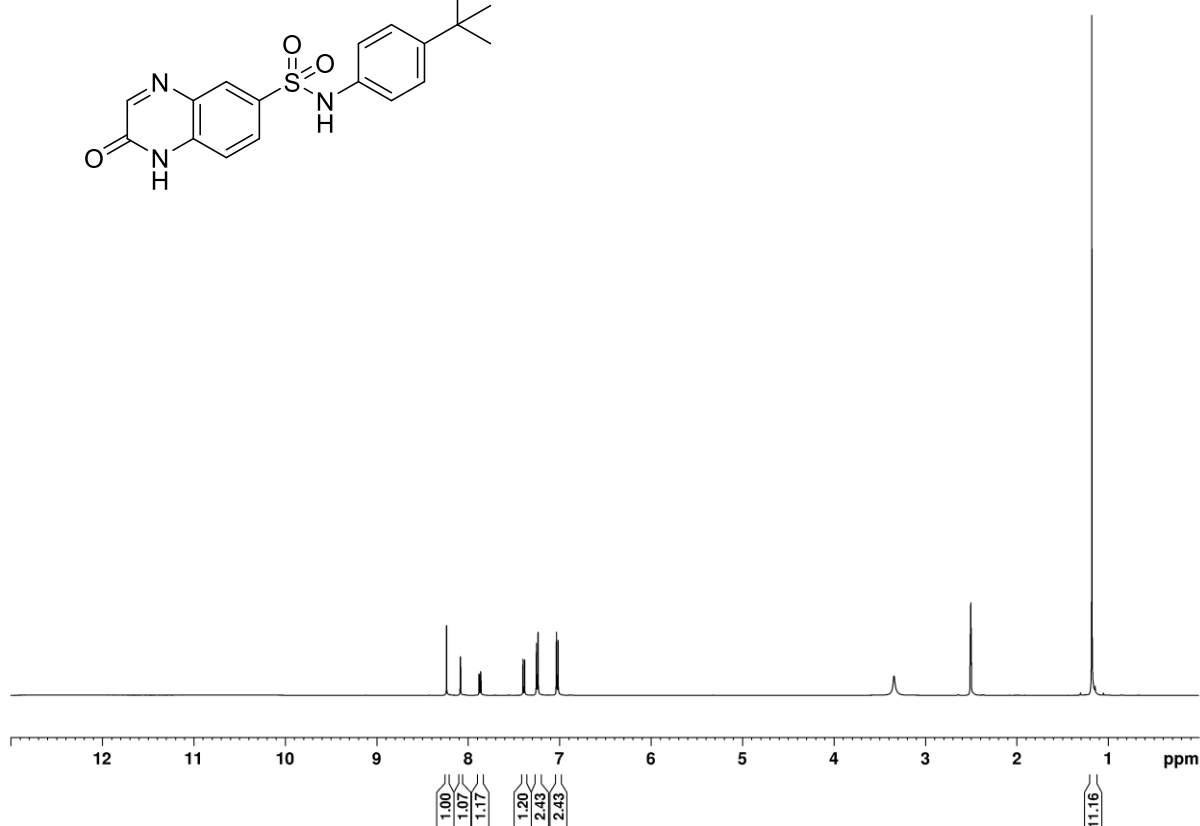
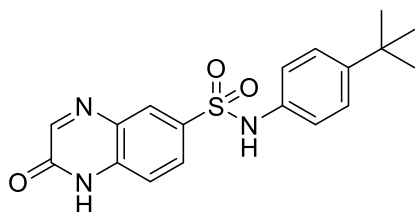
N-(4-Isopropylphenyl)-2-oxo-1,2-dihydroquinoxaline-6-sulfonamide (S7)



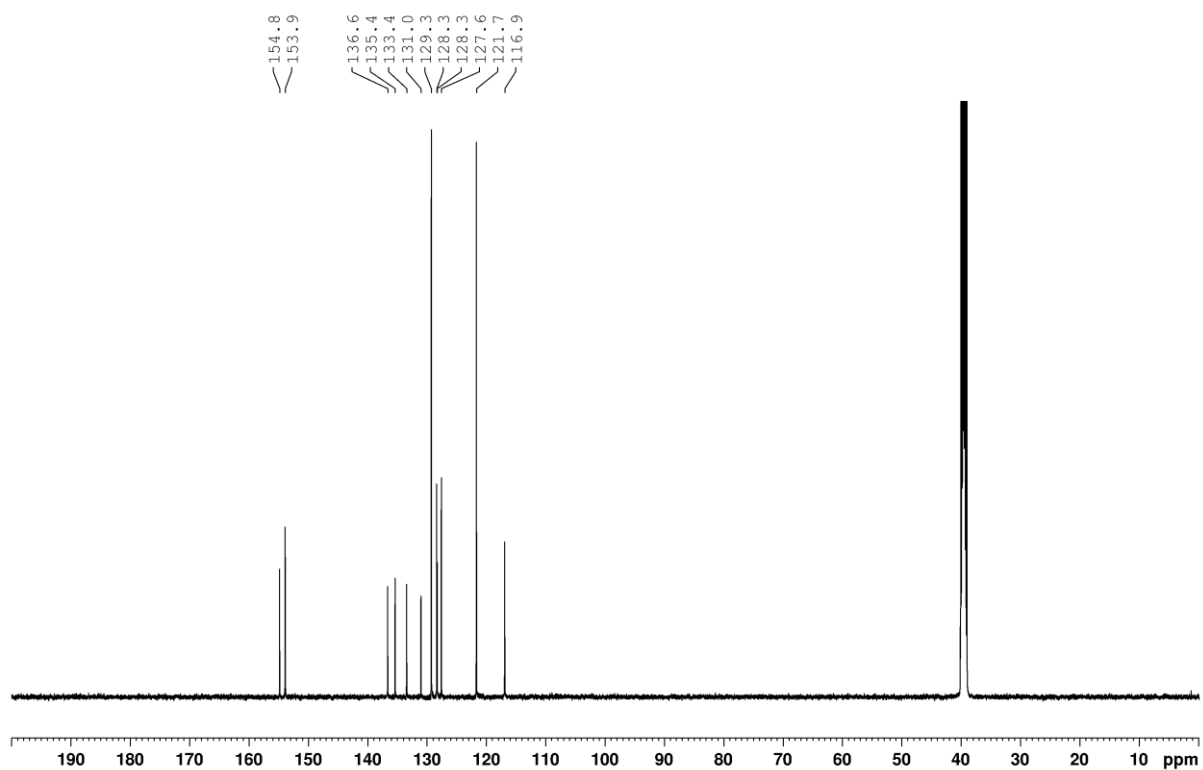
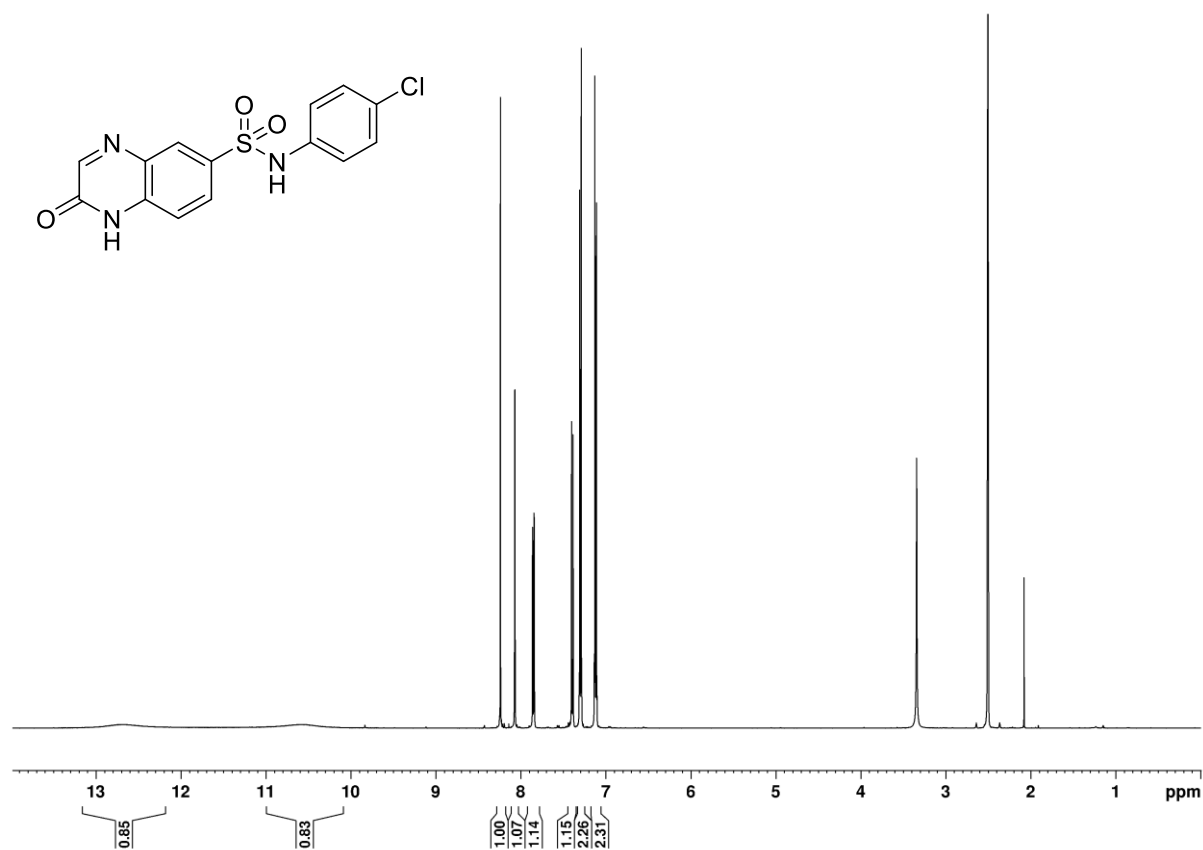
***N*-(4-bromo-3-methylphenyl)-2-oxo-1,2-dihydroquinoxaline-6-sulfonamide (S8)**



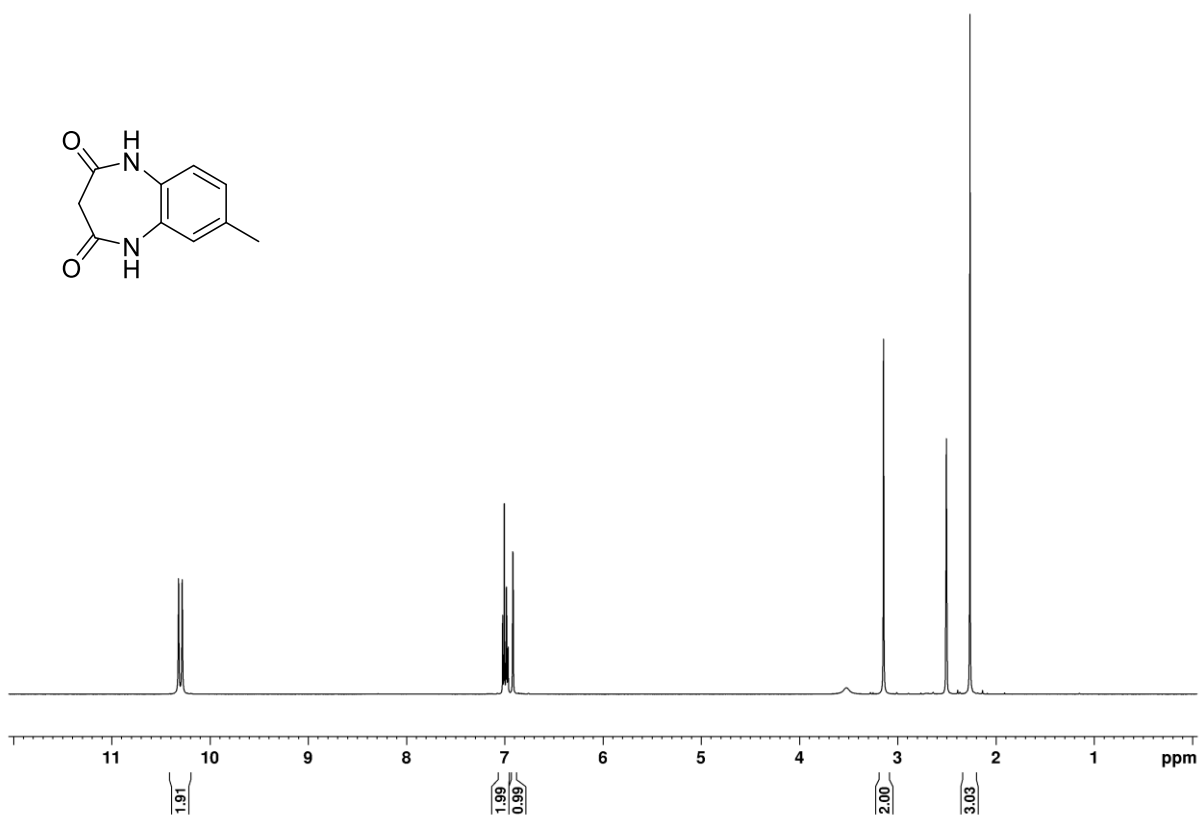
***N*-(4-(*tert*-Butyl)phenyl)-2-oxo-1,2-dihydroquinoxaline-6-sulfonamide (S9)**



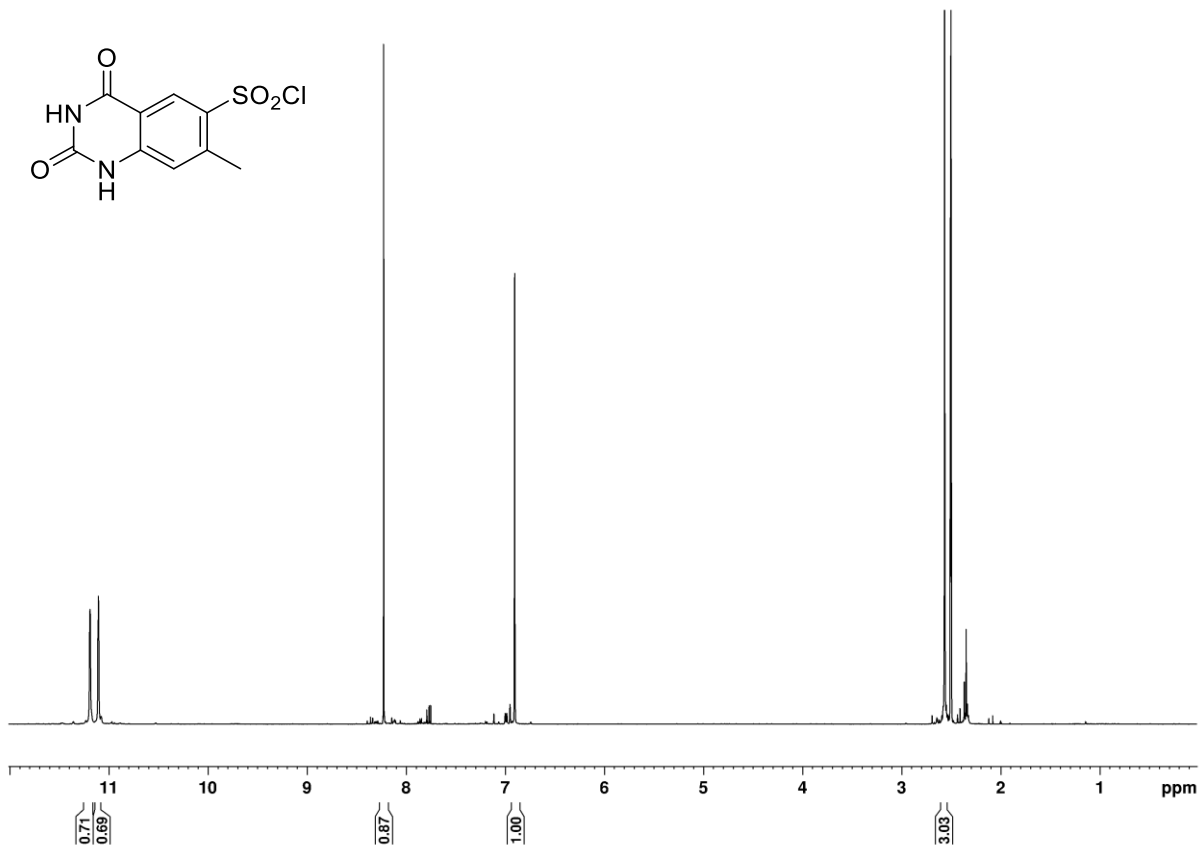
***N*-(4-chlorophenyl)-2-oxo-1,2-dihydroquinoxaline-6-sulfonamide (S10)**



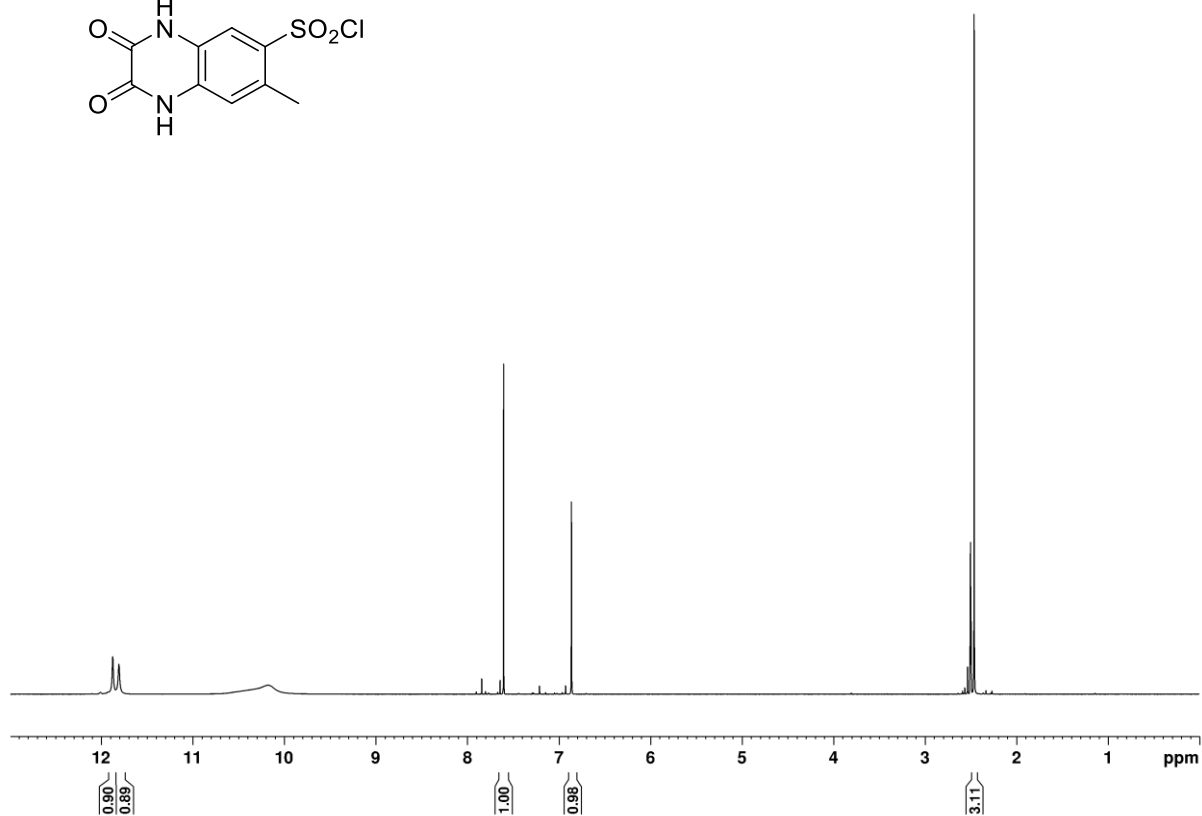
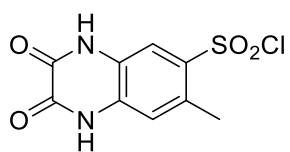
7-Methyl-1,5-dihydro-2H-benzo[b][1,4]diazepine-2,4(3H)-dione (S26)



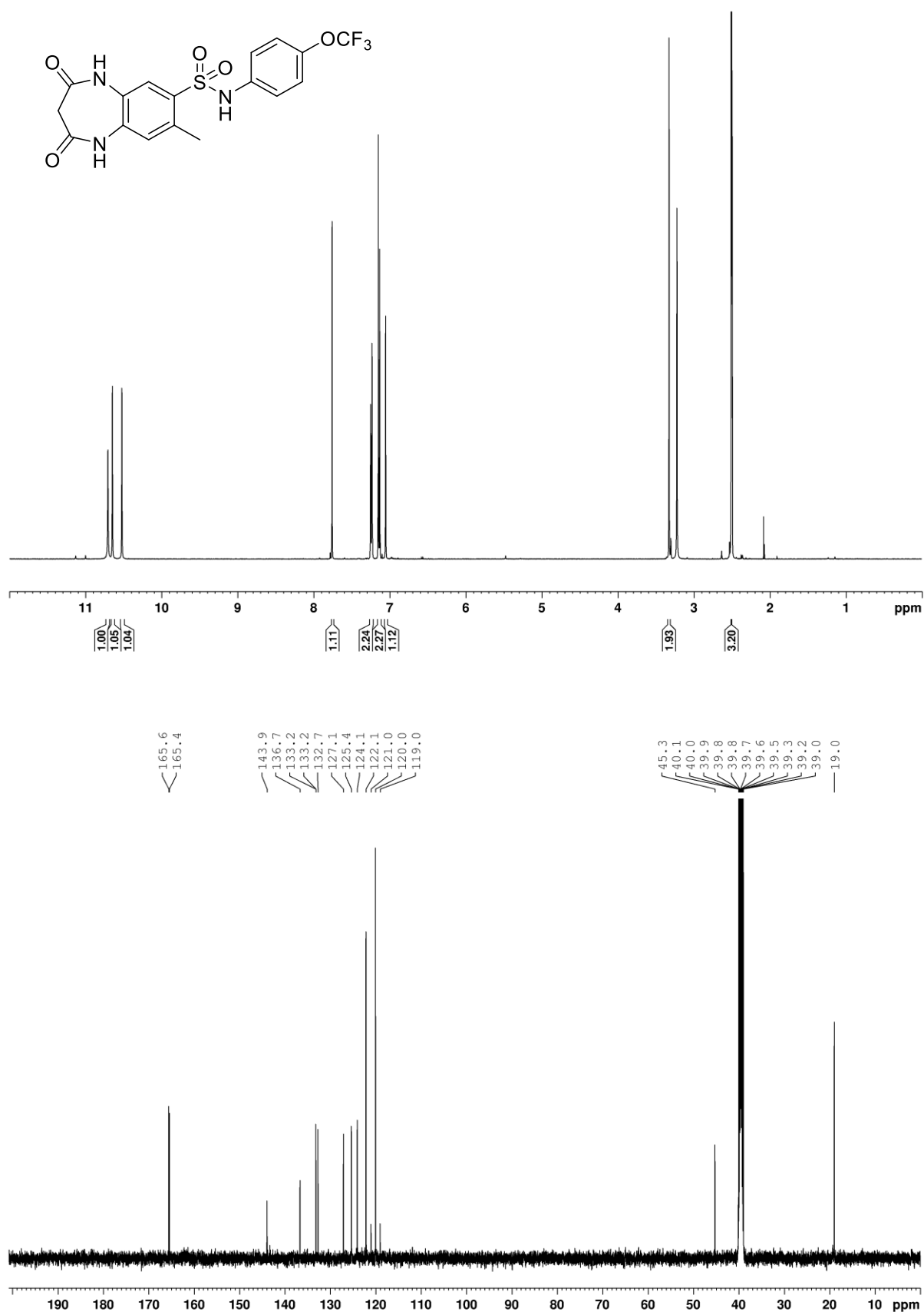
7-Methyl-2,4-dioxo-1,2,3,4-tetrahydroquinazoline-6-sulfonyl chloride (S28)



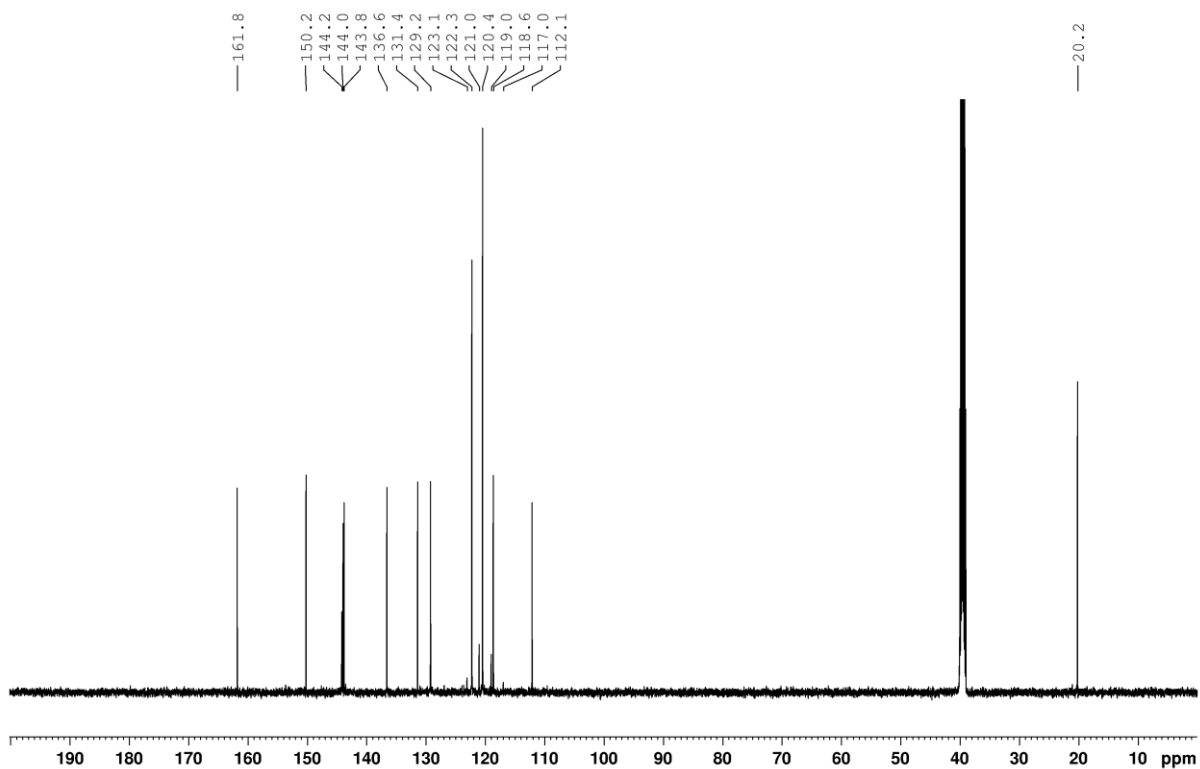
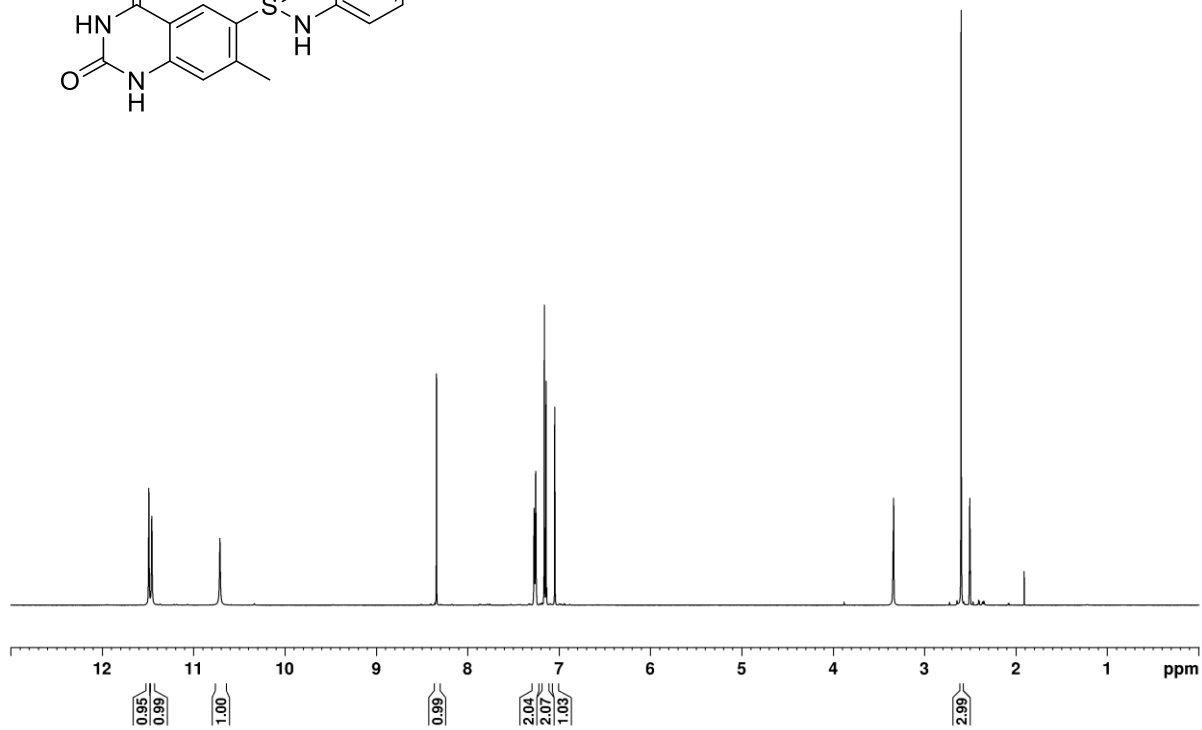
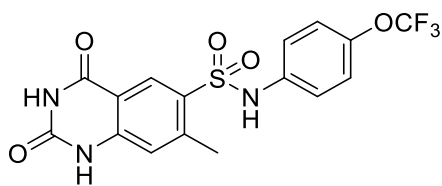
7-Methyl-2,3-dioxo-1,2,3,4-tetrahydroquinoxaline-6-sulfonyl chloride (S30)



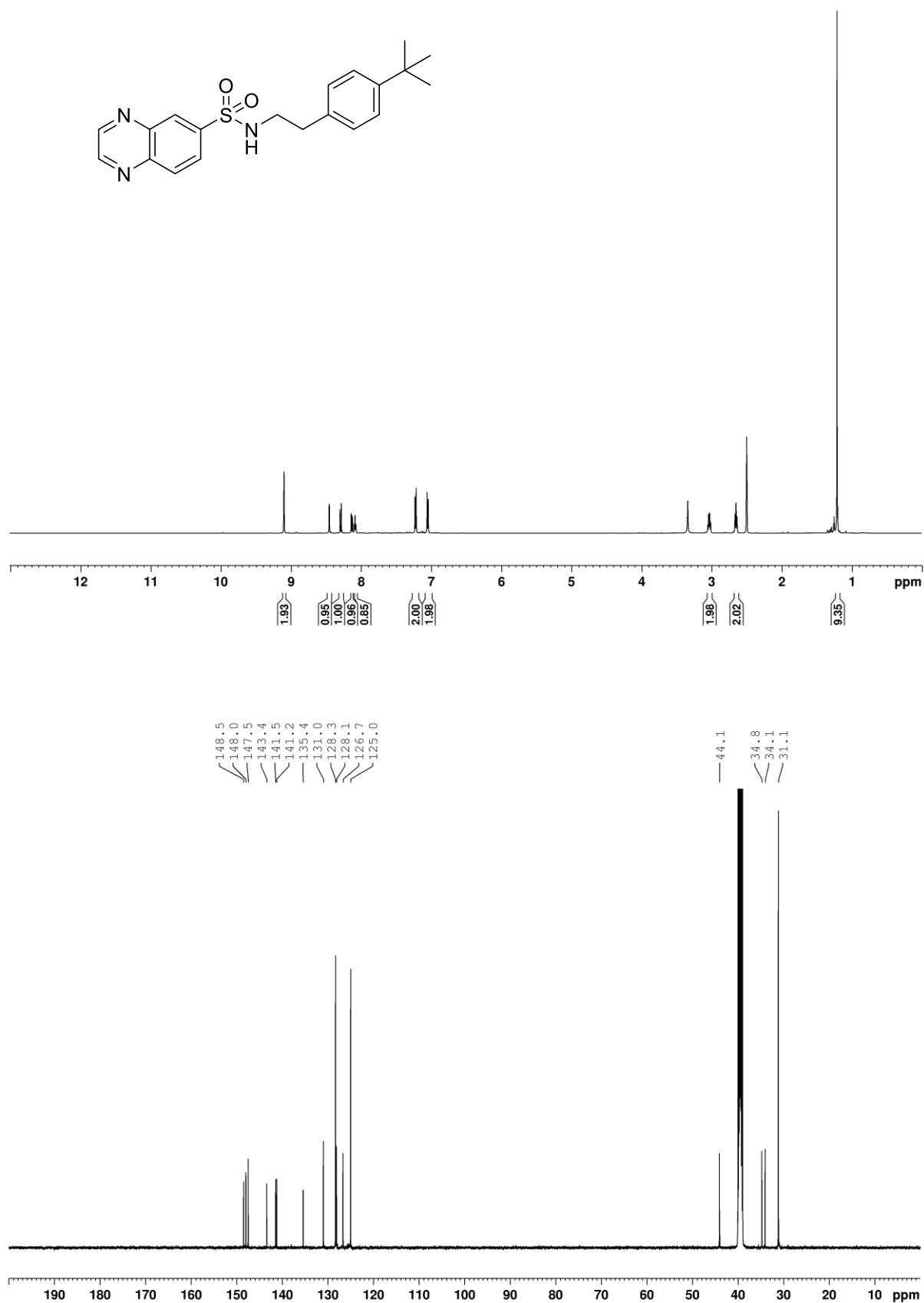
8-Methyl-2,4-dioxo-*N*-(4-(trifluoromethoxy)phenyl)-2,3,4,5-tetrahydro-1H-benzo[b][1,4]diazepine-7-sulfonamide (S17)



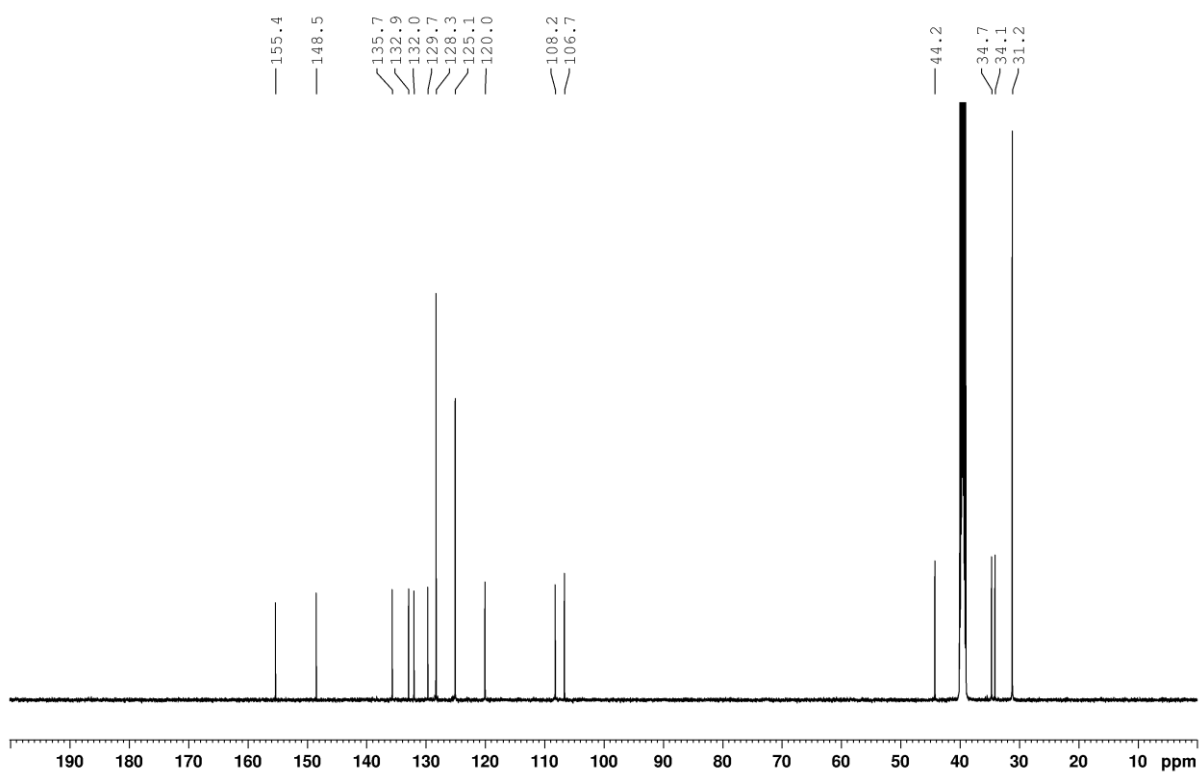
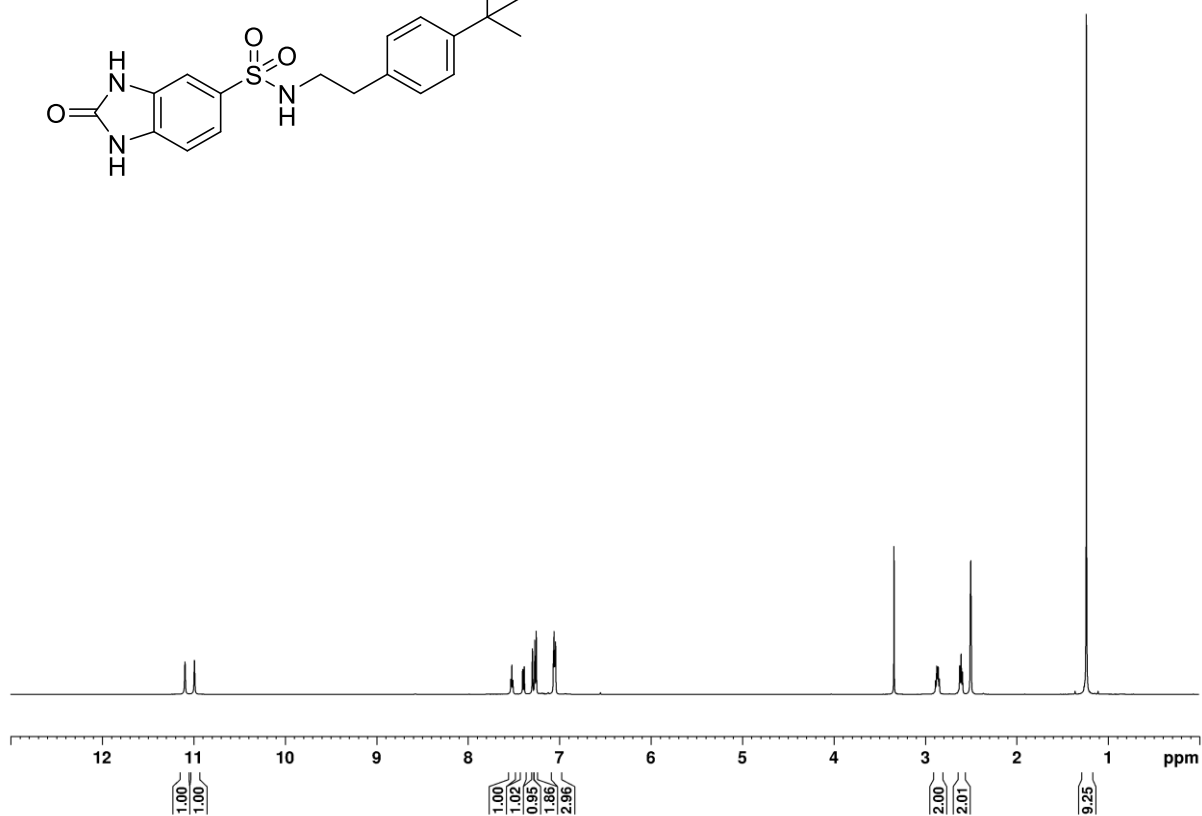
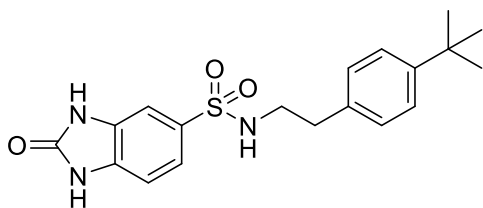
7-Methyl-2,4-dioxo-*N*-(4-(trifluoromethoxy)phenyl)-1,2,3,4-tetrahydroquinazoline-6-sulfonamide
(7)



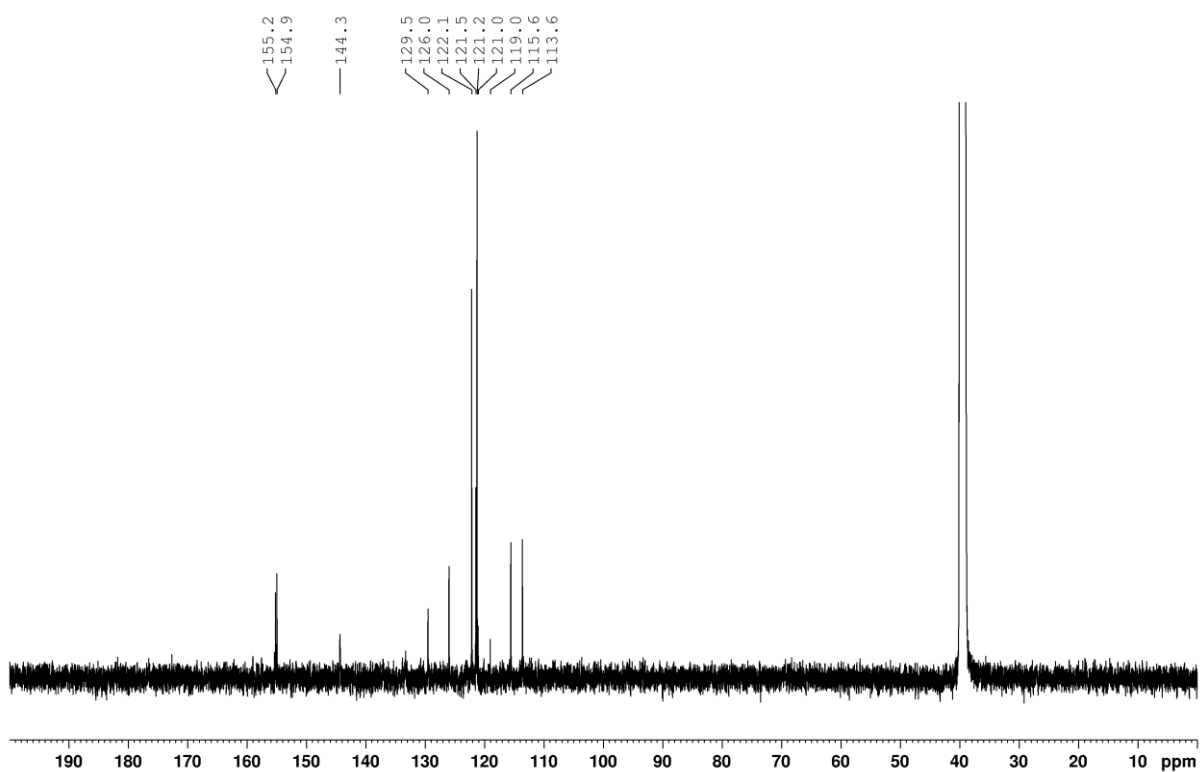
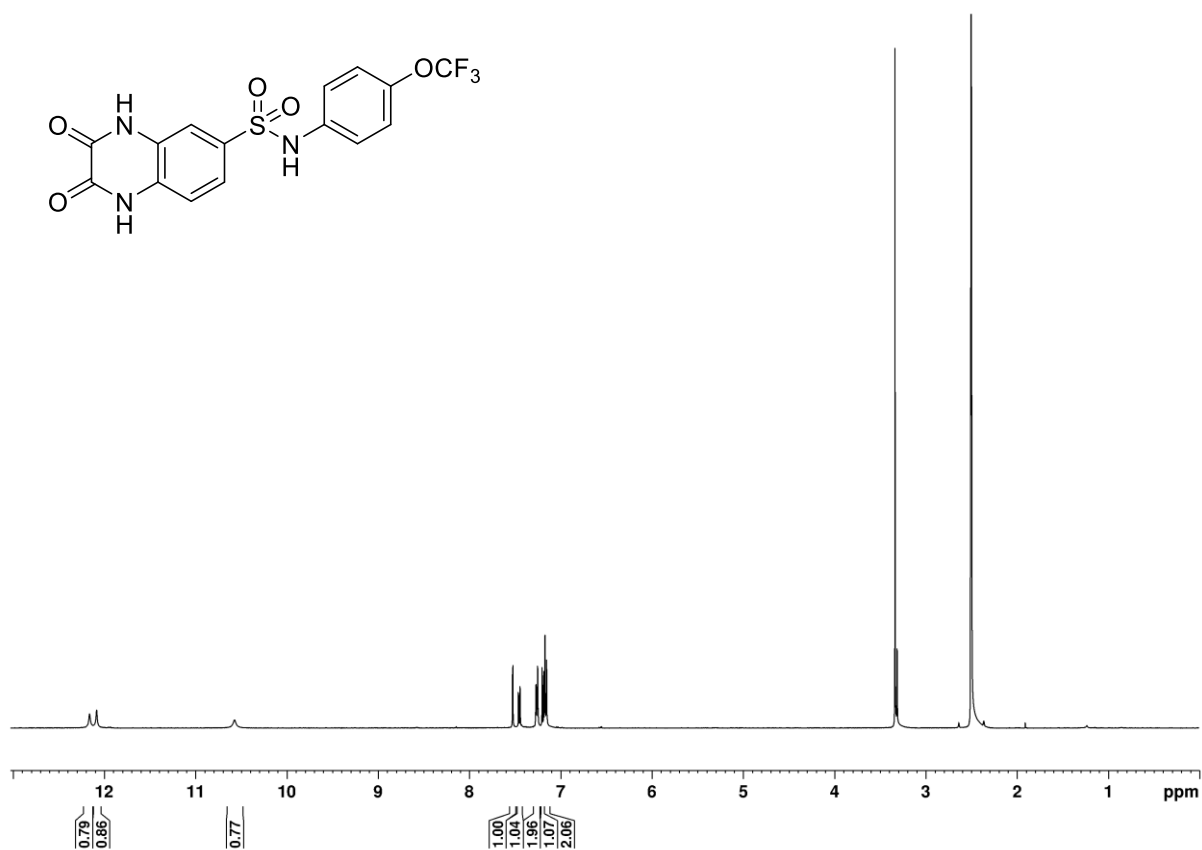
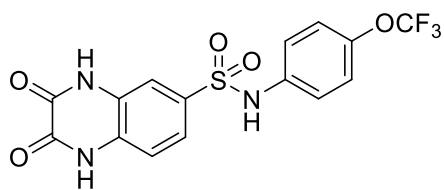
***N*-(4-(*tert*-Butyl)phenethyl)quinoxaline-6-sulfonamide (S13)**



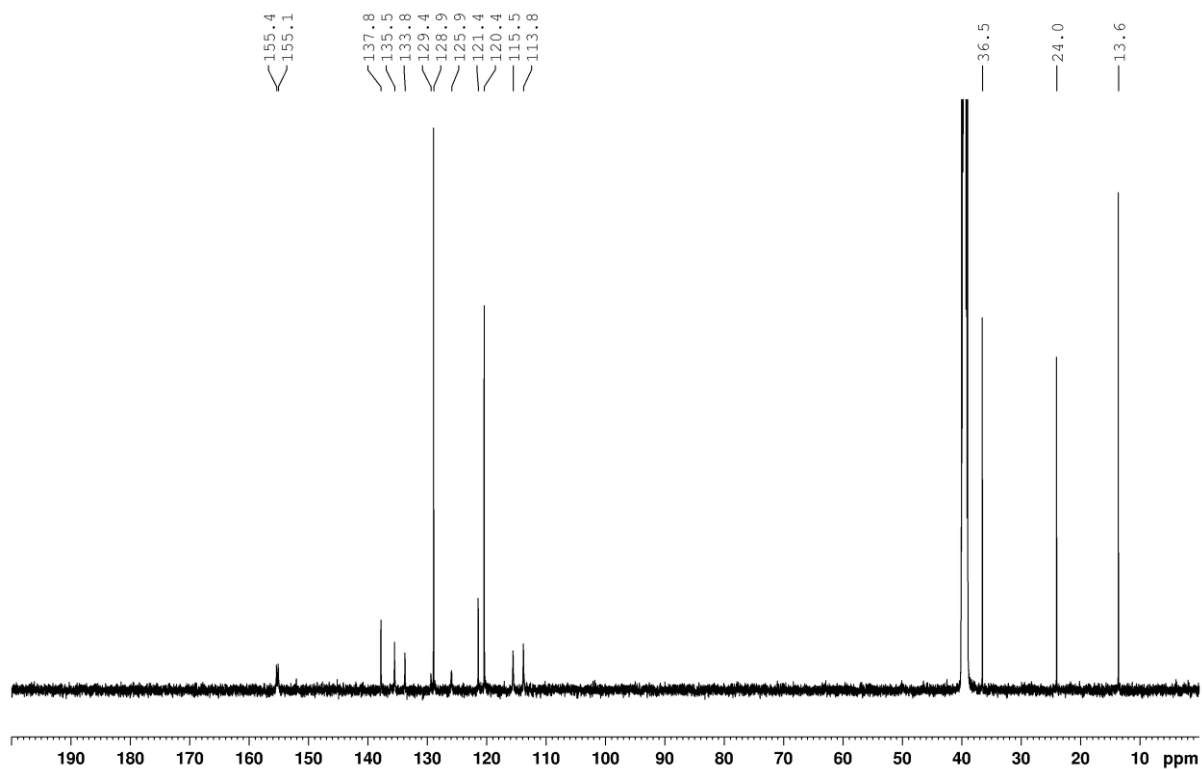
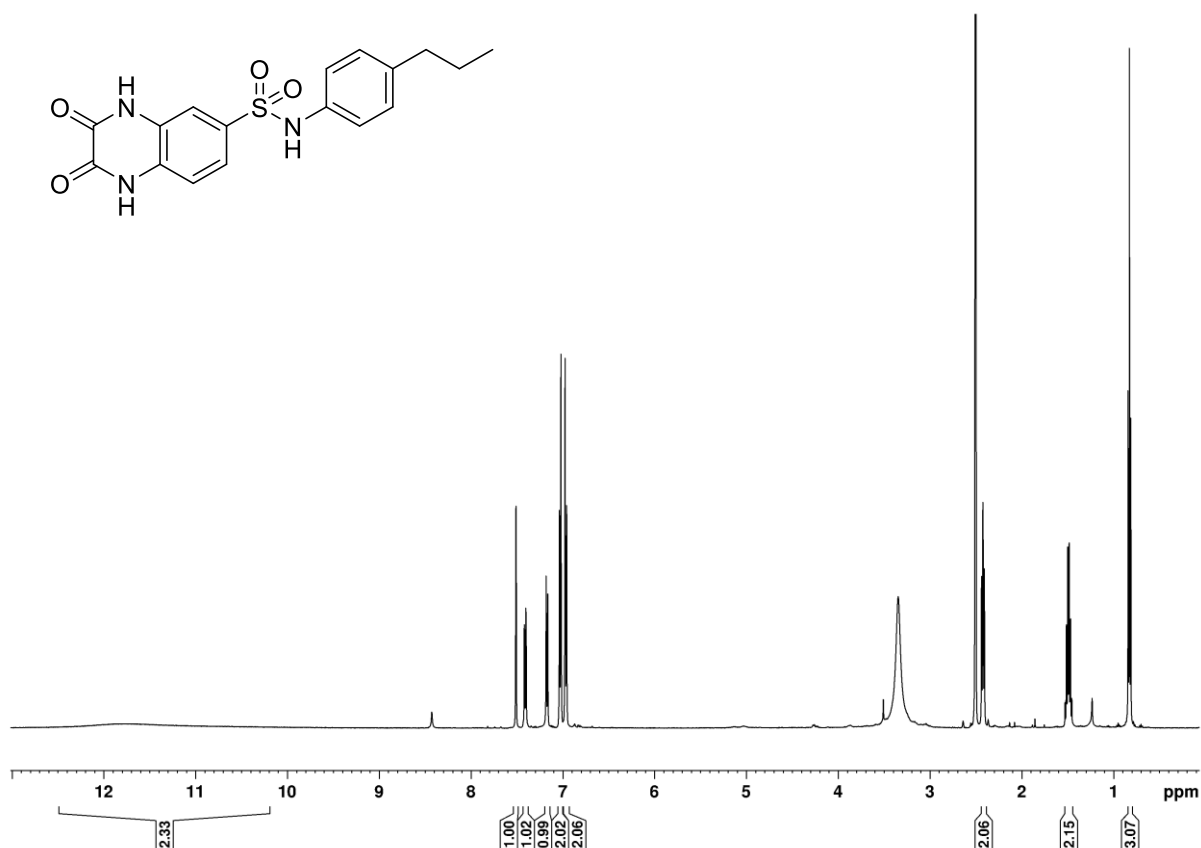
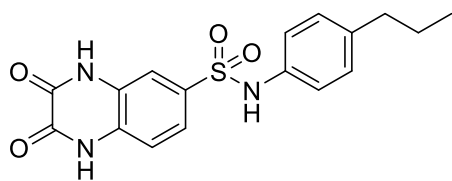
***N*-(4-(*tert*-Butyl)phenethyl)-2-oxo-2,3-dihydro-1H-benzo[d]imidazole-5-sulfonamide (S14)**



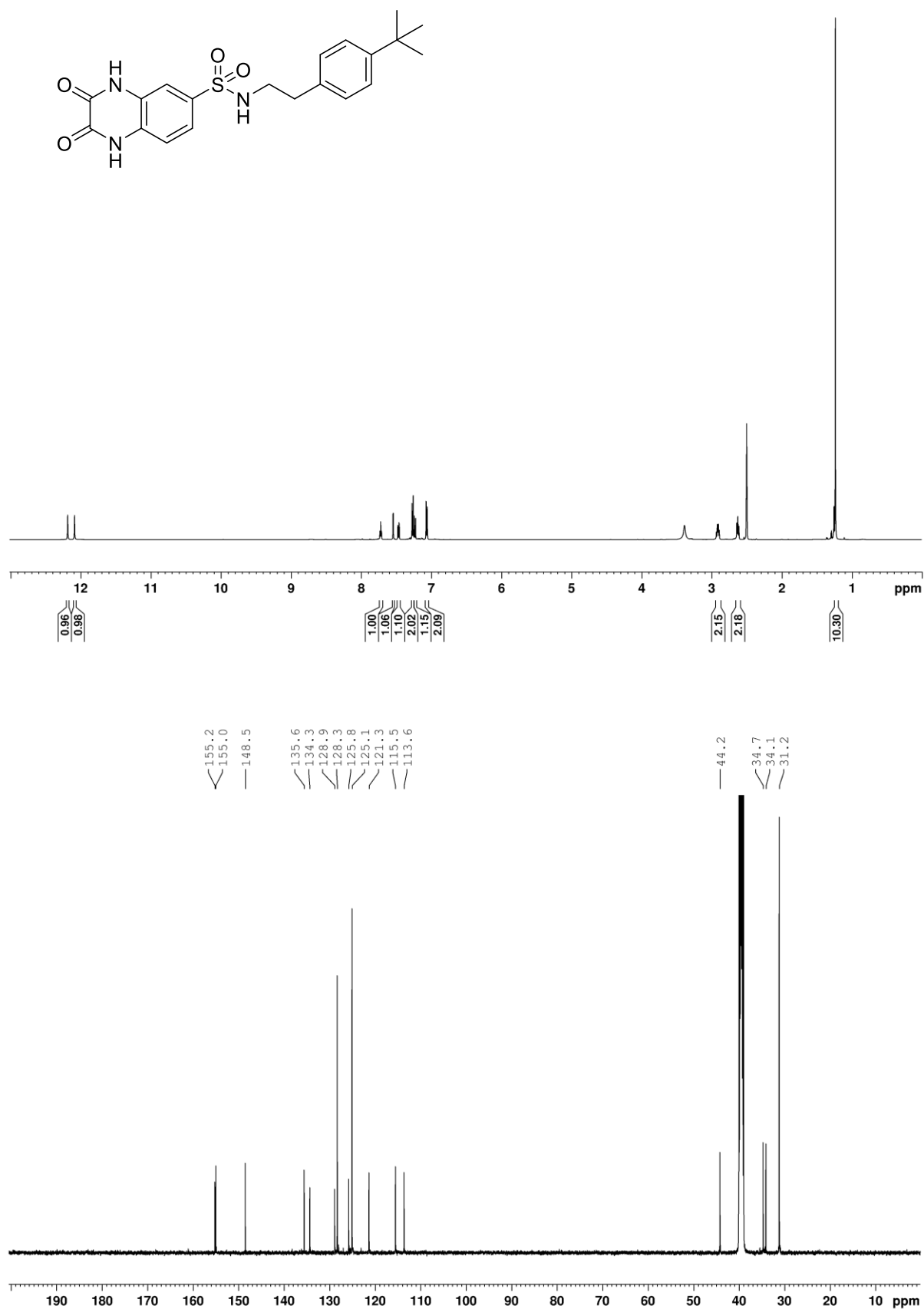
2,3-Dioxo-*N*-(4-(trifluoromethoxy)phenyl)-1,2,3,4-tetrahydroquinoxaline-6-sulfonamide (S2)



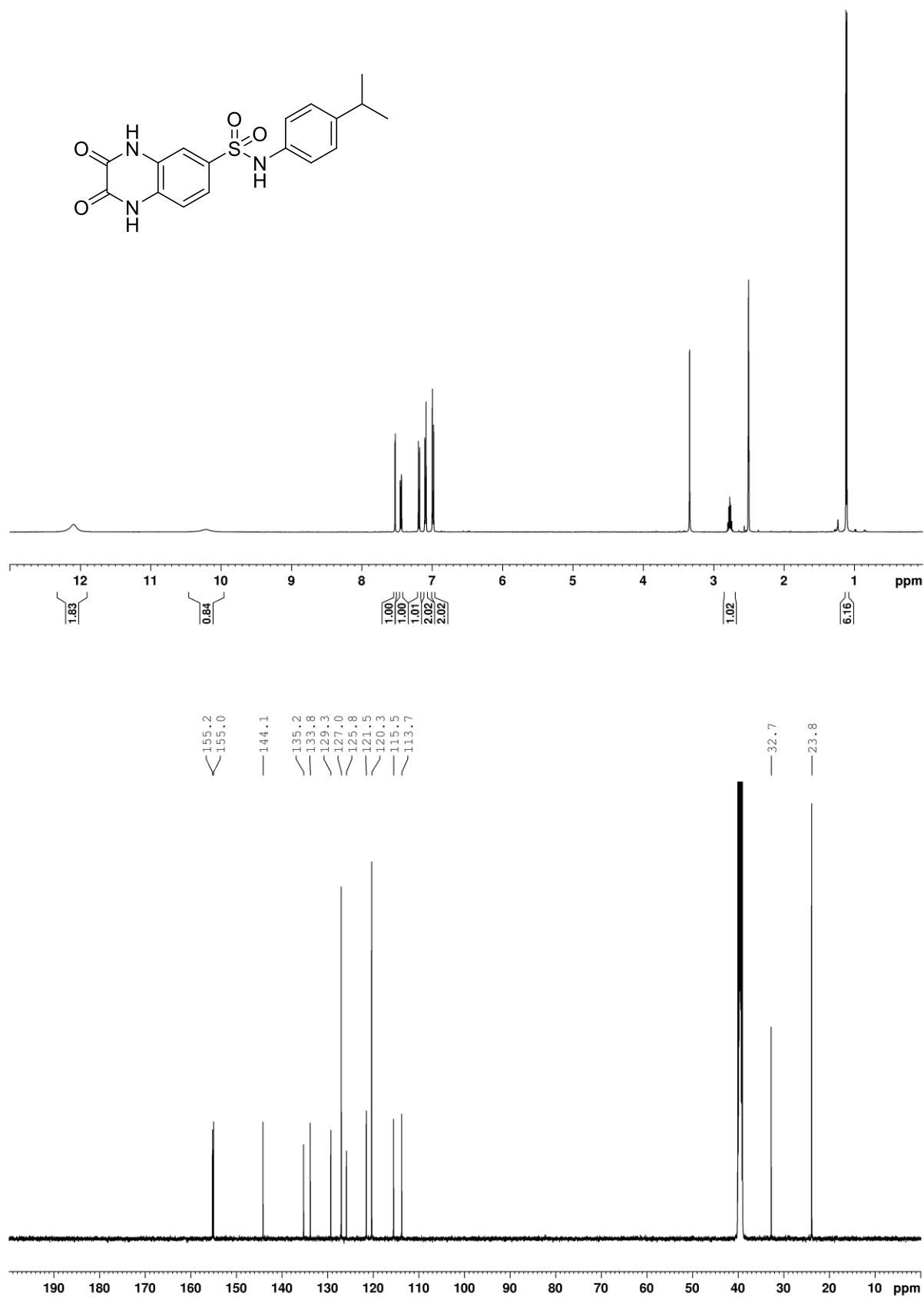
2,3-Dioxo-*N*-(4-propylphenyl)-1,2,3,4-tetrahydroquinoxaline-6-sulfonamide (S1)



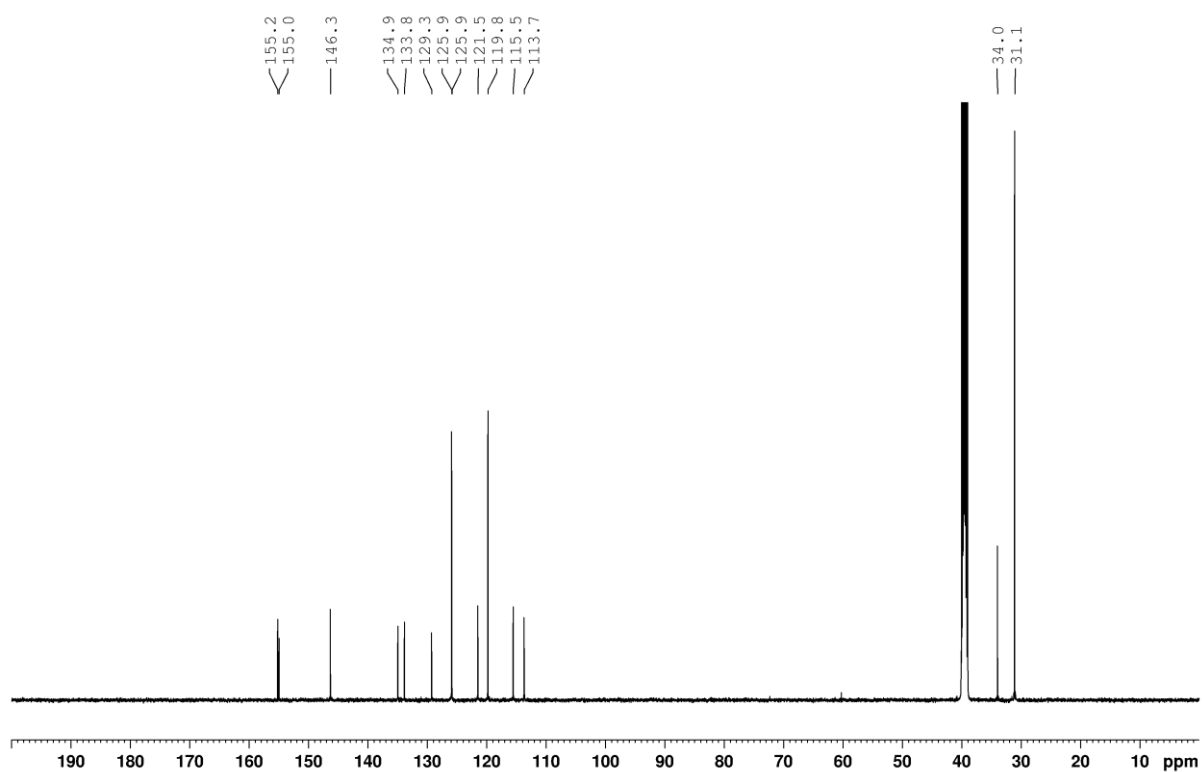
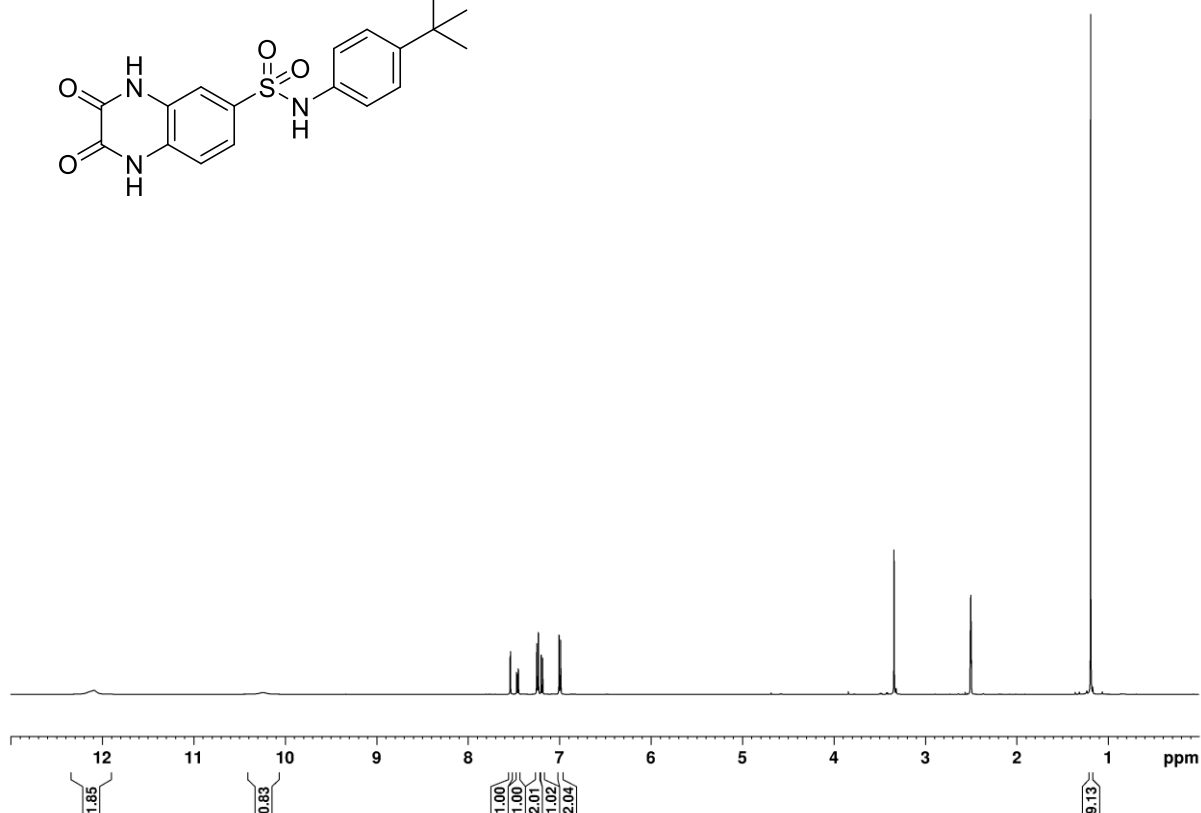
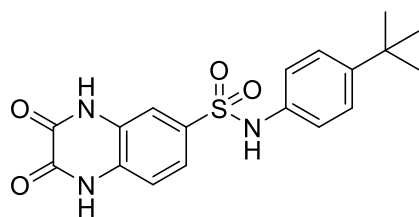
***N*-(4-(*tert*-Butyl)phenethyl)-2,3-dioxo-1,2,3,4-tetrahydroquinoxaline-6-sulfonamide (4)**



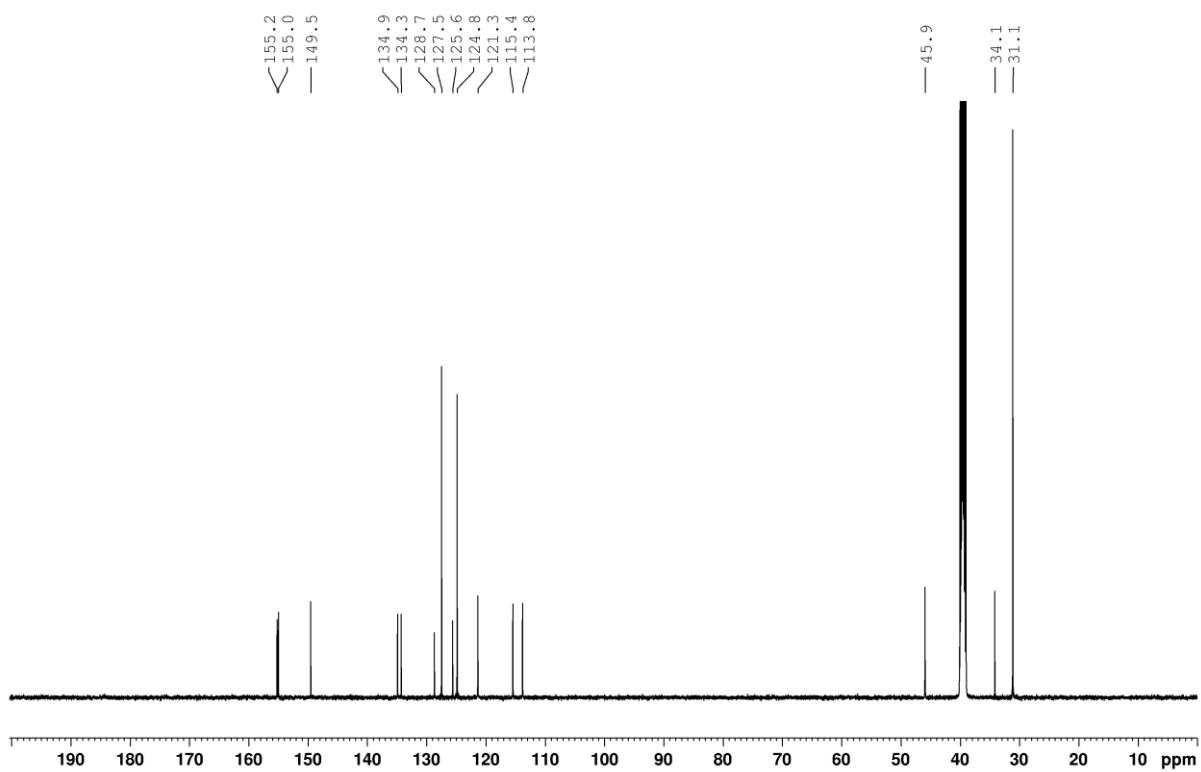
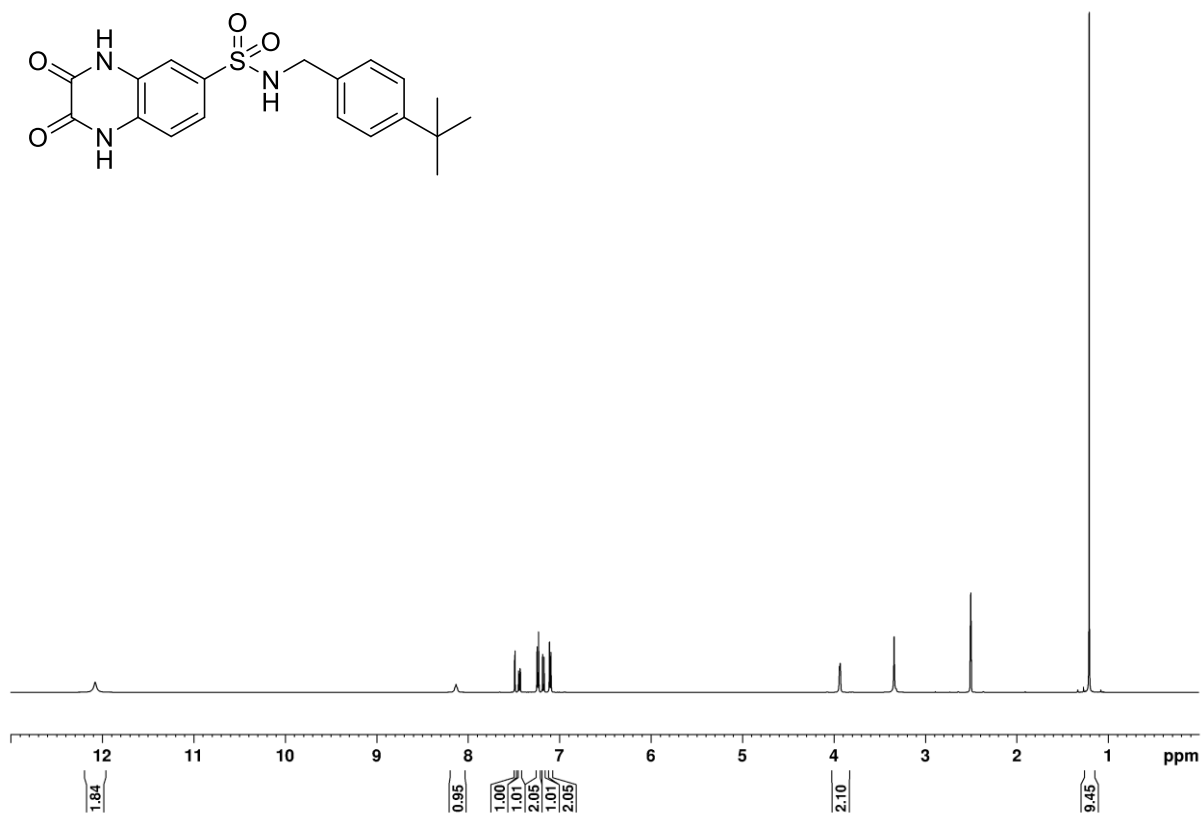
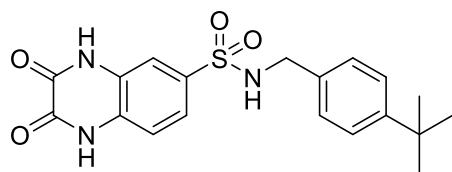
***N*-(4-Isopropylphenyl)-2,3-dioxo-1,2,3,4-tetrahydroquinoxaline-6-sulfonamide (10)**



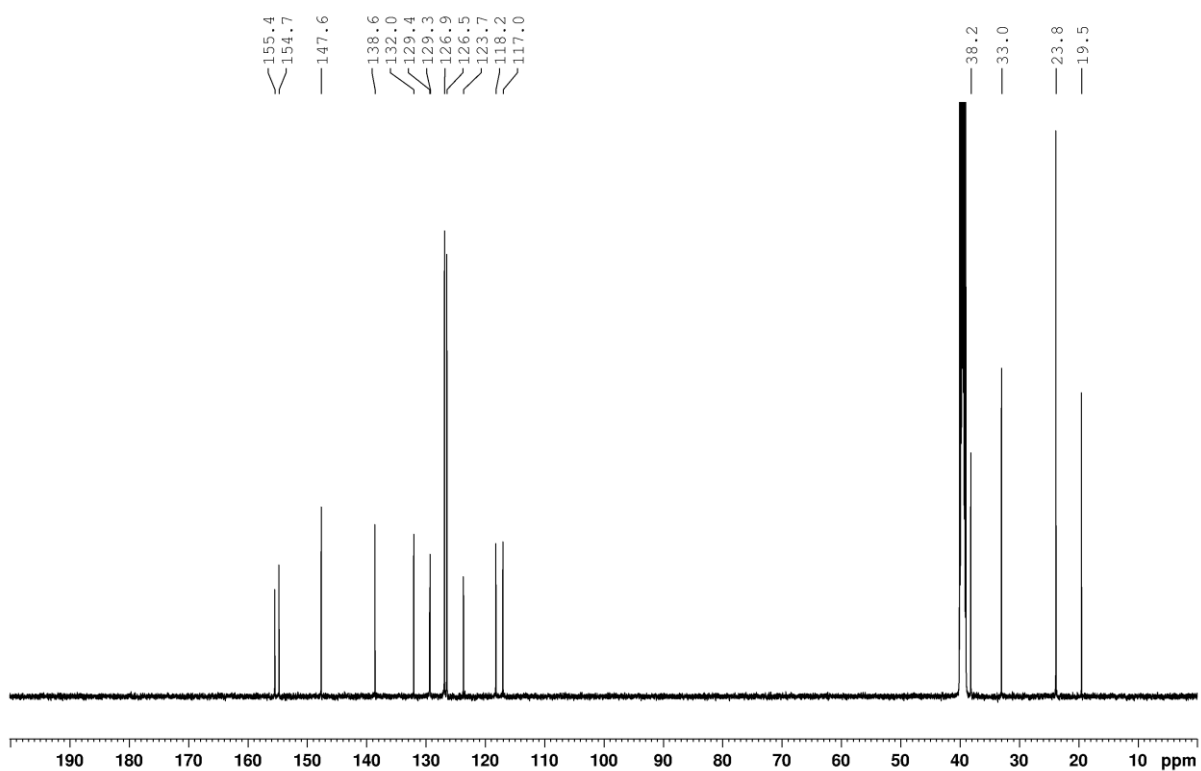
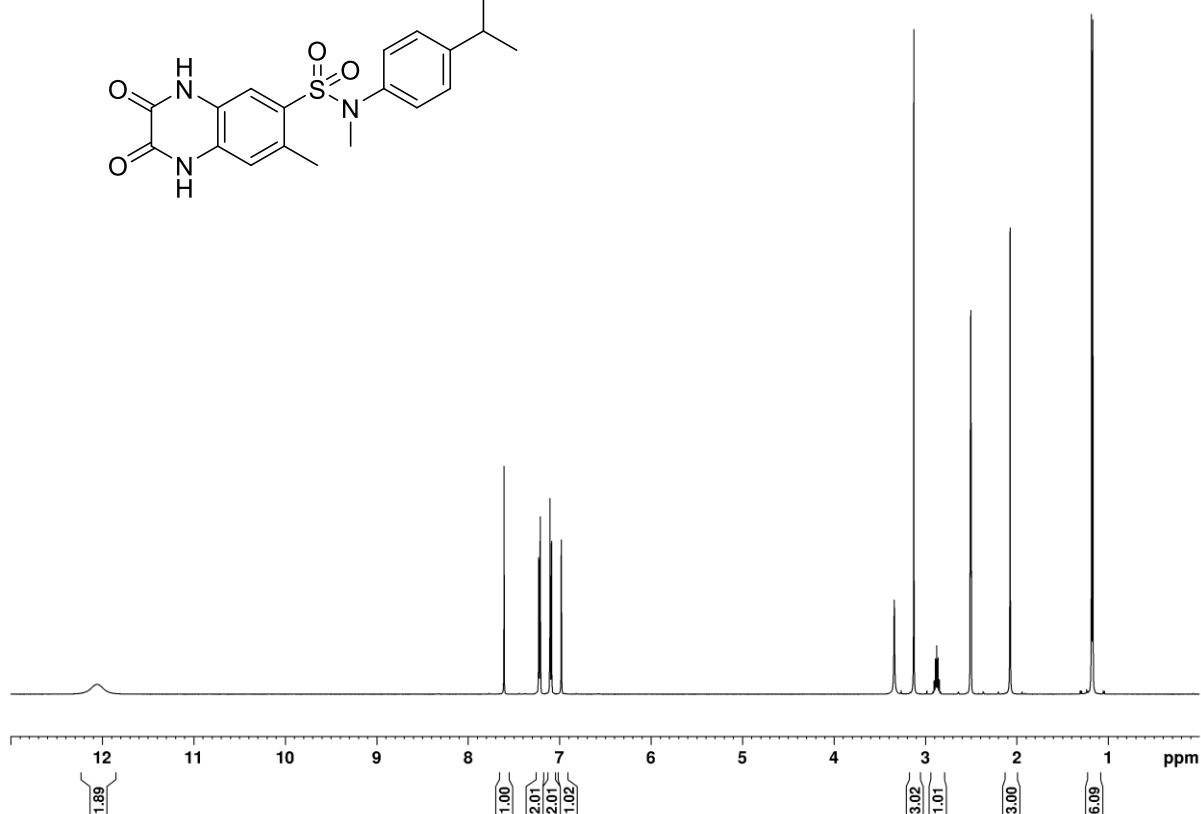
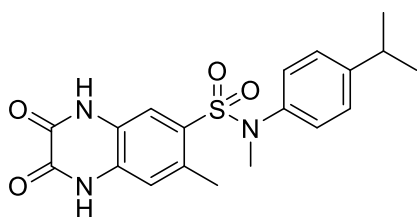
***N*-(4-(*tert*-Butyl)phenyl)-2,3-dioxo-1,2,3,4-tetrahydroquinoxaline-6-sulfonamide (5)**



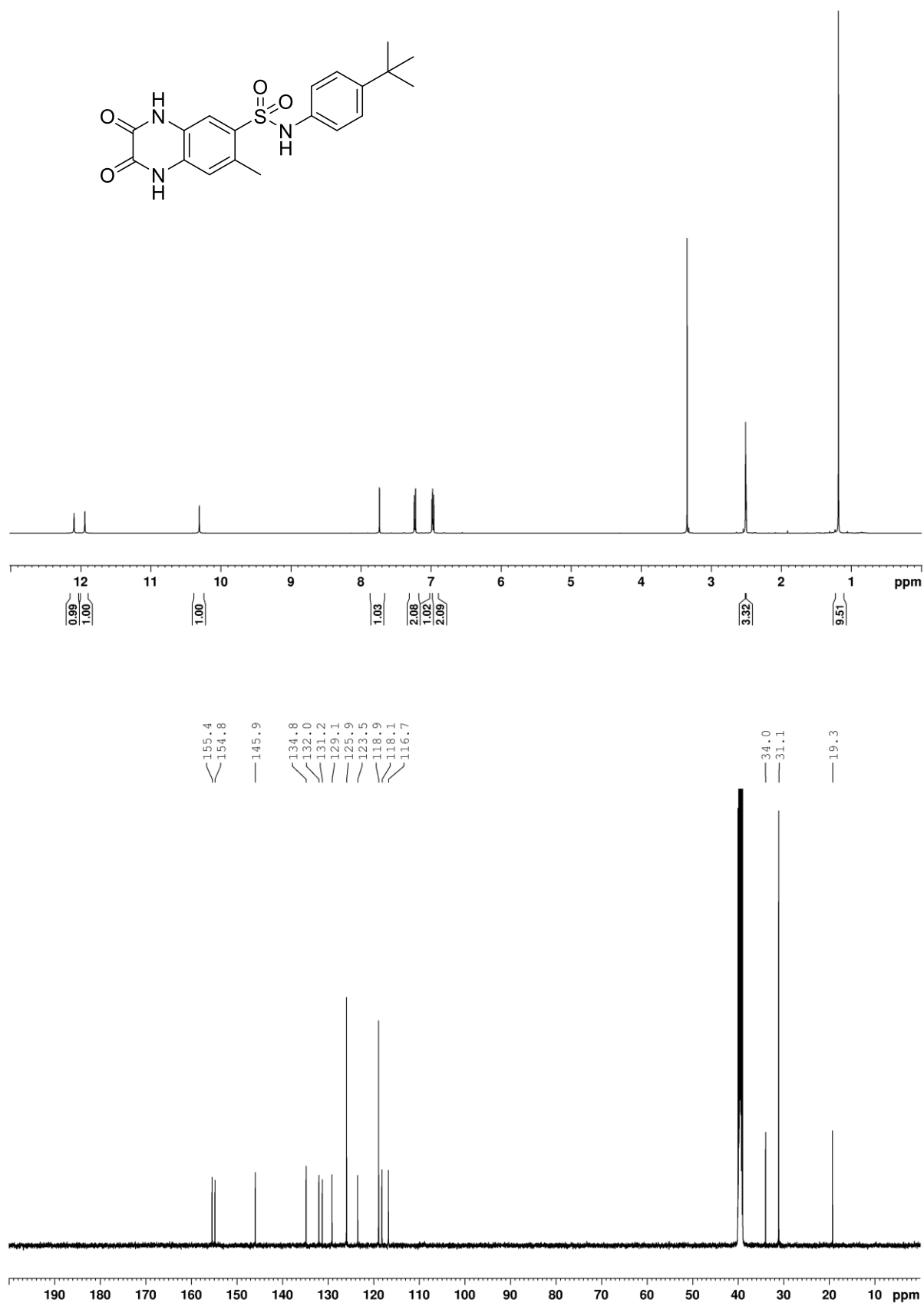
***N*-(4-(*tert*-Butyl)benzyl)-2,3-dioxo-1,2,3,4-tetrahydroquinoxaline-6-sulfonamide (17)**



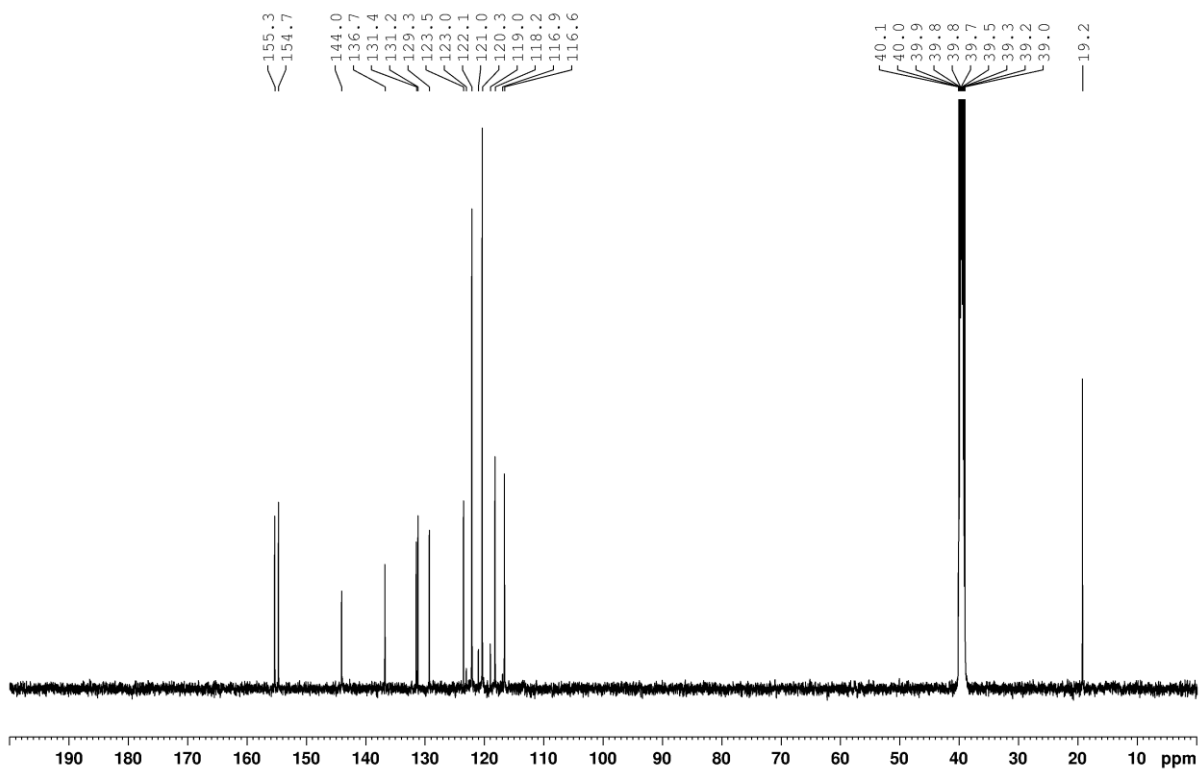
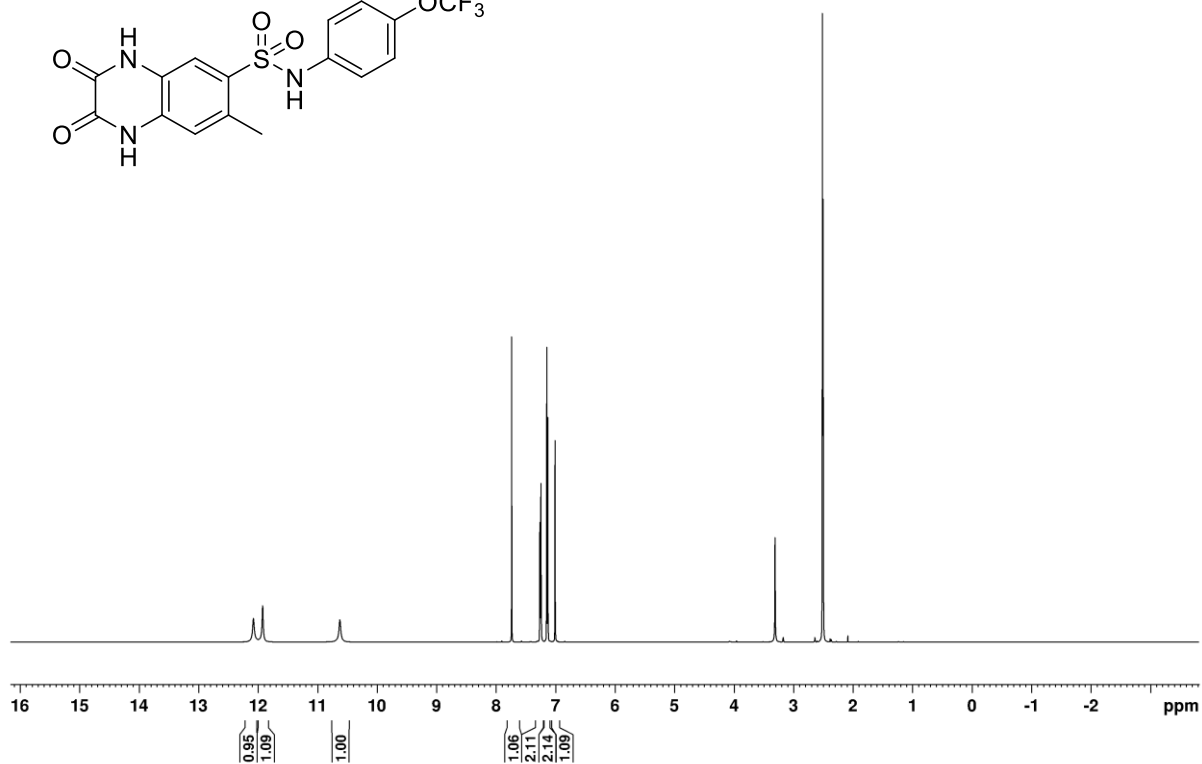
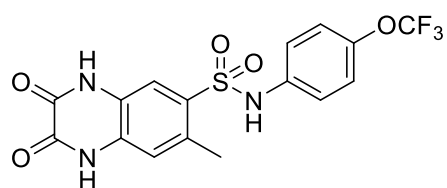
***N*-(4-Isopropylphenyl)-*N*,7-dimethyl-2,3-dioxo-1,2,3,4-tetrahydroquinoxaline-6-sulfonamide (6)**



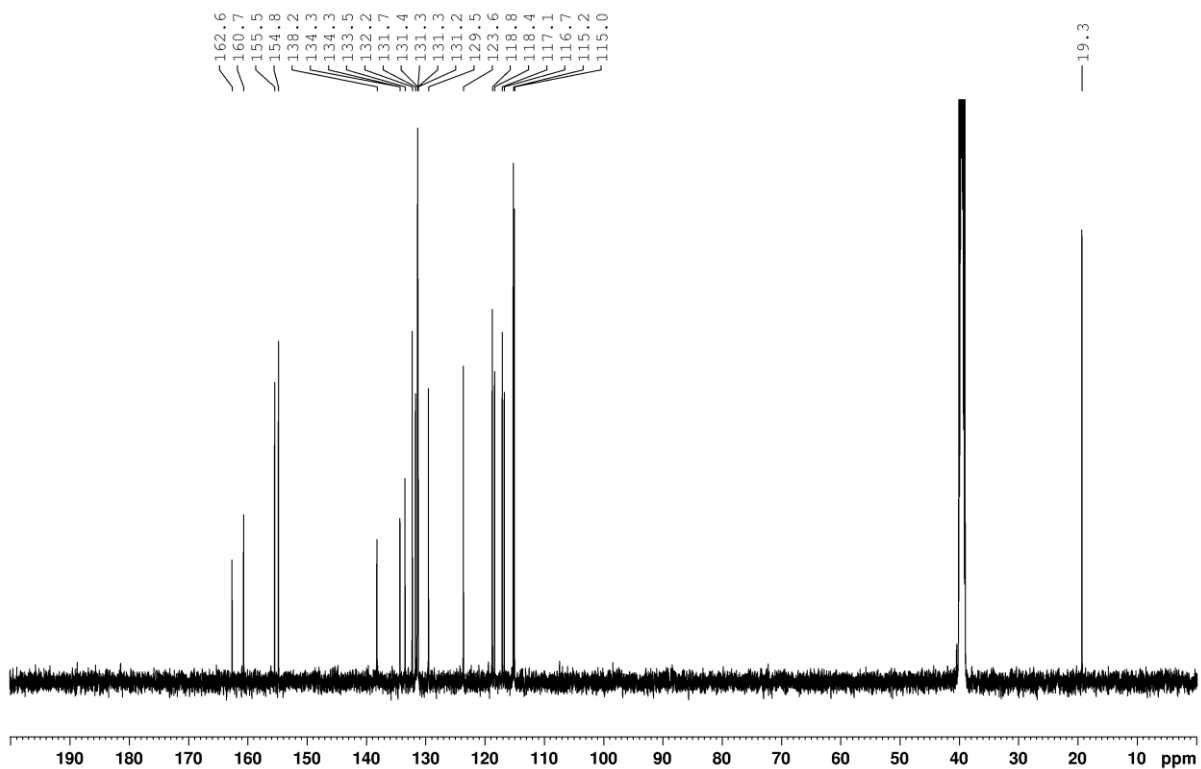
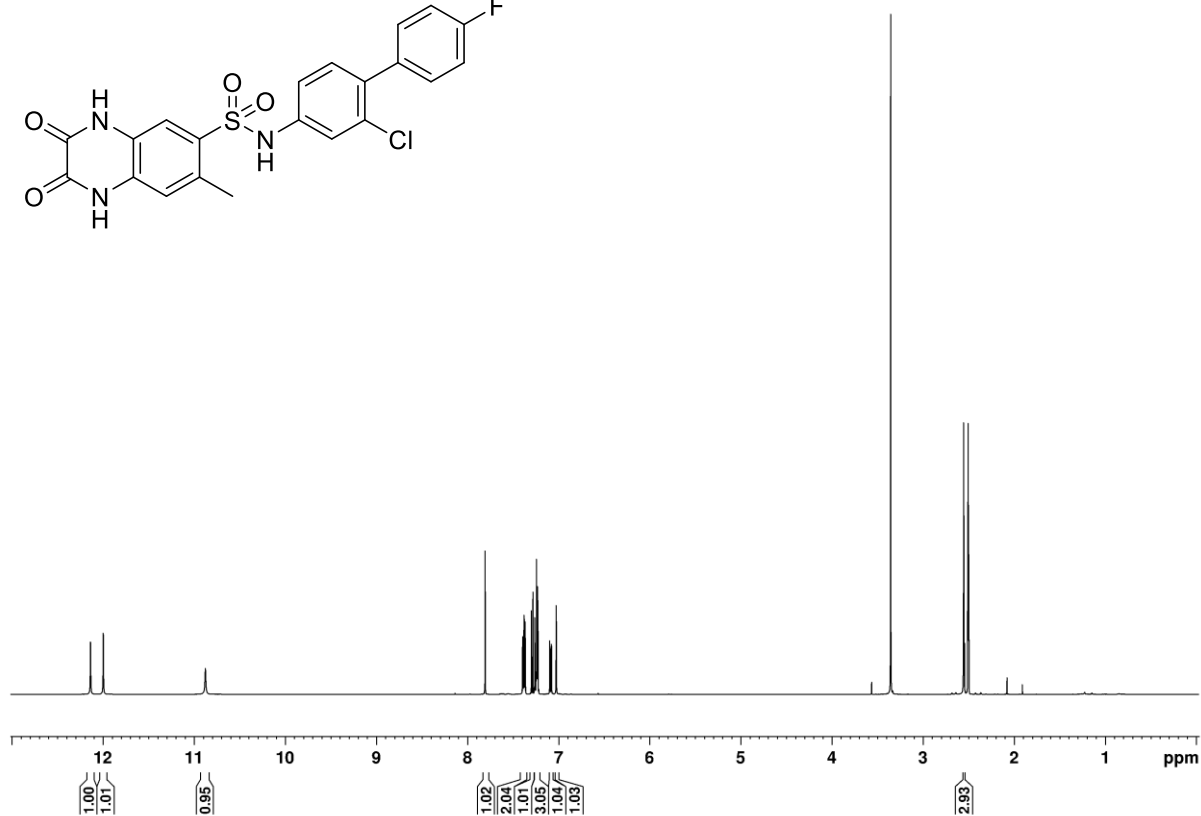
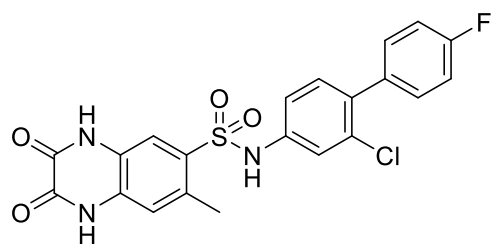
***N*-(4-(*tert*-Butyl)phenyl)-7-methyl-2,3-dioxo-1,2,3,4-tetrahydroquinoxaline-6-sulfonamide (11)**



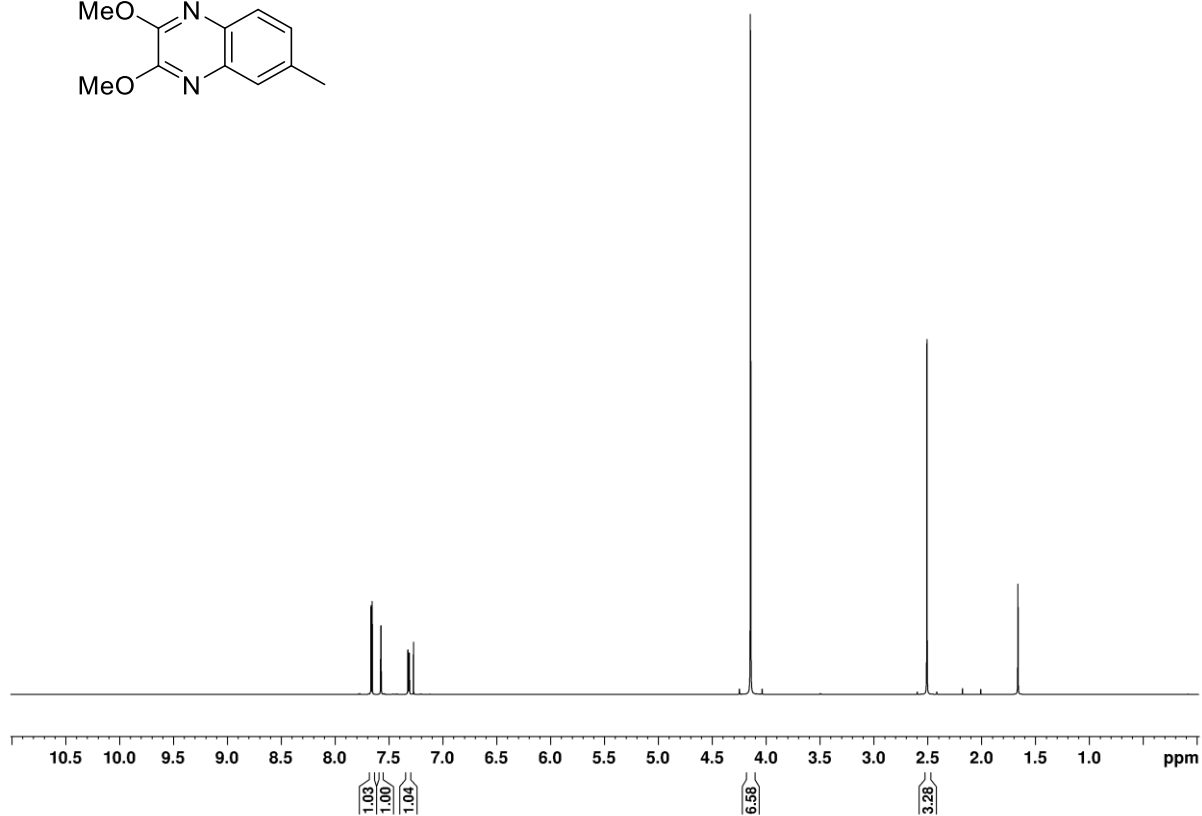
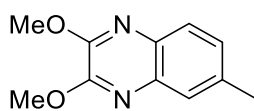
7-Methyl-2,3-dioxo-*N*-(4-(trifluoromethoxy)phenyl)-1,2,3,4-tetrahydroquinoxaline-6-sulfonamide (H831)



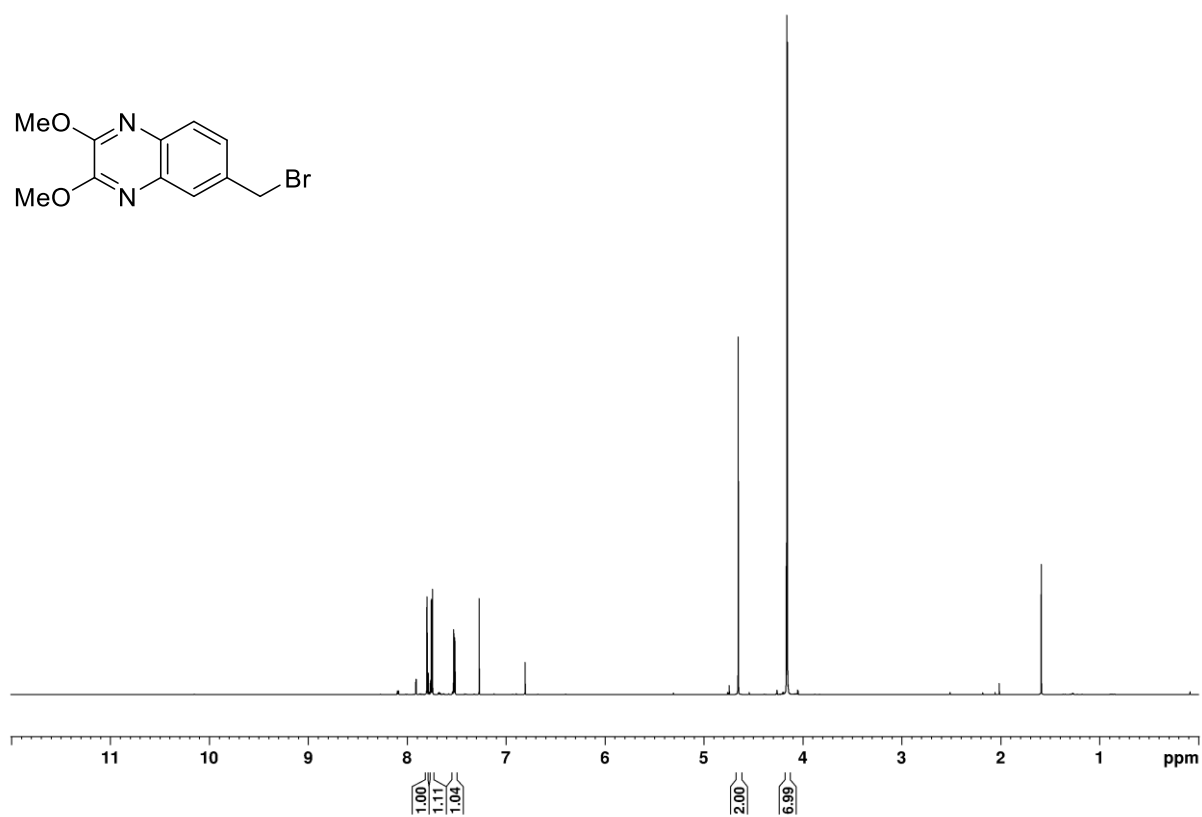
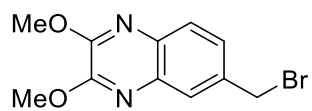
***N*-(2-chloro-4'-fluoro-[1,1'-biphenyl]-4-yl)-7-methyl-2,3-dioxo-1,2,3,4-tetrahydroquinoxaline-6-sulfonamide (H052)**



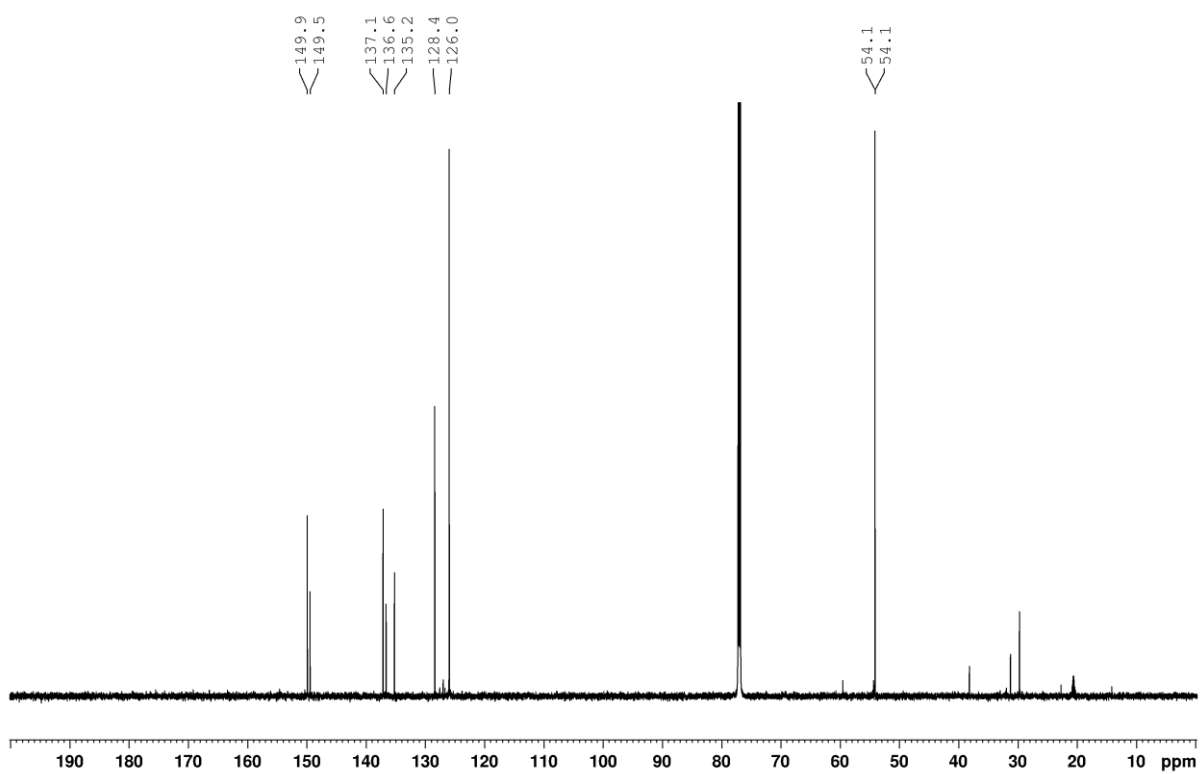
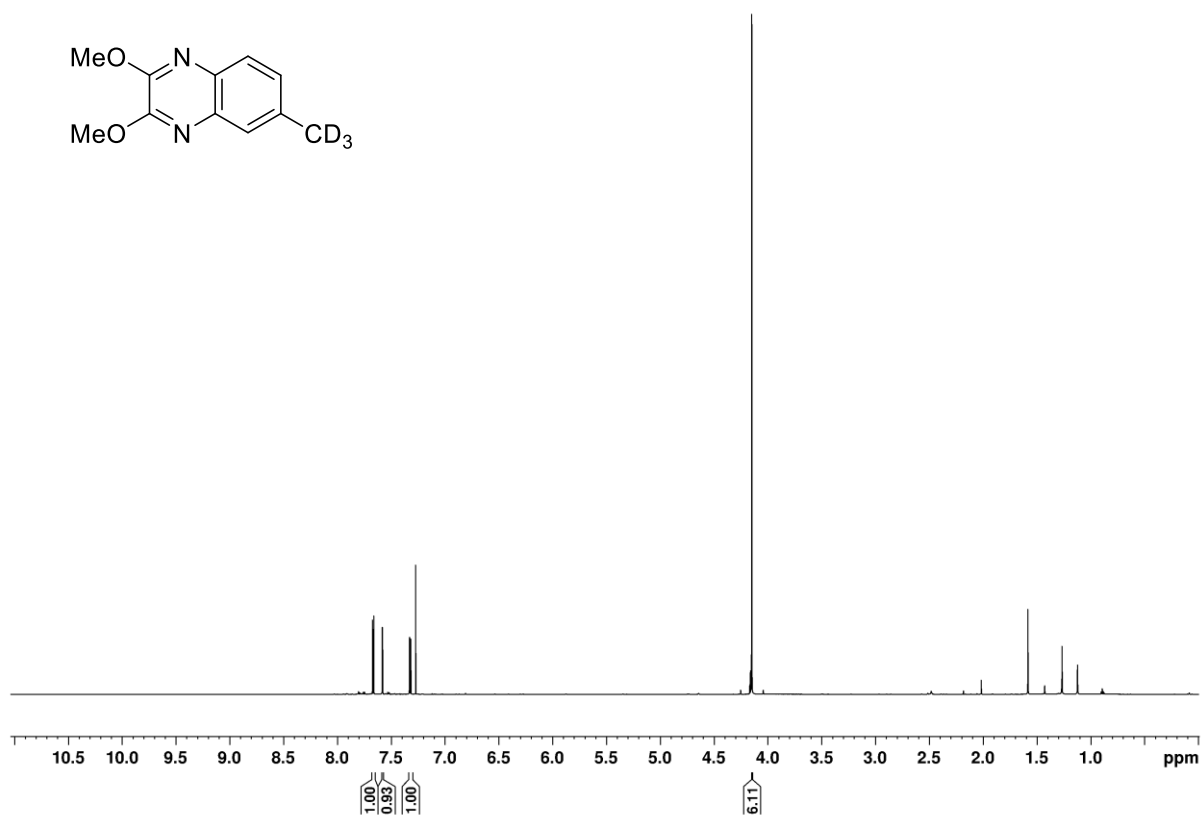
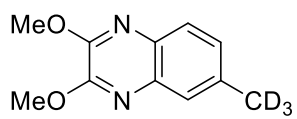
2,3-Dimethoxy-6-methylquinoxaline (S31)



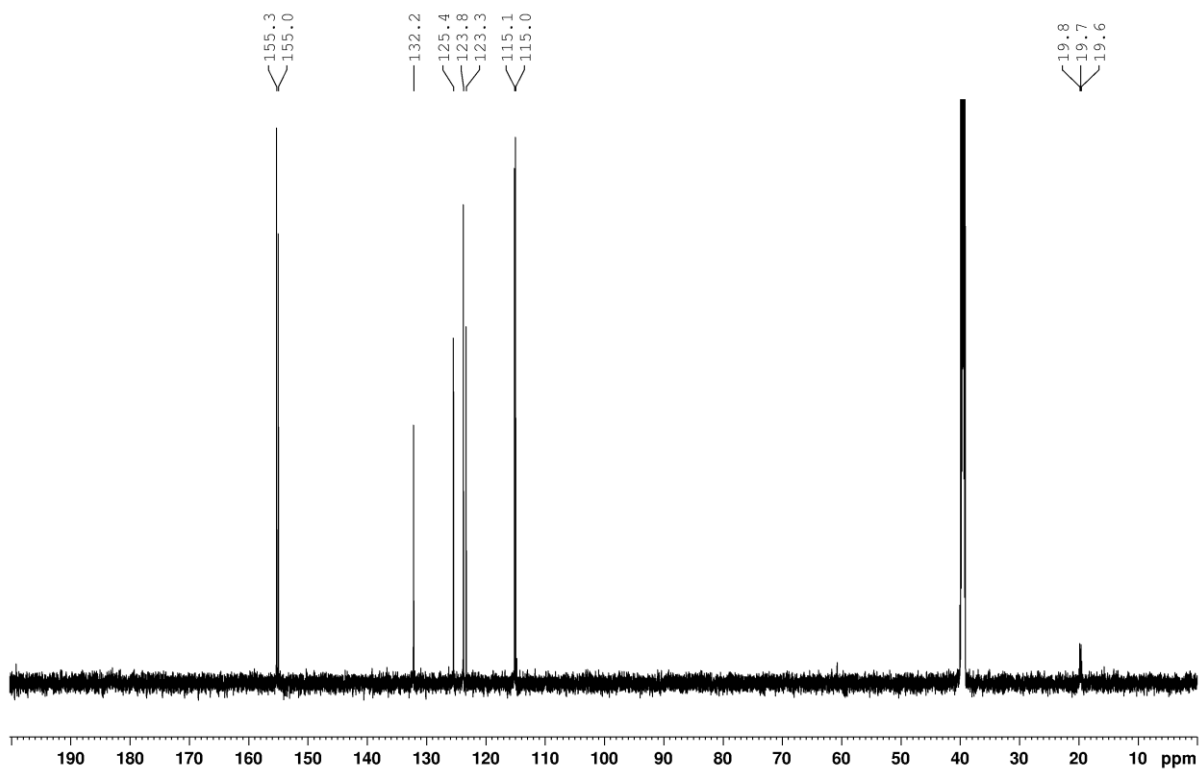
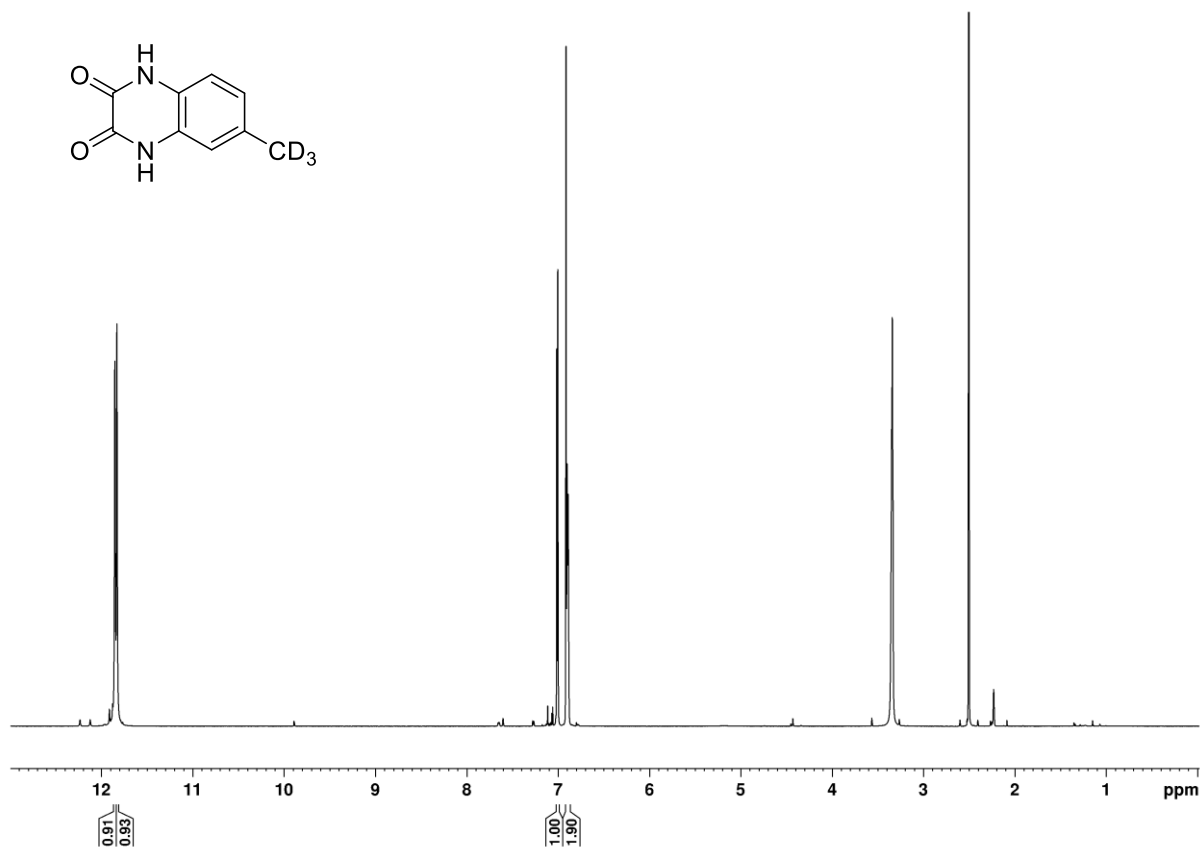
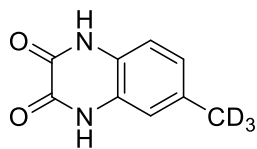
6-(Bromomethyl)-2,3-dimethoxyquinoxaline (S32)



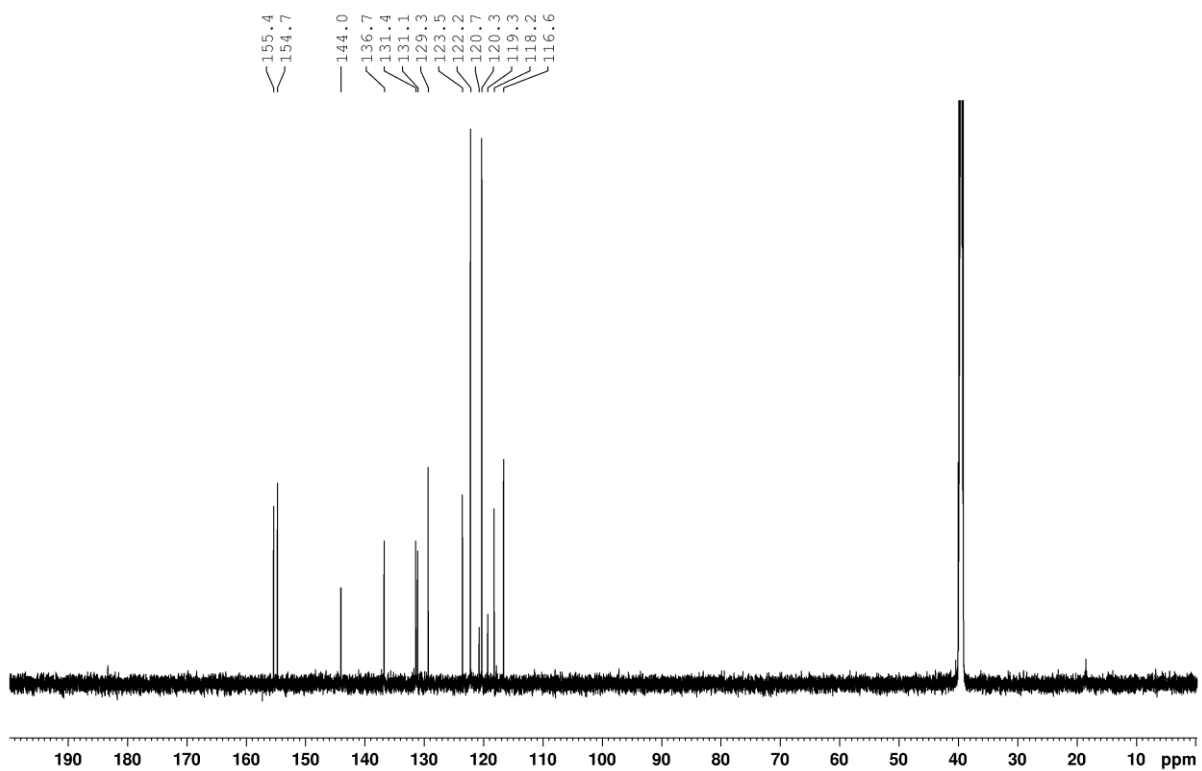
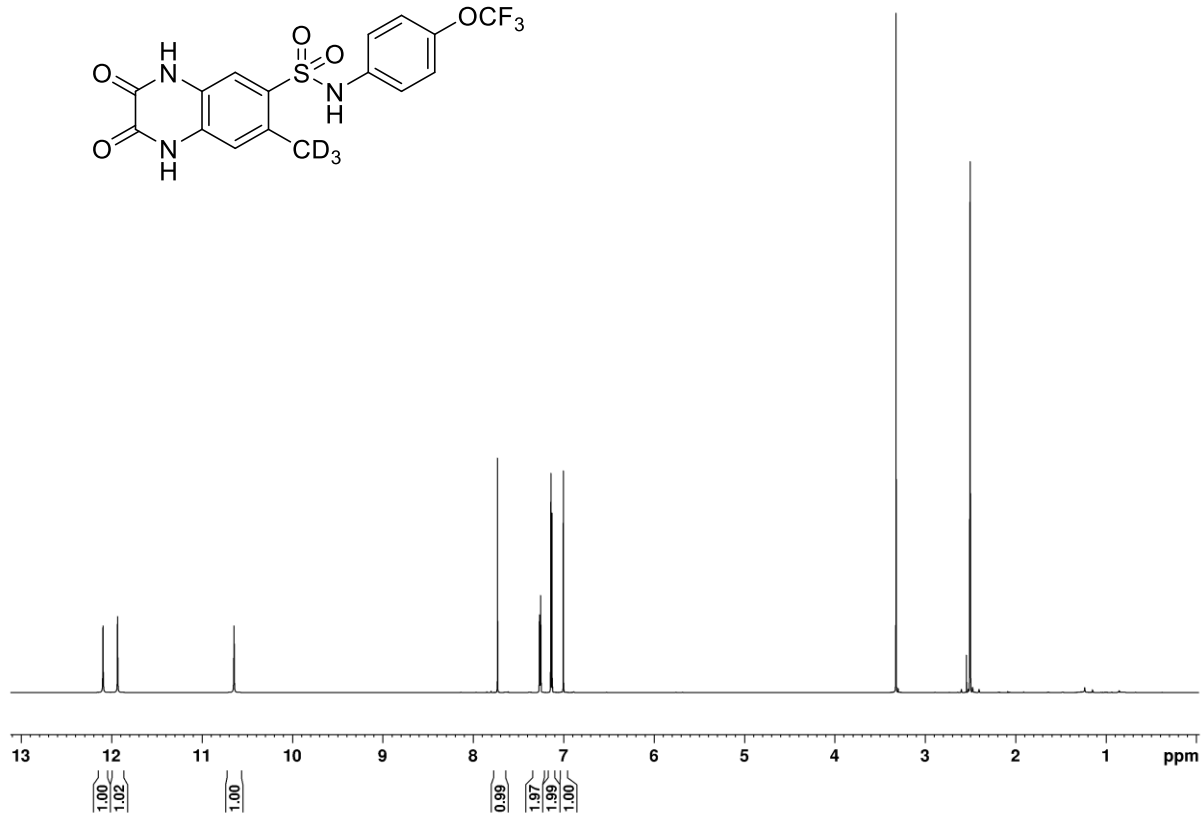
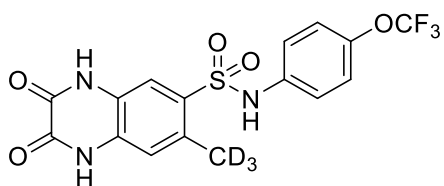
2,3-Dimethoxy-6-(methyl- d_3)quinoxaline (S34)



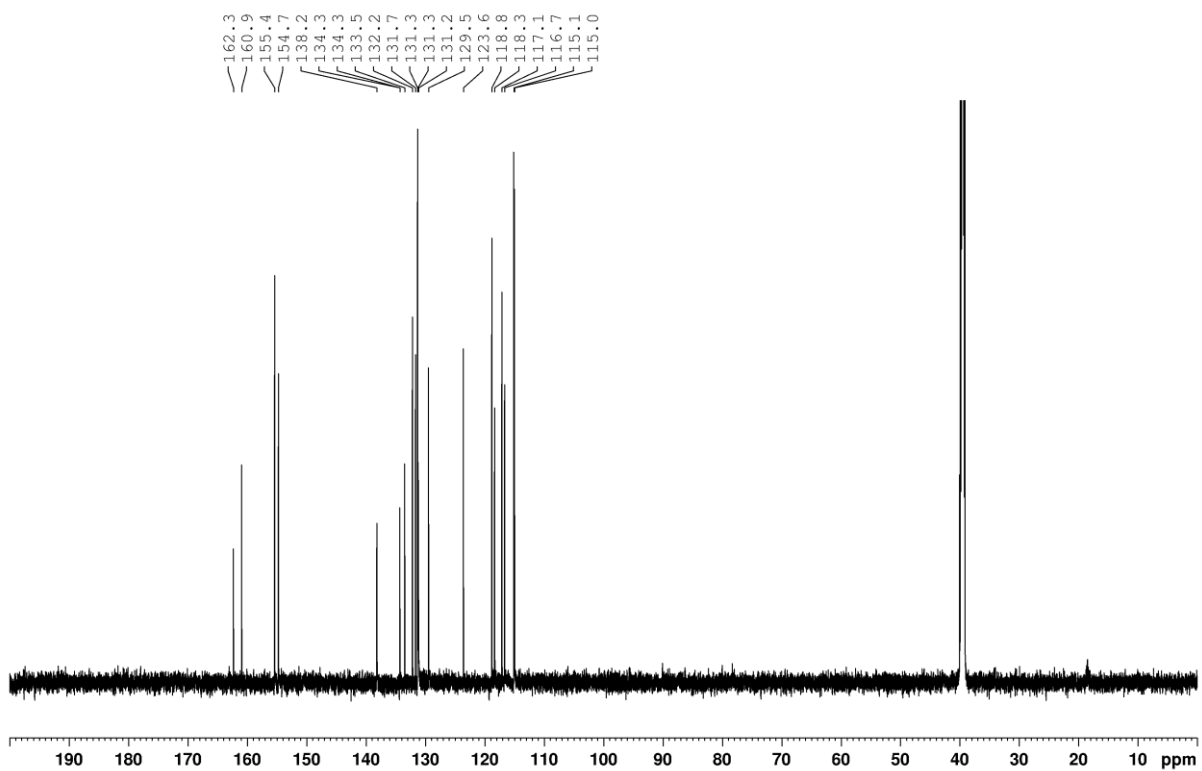
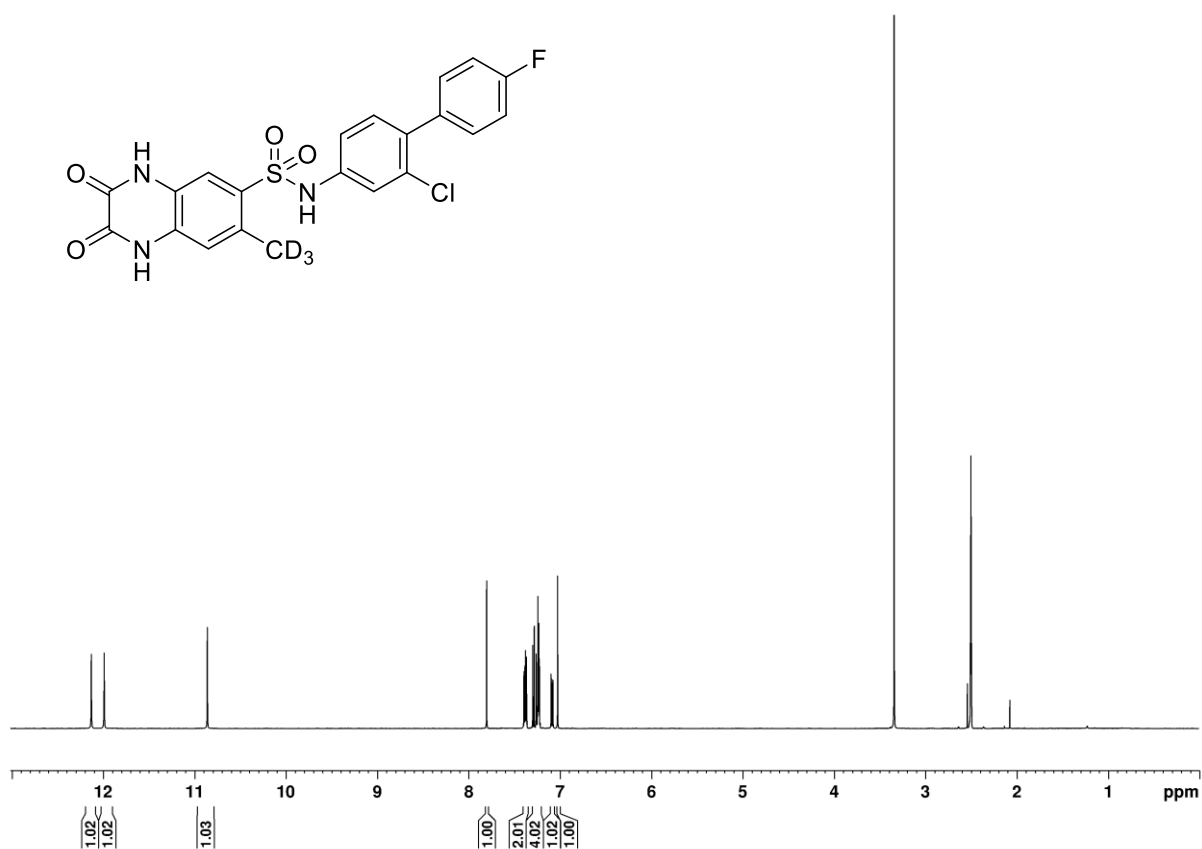
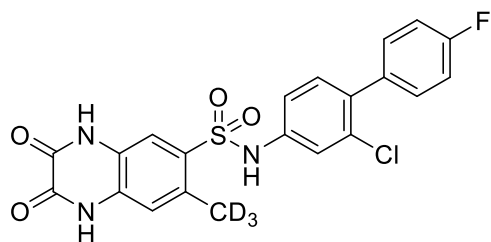
6-(Methyl- d_3)-1,4-dihydroquinoxaline-2,3-dione (S35)



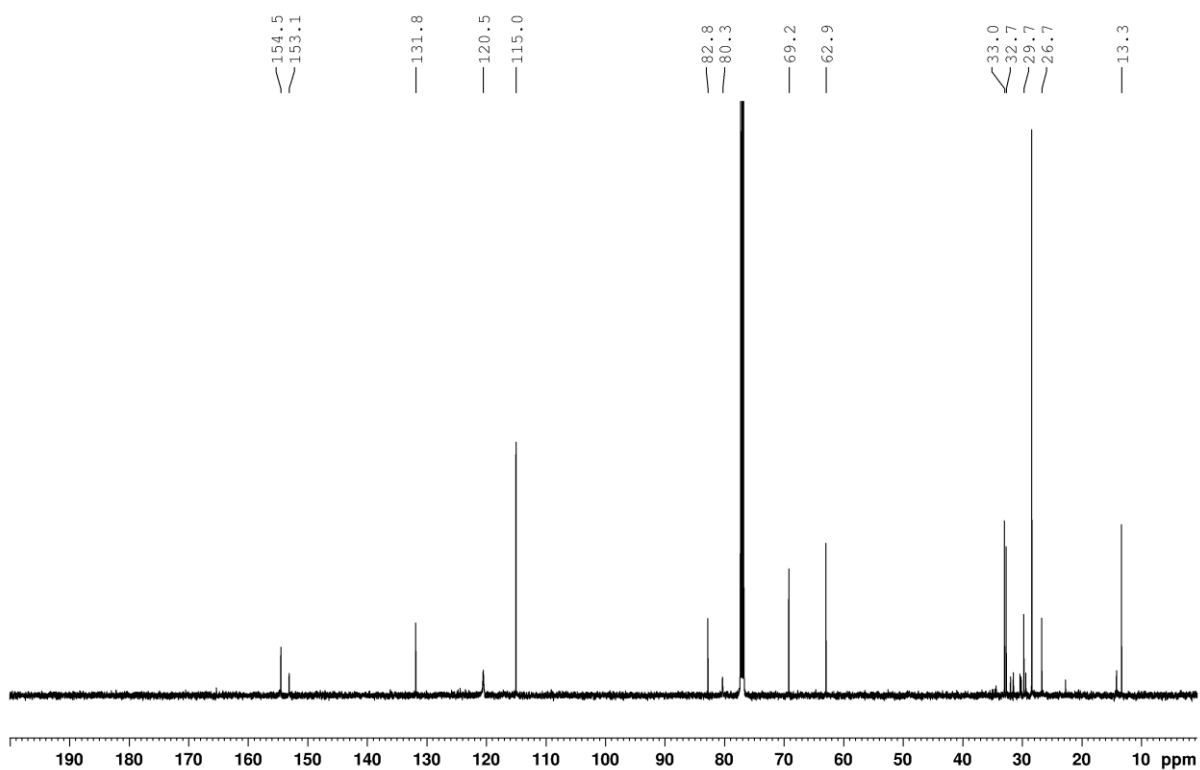
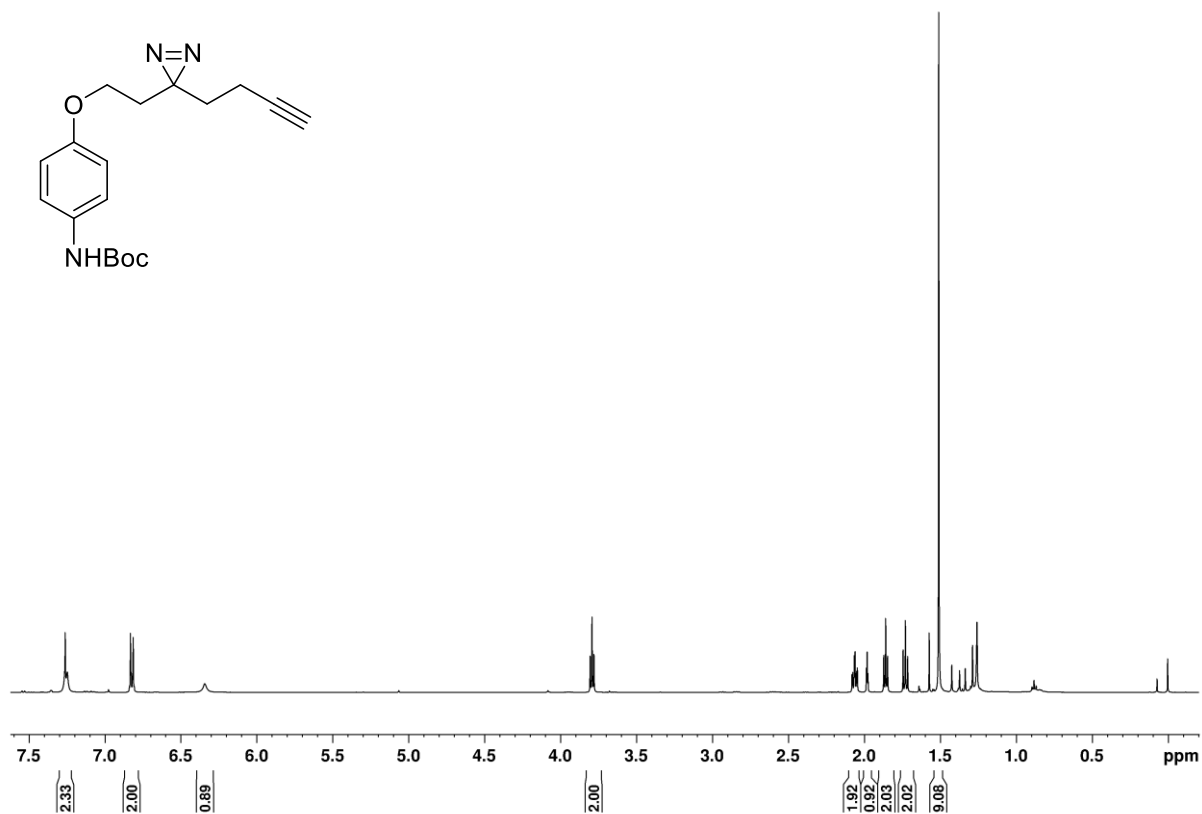
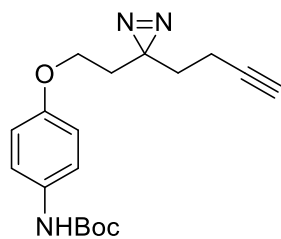
7-(Methyl- d_3)-2,3-dioxo-*N*-(4-(trifluoromethoxy)phenyl)-1,2,3,4-tetrahydroquinoxaline-6-sulfonamide (S4)



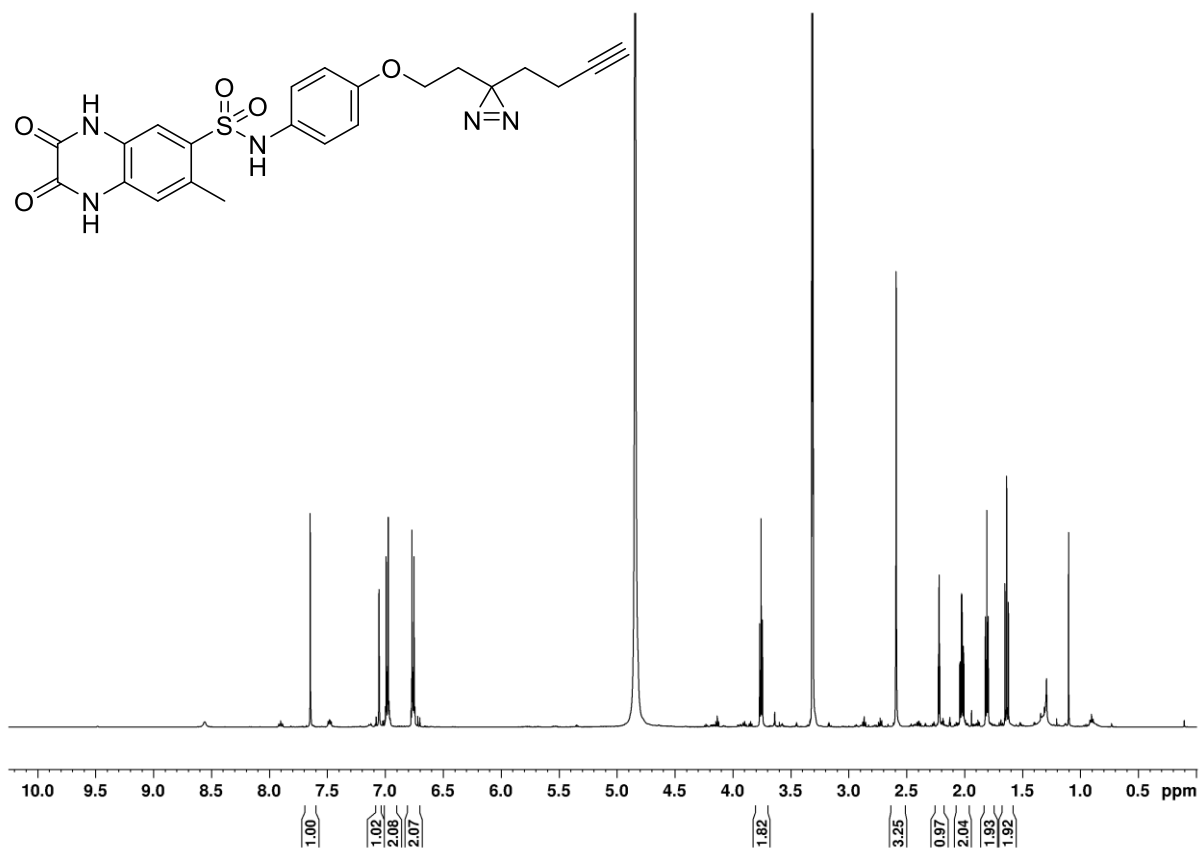
***N*-(2-chloro-4'-fluoro-[1,1'-biphenyl]-4-yl)-7-(methyl-*d*₃)-2,3-dioxo-1,2,3,4-tetrahydroquinoxaline-6-sulfonamide (S5)**



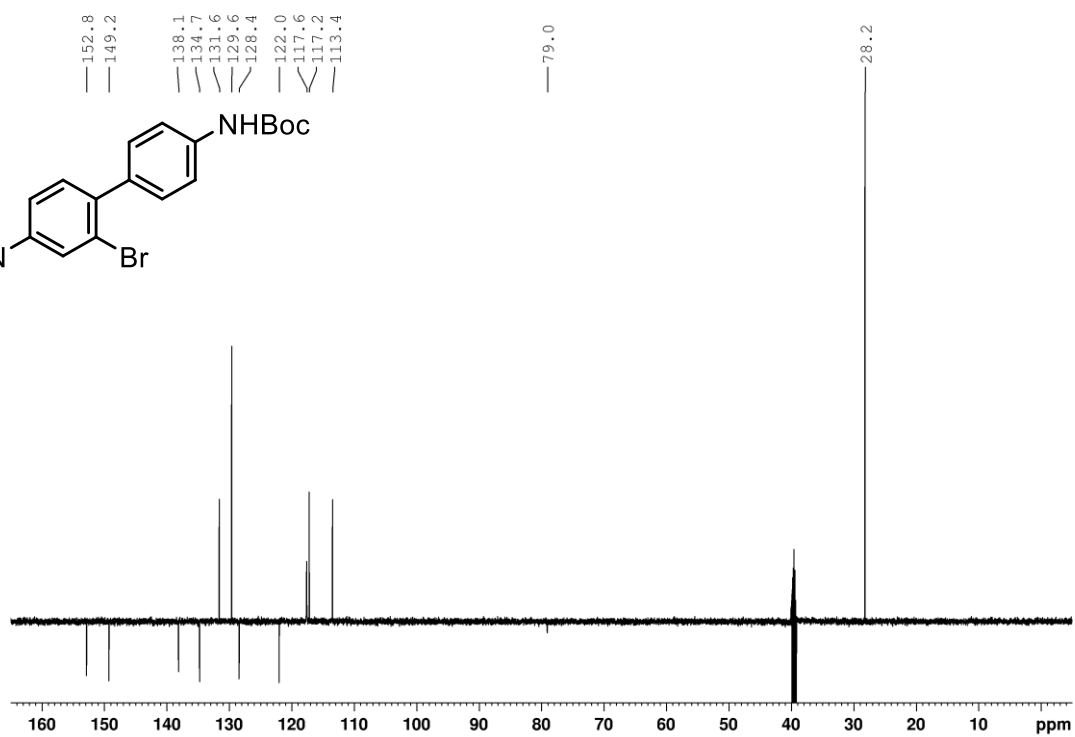
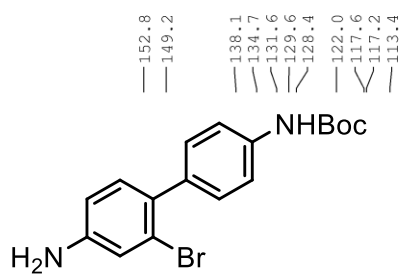
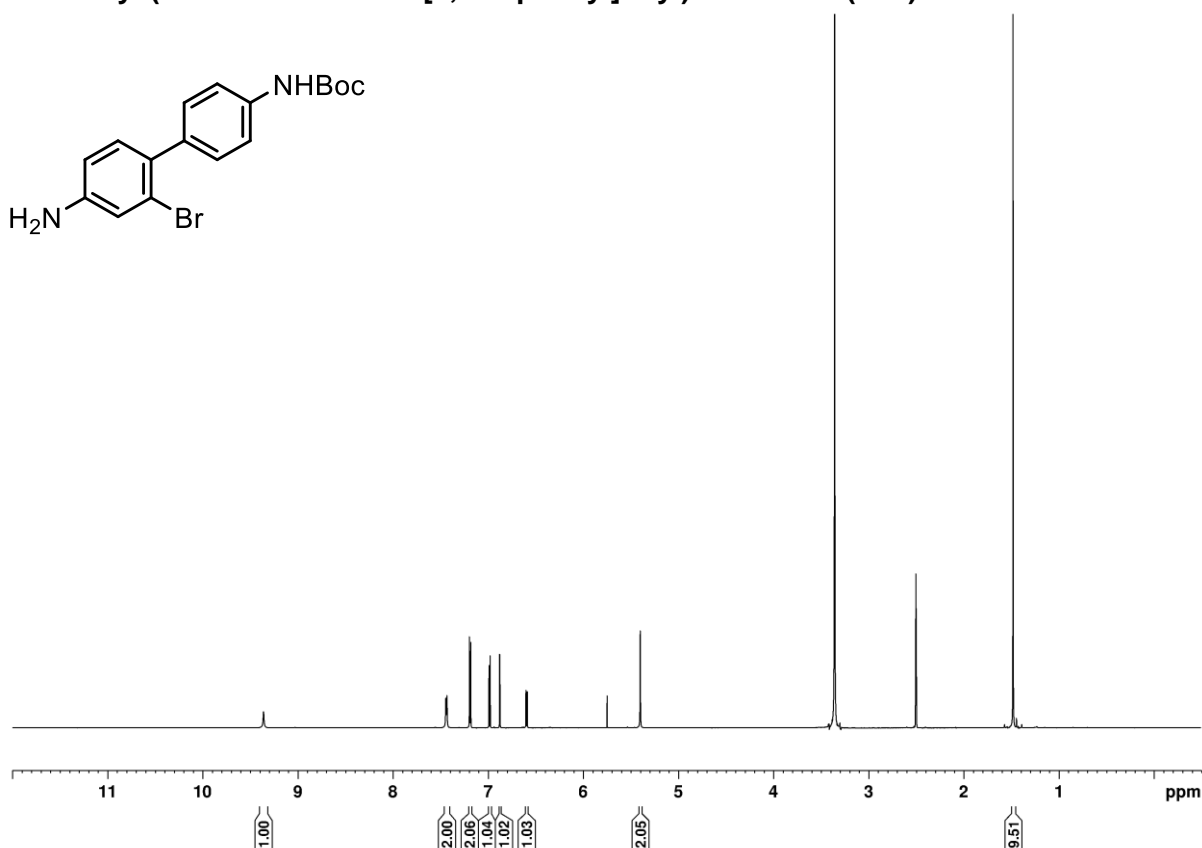
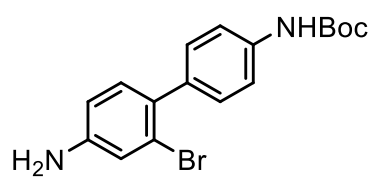
Tert-butyl (4-(2-(3-(but-3-yn-1-yl)-3H-diazirin-3-yl)ethoxy)phenyl)carbamate (S44)



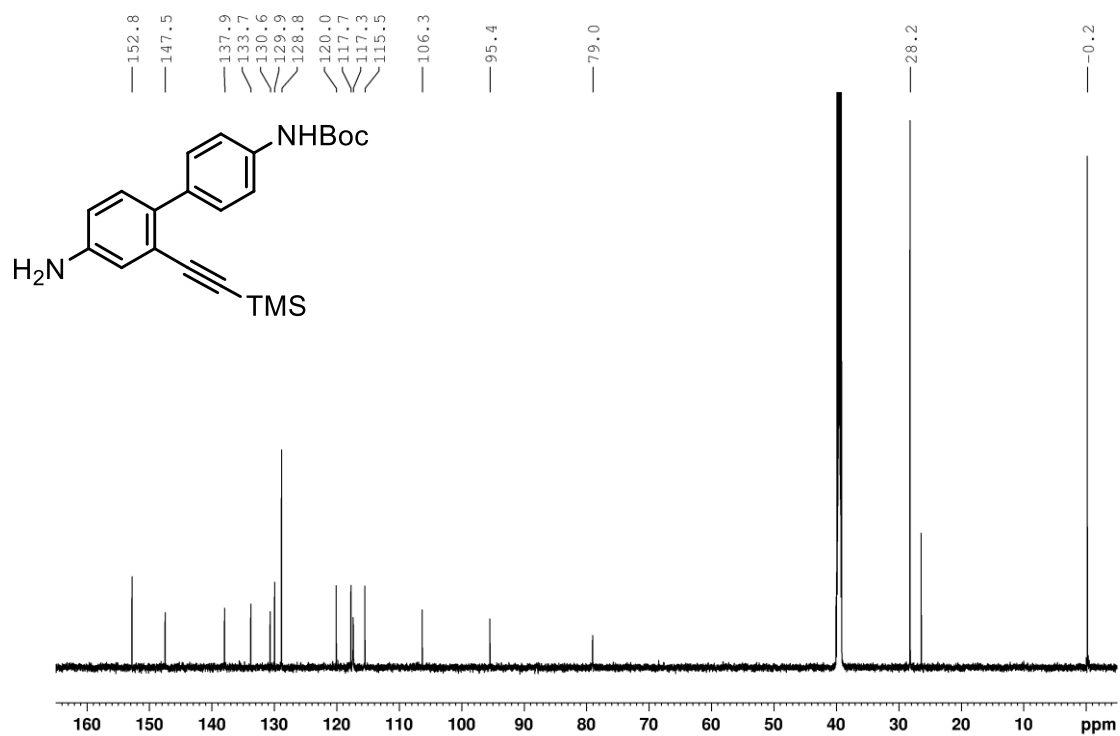
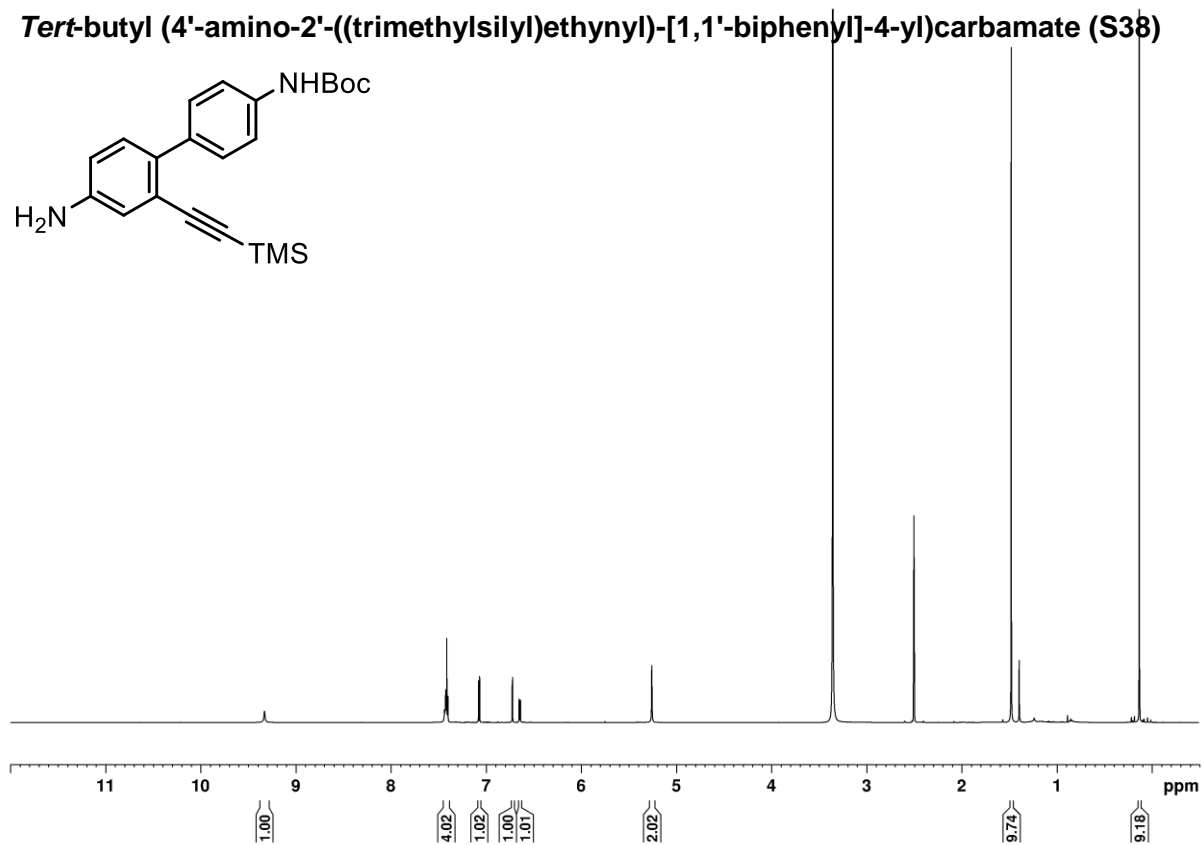
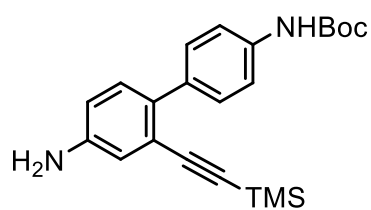
***N*-(4-(2-(3-(But-3-yn-1-yl)-3*H*-diazirin-3-yl)ethoxy)phenyl)-7-methyl-2,3-dioxo-1,2,3,4-tetrahydroquinoxaline-6-sulfonamide (14)**



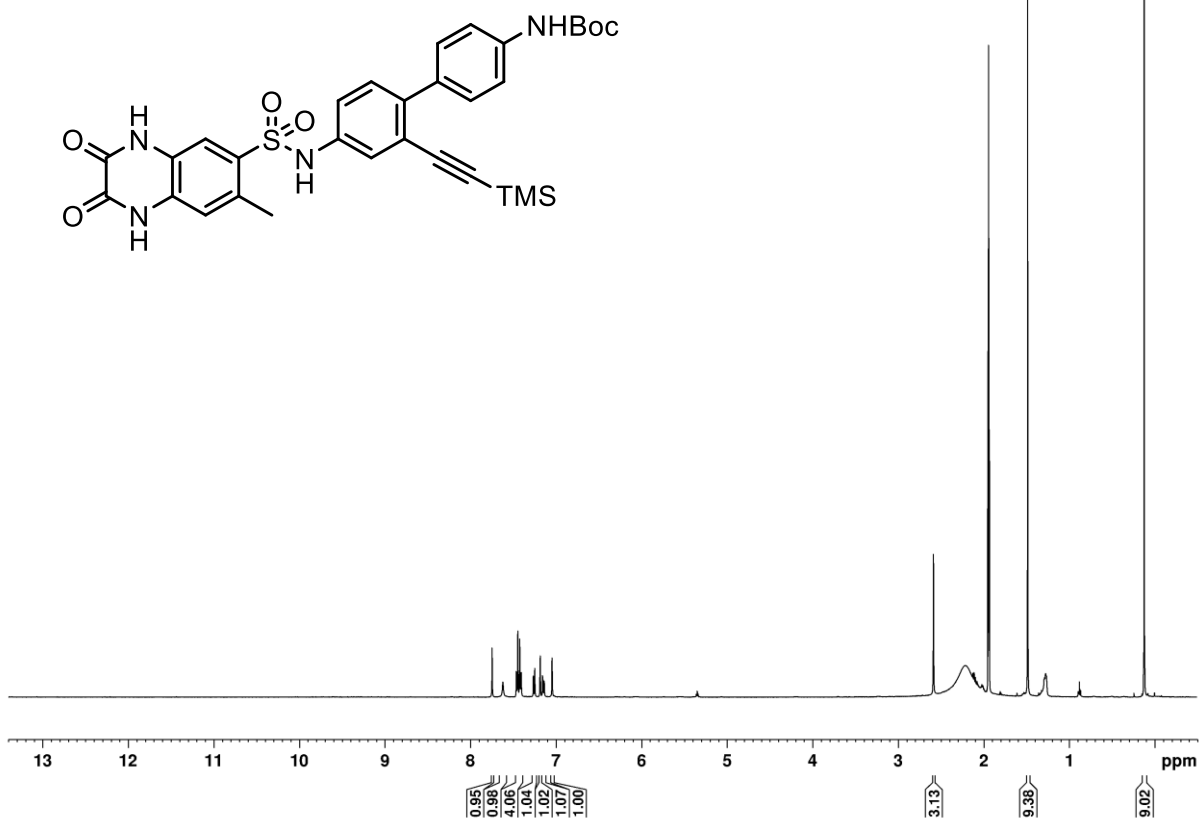
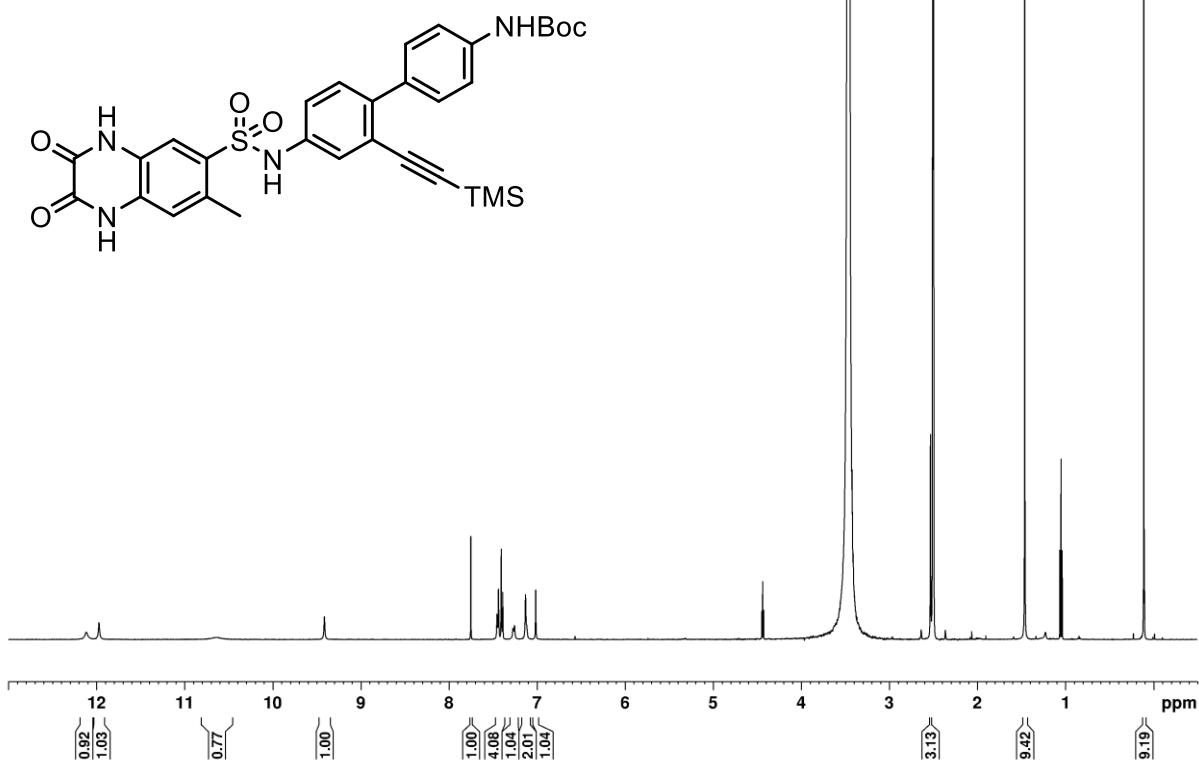
***Tert*-butyl (4'-amino-2'-bromo-[1,1'-biphenyl]-4-yl)carbamate (S37)**

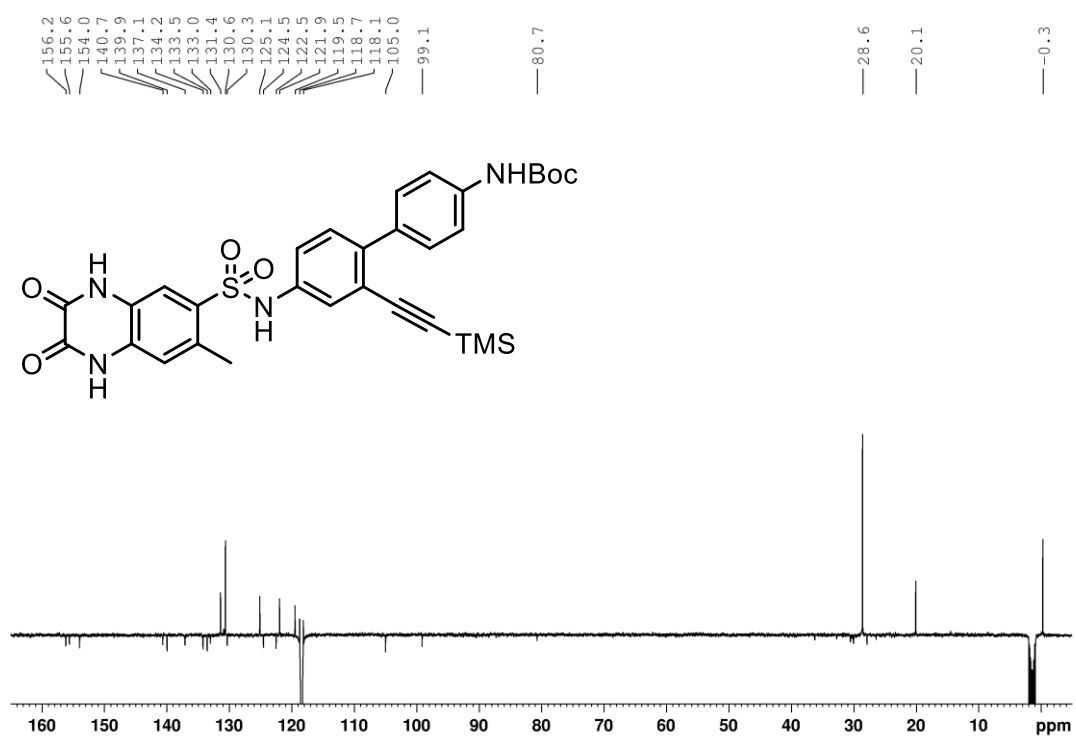


***Tert*-butyl (4'-amino-2'-((trimethylsilyl)ethynyl)-[1,1'-biphenyl]-4-yl)carbamate (S38)**

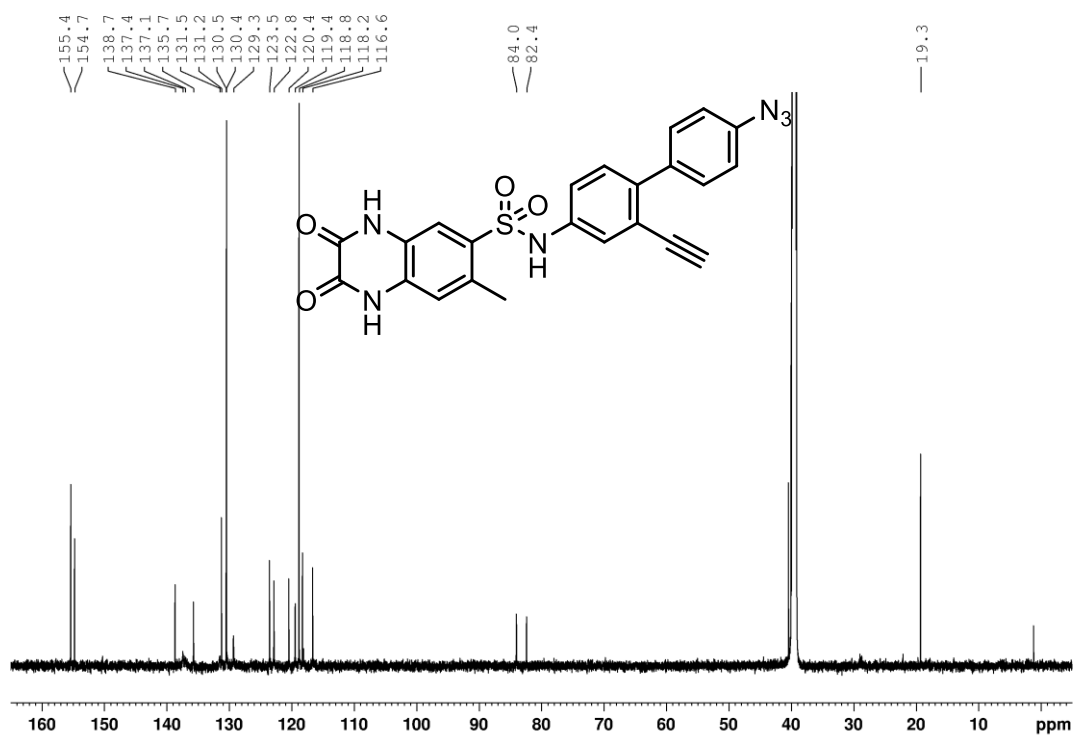
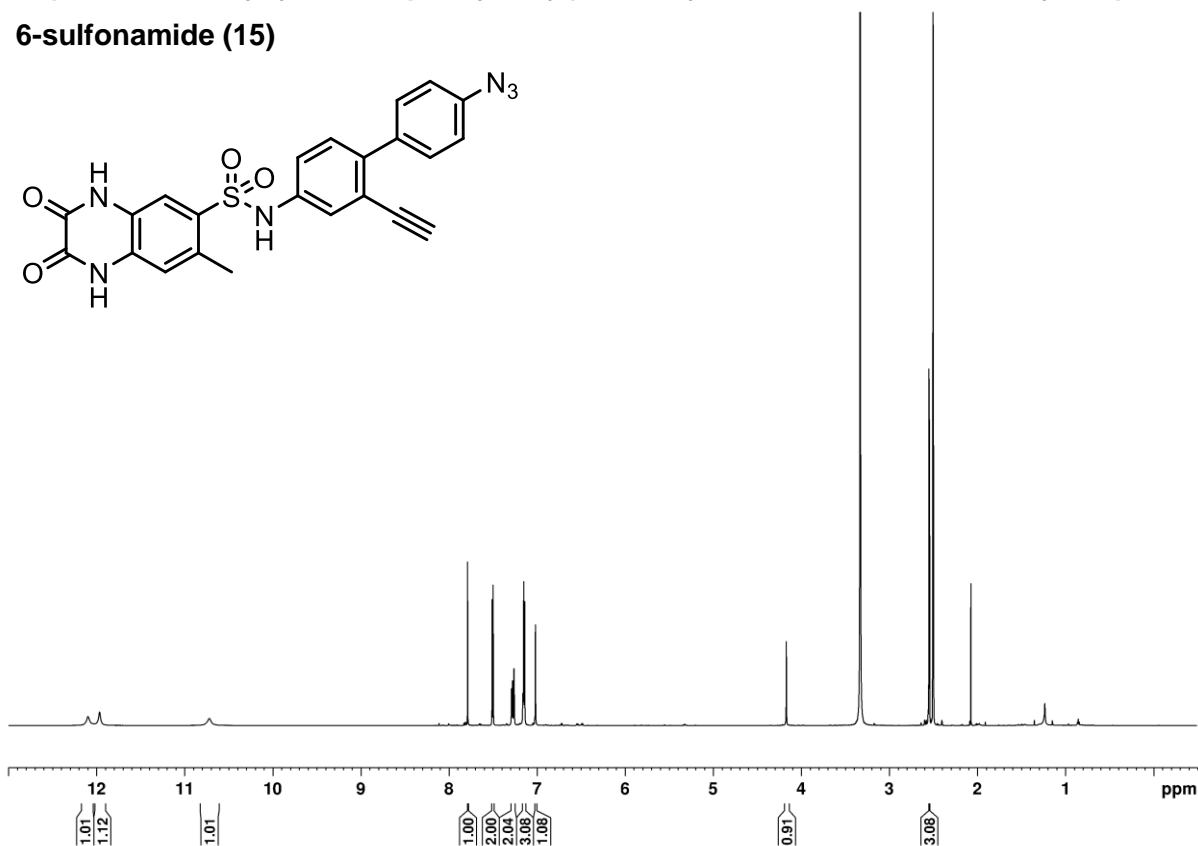


***Tert*-butyl (4'-((7-methyl-2,3-dioxo-1,2,3,4-tetrahydroquinoxaline)-6-sulfonamido)-2'-((trimethylsilyl)ethynyl)-[1,1'-biphenyl]-4-yl)carbamate (S39)**

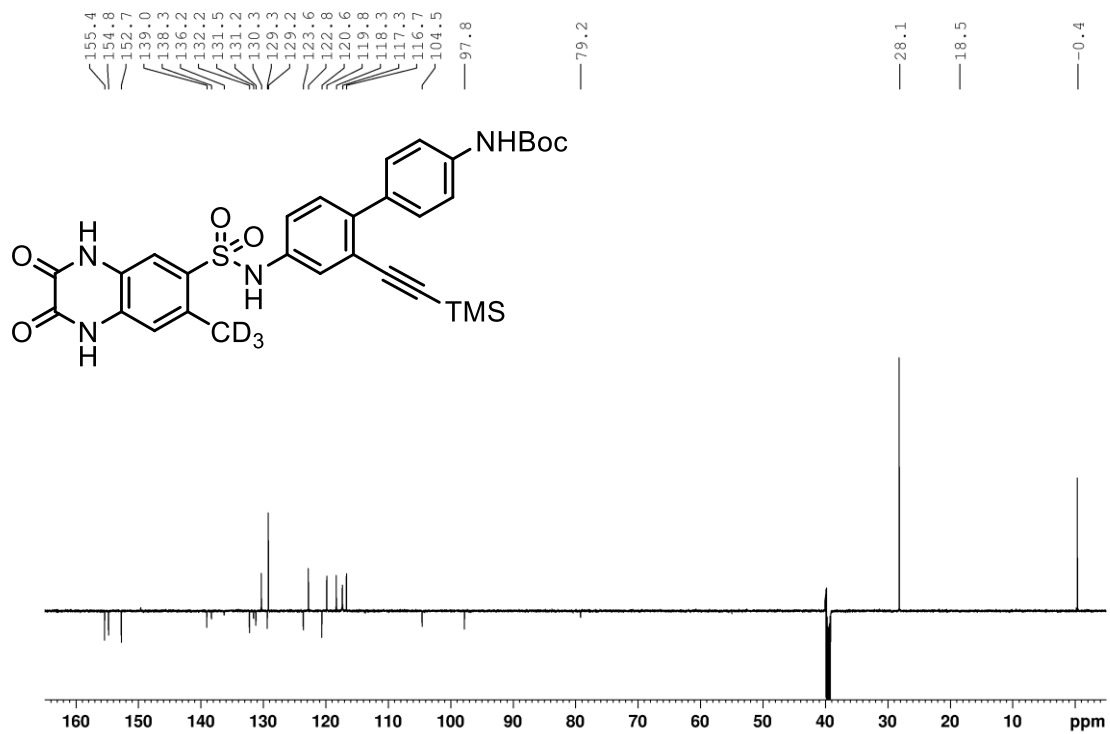
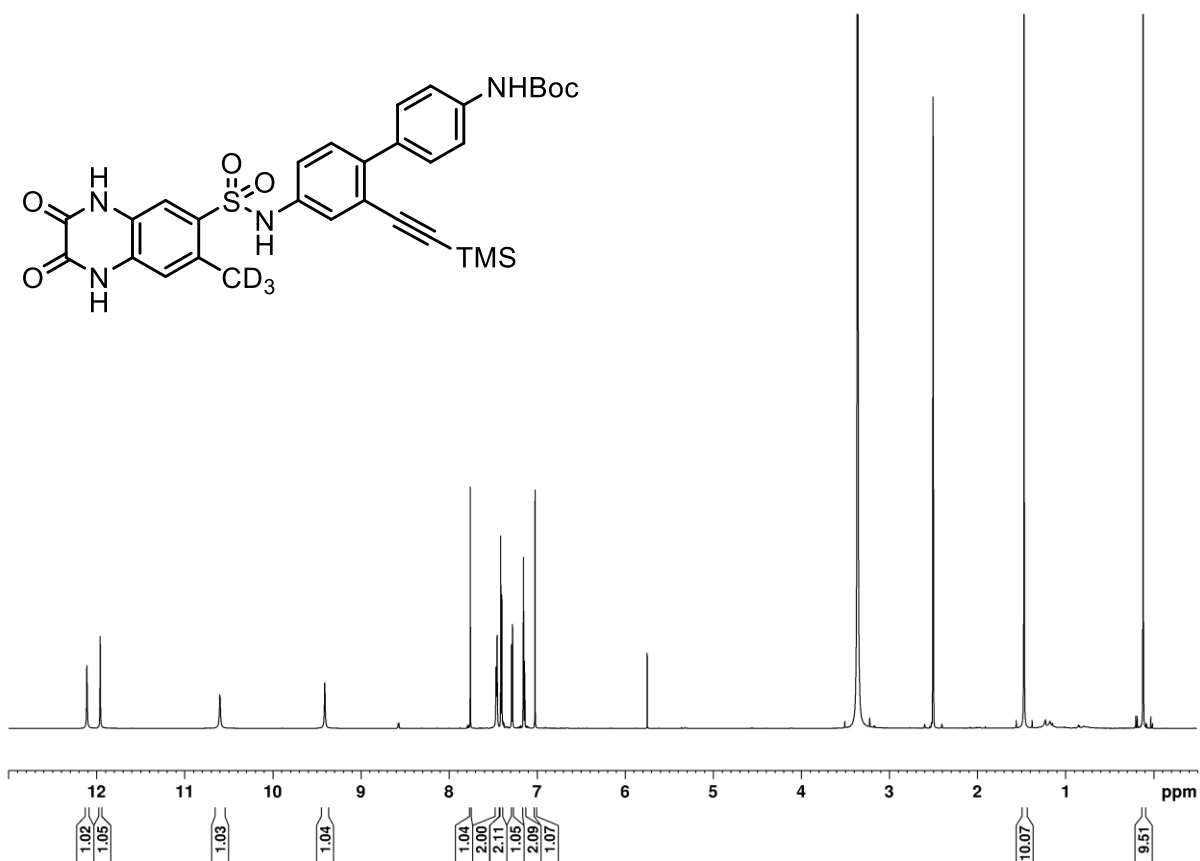




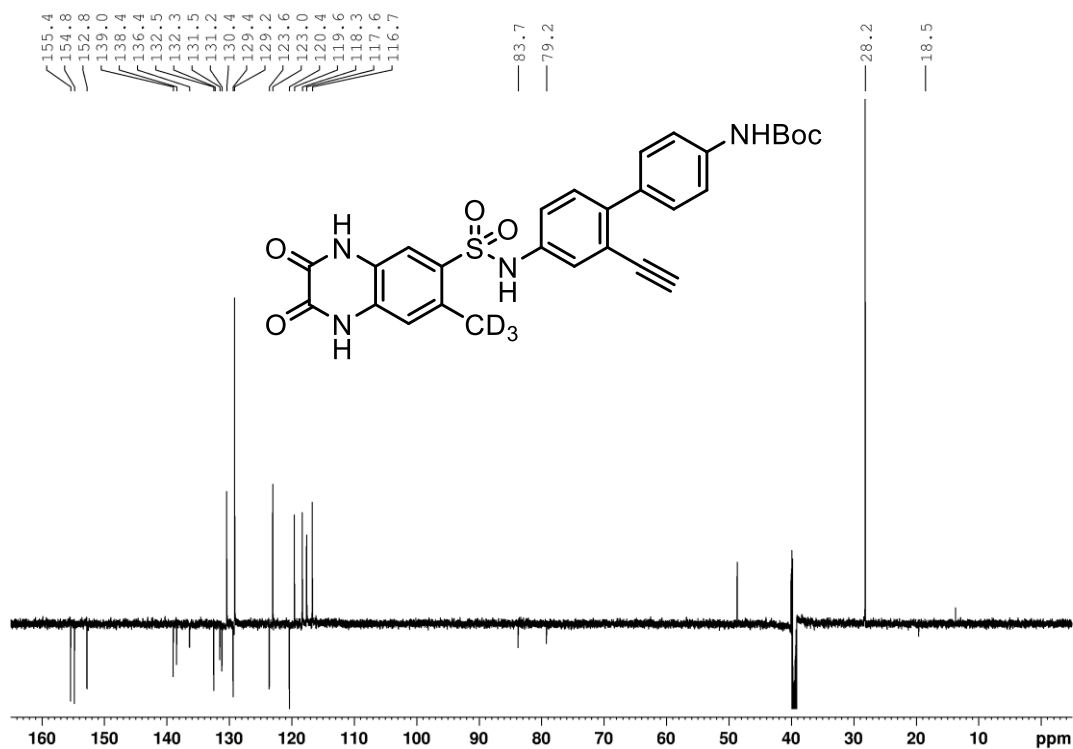
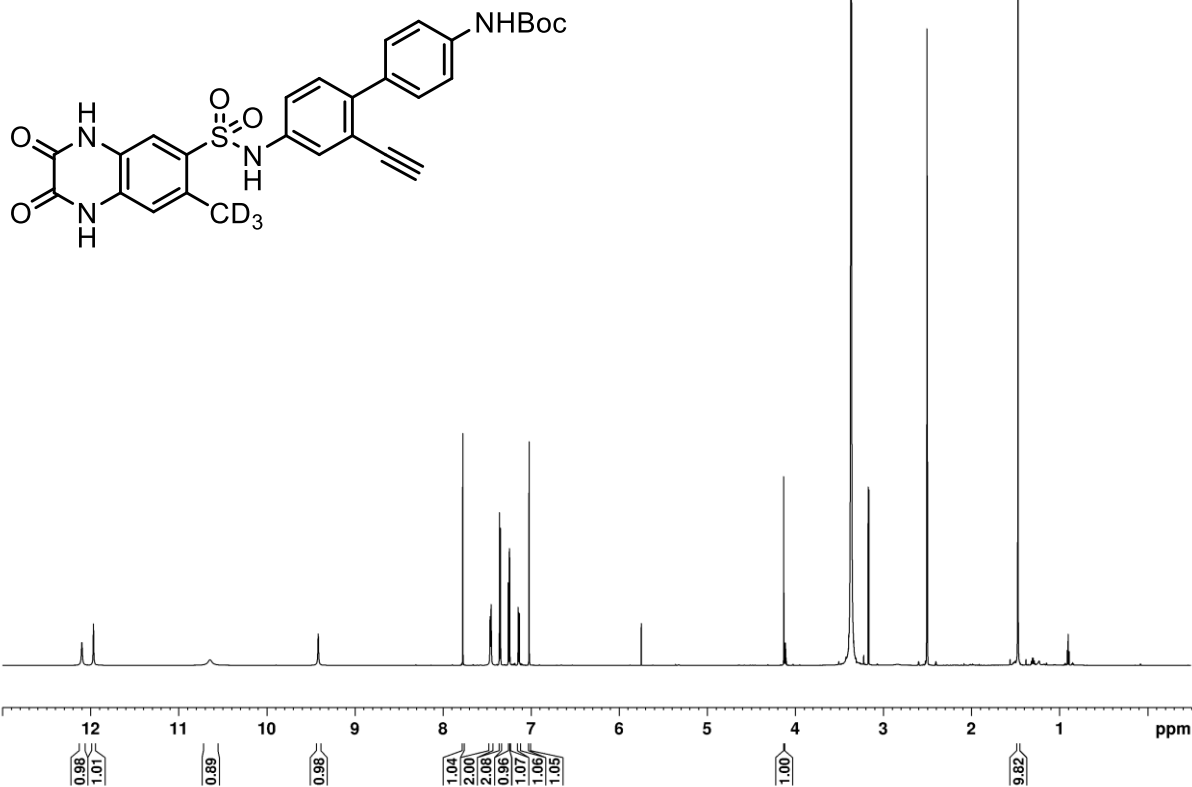
***N*-(4'-azido-2-ethynyl-[1,1'-biphenyl]-4-yl)-7-methyl-2,3-dioxo-1,2,3,4-tetrahydroquinoxaline-6-sulfonamide (15)**



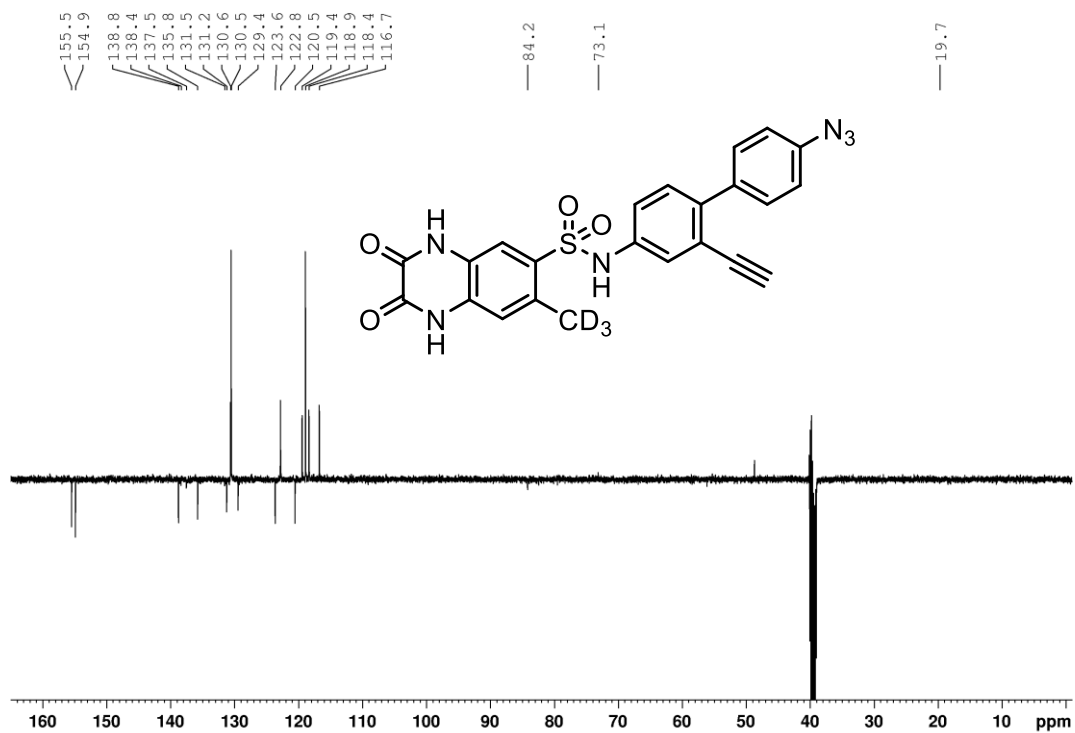
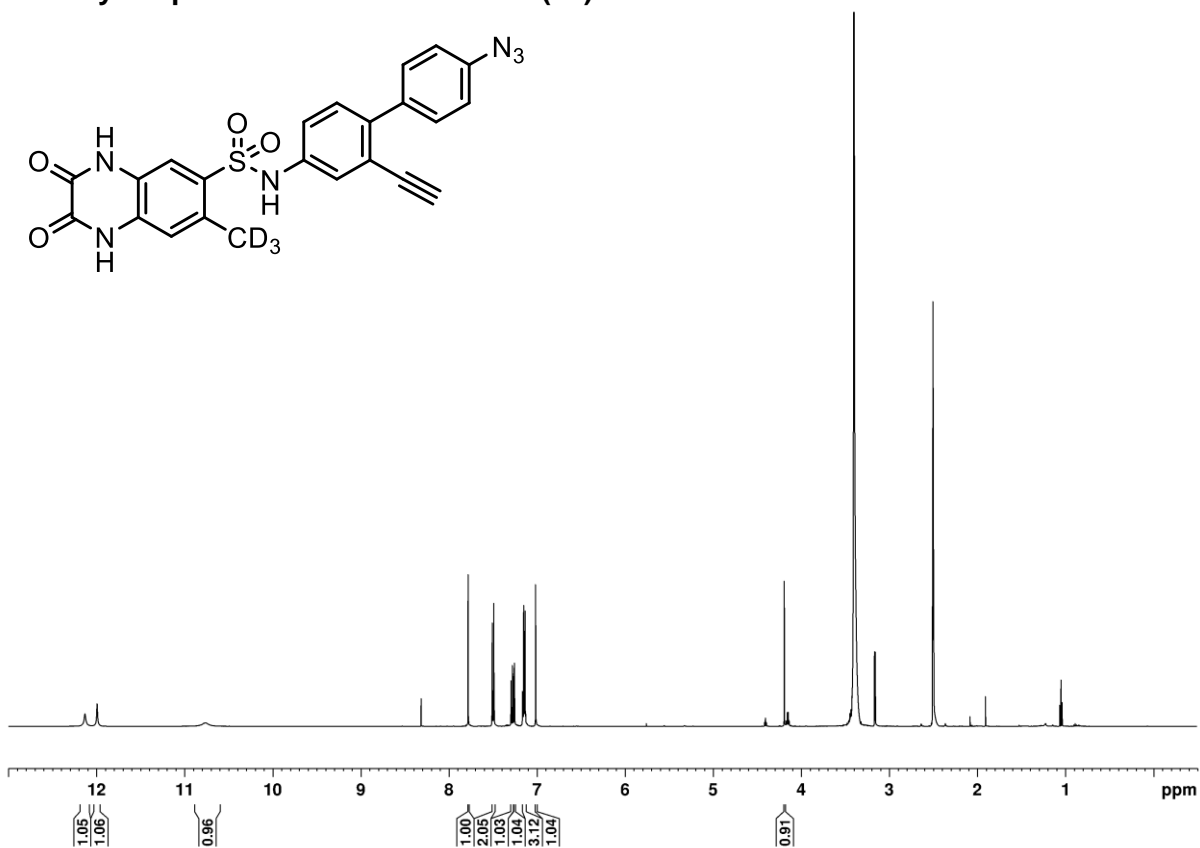
Tert-butyl (4'-((7-(methyl-*d*₃)-2,3-dioxo-1,2,3,4-tetrahydroquinoxaline)-6-sulfonamido)-2'-((trimethylsilyl)ethynyl)-[1,1'-biphenyl]-4-yl)carbamate (S41)



Tert-butyl (2'-ethynyl-4'-((7-(methyl-*d*₃)-2,3-dioxo-1,2,3,4-tetrahydroquinoxaline)-6-sulfonamido)-[1,1'-biphenyl]-4-yl)carbamate (S42)



***N*-(4'-azido-2-ethynyl-[1,1'-biphenyl]-4-yl)-7-(methyl-*d*₃)-2,3-dioxo-1,2,3,4-tetrahydroquinoxaline-6-sulfonamide (16)**



Supplemental References

- S1. Angulo, J., and Nieto, P.M. (2011). STD-NMR: application to transient interactions between biomolecules-a quantitative approach. *Eur Biophys J* 40, 1357-1369. 10.1007/s00249-011-0749-5.
- S2. Tabor, D.E., Yu, L., Mok, H., Tkaczyk, C., Sellman, B.R., Wu, Y., Oganessian, V., Slidel, T., Jafri, H., McCarthy, M., et al. (2016). Staphylococcus aureus Alpha-Toxin Is Conserved among Diverse Hospital Respiratory Isolates Collected from a Global Surveillance Study and Is Neutralized by Monoclonal Antibody MEDI4893. *Antimicrob Agents Chemother* 60, 5312-5321. 10.1128/AAC.00357-16.
- S3. Tavares, A., Nielsen, J.B., Boye, K., Rohde, S., Paulo, A.C., Westh, H., Schønning, K., de Lencastre, H., and Miragaia, M. (2014). Insights into alpha-hemolysin (Hla) evolution and expression among Staphylococcus aureus clones with hospital and community origin. *PLoS One* 9, e98634. 10.1371/journal.pone.0098634.